Structural Investigation of Helical Intermediates in the Misfolding Pathway of Amyloid Peptides Associated with Type II Diabetes and HIV

by

Ravi Prakash Reddy Nanga

A dissertation submitted in partial fulfillment
of the requirements for the degree of
Doctor of Philosophy
(Chemistry)
in The University of Michigan
2011

Doctoral Committee:

Professor Ayyalusamy Ramamoorthy, Chair
Professor E. Neil Marsh
Professor Zhan Chen
Professor Malini Raghavan
Assistant Professor Mi Hee Lim

To my family and to all those sincere and dedicated researchers, who worked and are working hard for the advancement of science towards the welfare of mankind.

ACKNOWLEDGEMENTS

First and foremost, I want to thank my father (Narasimha Reddy Nanga), my mother (Prameela Nanga), my uncle (Subramanyam Reddy Nanga), my aunt (Jyothi Nanga), my brother (Lakshmi Prasad Reddy Nanga), my sister-in-law (Divya Nanga), my wife (Sravani Chintalapalli), my sisters (Bindu Swaroopa Nanga and Jahnavi Nanga), my brother kids (Sahil Nanga and Neha Nanga) and my little daughter (Akshara Nanga) without whose love and affection as well as moral support I would have never been able to write this thesis. They were always encouraging, stood by me in times of troubles and have believed in me when I took my career path towards research.

I want to thank my Prof. Ayyalusamy Ramamoorthy whose has been a great mentor and without whose guidance I would not have progressed in my research. He is very friendly, highly motivated and always keeps the people in the lab motivated when they are down. Without his constant encouragement and support, I would never have been able to learn and realize the beautiful aspects of NMR spectroscopy in the field of membrane proteins. I am fortunate to have such a wonderful person as my mentor. I would also like to thank my committee members Prof. Neil Marsh, Prof. Zhan Chen, Prof. Malini Raghavan and Asst Prof. Mi Hee Lim for their helpful comments and discussions on my research work.

I want to thank all the lab members of the Ramamoorthy lab who have been very friendly and helpful at all times. In particular, Dr. Jeffrey Brender with whom I have worked for most of my research. He is very friendly, helpful at all times, and the only one person with highest probability to encounter in the lab at any given time. I also want to thank Dr. Sathan Thennarasu, Dr. Vivekanandan Subramanian who had been great friends of me and in particular Dr. Vivek from whom I have learned most of the solution NMR aspects and ended up from being a computational chemist to NMR spectroscopist. I also want to thank my friends Dr. Pieter Smith, Marchello Cavitt, Kevin Hartmann, Dr. Jiadi Xu, Kazutoshi Yamamoto, Dr. Neil MacKinnon, Dr. Nataliya Popovych, Dr. Shivani Ahuja and Stephanie Le Clair. Also not to forget the undergraduates Jeffrey Barry, Michelle Fritz, Daniel Youngstrom, Samer Salamekh and Austin McHenry who are also great contributors to our research in the lab.

I would also like to thank my home department (Chemistry) for providing the winter 2010 departmental fellowship and its staff in particular Laura Labut, Stryker Anna as well as the Biophysics staff in particular Tony Markel and the staff of NMR facility at the Michigan State University, Lansing where I have collected most of the NMR data for my research work.

Table of Contents

LIST OF FIGURES

LIST OF TABLES

LIST OF ABBREVIATIONS

Aβ: Amyloid Beta
CD: Circular Dichroism
CSI: Chemical Shift Index
CGRP: Calcitonin Gene Related Peptide
DPC: Dodecylphosphocholine
DSC: Differential Scanning Calorimetry
DMPG: Dimyristoyl Phosphatidyl Glycerol
DMPC: Dimyristoyl Phosphatidyl Choline
EPR: Electron Paramagnetic Resonance
HIV: Human Immunodeficiency Virus
HFIP: Hexafluoroisopropanol
hIAPP: Human Islet Amyloid Polypeptide
IAPP: Islet Amyloid Polypeptide
NMR: Nuclear Magnetic Resonance
NOE: Nuclear Overhauser Effect
NOESY: Nuclear Overhauser Enhancement Spectroscopy
PAP: Prostatic Acid Phosphatase
POPG: Palmitoyl Oleoyl Phosphatidyl Glycerol
RMS: Root Mean Square
RMSD: Root Mean Square Deviation
rIAPP: Rat Islet Amyloid Polypeptide
SA: Simulated Annealing
SDS: Sodium Dodecyl Sulfate
SDS-PAGE: Sodium Dodecyl Sulfate – Poly Acrylamide Gel Electrophoresis
SEVI: Semen-derived Enhancer of Viral Infection
1D: One Dimension

2D: Two Dimension

TFA: Trifluoroacetic acid

TOCSY: Total Correlation Spectroscopy

ABSTRACT

A variety of aging related diseases including Alzheimer's, Type II diabetes, Huntington's, Parkinson's, and Creutzfeldt-Jakob are characterized by the formation of abnormal proteinaceous deposits. These deposits, known as amyloid, are abnormal accumulations of misfolded proteins with a characteristic cross β-sheet conformation. The formation of amyloid fibers can occur through many pathways, of which one of the most important pathway is catalyzed by binding to the cell membrane. The peptide-membrane interaction can disrupt the integrity of the cell membrane, causing disruption of calcium homeostasis and eventual cell death.

In membrane-mediated aggregation, the protein is thought to initially bind with the membrane in an α-helical conformation before undergoing a conformational change during aggregation to a β-sheet form characterstic of the amyloid fiber. Therefore, it is important to determine atomic-level structures of these intermediates, as they can provide insights into the toxic mechanism exhibited by these amyloidogenic proteins and into the design of drugs that can suppress these intermediate helical species to stop further progression into toxic states.

This dissertation reports high-resolution NMR structural studies of two different membrane bound amyloid proteins: (1) IAPP (an amyloidogenic peptide

related to Type II diabetes), in order to understand the role of α-helical intermediate structures in causing membrane disruption, (2) $PAP_{248-286}$ (the corresponding amyloid fiber (SEVI) enhances the infectivity of the HIV virus), in order to understand the bridging interactions it exhibits between the host and viral cell membranes.

Our studies on the membrane bound α-helical intermediates of rat and human IAPP/$IAPP_{1-19}$ reveal a pH dependent membrane orientation for $IAPP_{1-19}$, which correlates well with its ability to disrupt synthetic membrane vesicles and β-cells, and that the position of the disulfide bridge with respect to the hydrophobic interface of the N-terminal helix could be one of the factors that modulate the membrane disruptive behaviour of these peptides.

Our study on membrane bound $PAP_{248-286}$, reveals an unusual amount of structural disorder that, in combination with high positive charge at the N-terminus could play an important role in the fusion of host and viral cell membranes by weakening the electrostatic interactions that repel similarly charged membranes.

CHAPTER 1. AN INTRODUCTION TO THE AMYLOID PEPTIDES INVOLVED IN TYPE II DIABETES AND HIV

1.1 WHAT ARE AMYLOIDS?

Amyloids are cross-beta fibril protein deposits that have been found in many amyloidogenic diseases such as Alzheimer's disease, Type II diabetes, Huntington's disease, Parkinson's disease and Creutzfeldt-Jakob disease [*1-5*]. A recent study by Muench et al., [*6*] has led to the discovery of another amyloidogenic peptide known as $PAP_{248-286}$ that has been related to the transmission of human immunodeficiency virus (HIV). The amyloidogenic peptides and proteins associated with these deposits undergo a misfolding upon binding to the membrane from their native random coil monomeric conformation to intermediate helical species which later tranforms to the β-sheet that are characteristic of fibril deposits. This misfolding on the cell surface can have several consequences for the cell including cell membrane fusion, disruption of the integrity of the plasma membrane, and cytotoxicity. In all of these pathways, the intermediate helical species play an important role in cell toxicity, cell membrane fusion or transformation into β-fibril deposits as shown in Figure 1-1.

The two systems we are interested in are : 1) Type II diabetes and 2) HIV, where the amyloid peptide associated with the former is cytotoxic to the cell and the latter is non-toxic but associated with the fusion of host cell membrane with viral cell membrane.

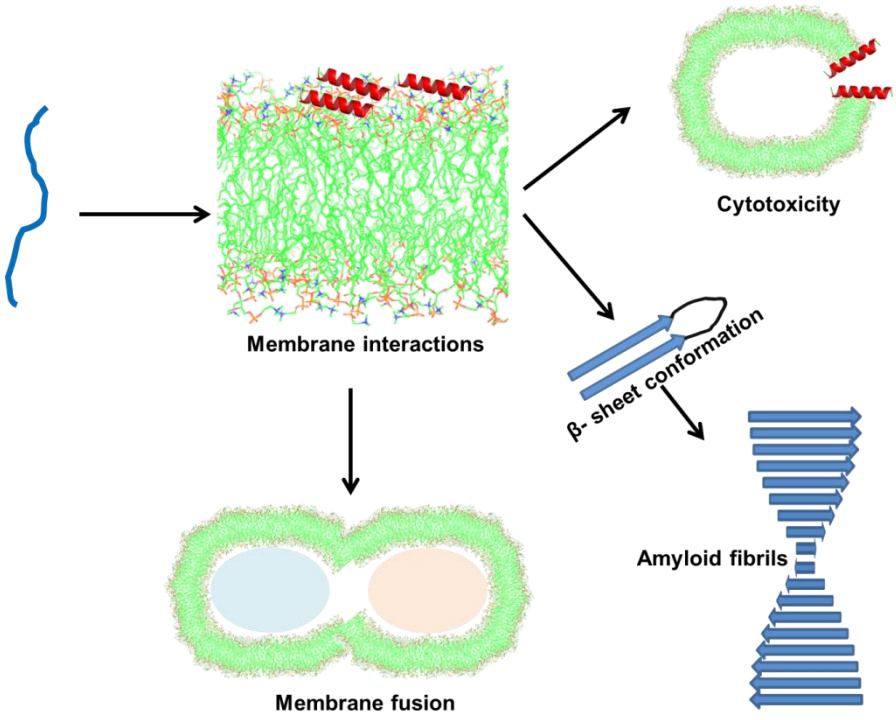

Figure 1-1. Aggregation pathway of amyloids

1.2 TYPE II DIABETES

Type II diabetes *aka* non-insulin-dependent diabetes mellitus or adult onset diabetes is one of the most common disease worldwide. It is characterized by an increase in insulin resistance as well as the decreased production of insulin due to loss of β-cell mass in the human pancreas. Around 20.8 million people in the year 2005 were affected by this disease in United States alone of which around 20.6 million were of age 20 years or older [*7*]. Some of the complications that arise from type II diabetes are high blood pressure, heart disease & stroke, blindness and kidney diseases. Direct medical costs associated with the treatment of this disease in United States alone, was around $92 billion in the year 2002 [*7*]. In recent years, there has an alarming increase in the number of people suffering with type II diabetes due to changes in diet and an increase in

the average age of the US population, which has prompted interest in the mechanism involved in its development.

Amyloid deposits are commonly isolated in the pancreatic islets from the subjects both suffering with type II diabetes, and to a lesser degree, older subjects without type II diabetes [*8-10*]. Although the amyloid-like material was first observed in the year 1901 by the pathologist Dr. Opie in specimens of human pancreas [*11*], its contents were only solubilized and identified as islet amyloid polypeptide (IAPP) in the year 1987 by Westermark, P., *et al* [*12, 13*].

IAPP *aka* Amylin, is derived from an 89 amino acid residue precursor by sequential enzymatic cleavage in pancreatic β-cells. The N-terminal residues of the IAPP precursor from 1-18 resembles a signal peptide with a possible signal peptidase cleavage site located at Ala22 [*14, 15*]. This initial cleavage and oxidation of disulfide-bridge occurs in the lumen of the endoplasmic reticulum and results in the proIAPP precursor [*16*]. The 11 residue N-terminal flanking peptide and the 16 residue C-terminal flanking peptide of proIAPP are then cleaved at the dibasic amino acids sites (K10, R11 & K50, R51 by the enzymes prohormone convertase 2 and 1/3, respectively, in immature secretory granules [*17-20*]. In the next step, the C-terminus Lys-Arg residues are cleaved by carboxypeptidase E resulting in the exposure of Gly residue for attack by the enzyme peptidylglycine α-amidating monooxygenase (PAM), which cleaves $C_{\alpha}H_2COOH$ from Gly, leaving only the amine resulting in the amidation of the Tyr residue. The final product is 37 residues with a calculated molecular mass of 3.9 kDa [*21-25*]. This entire processing scheme is shown in Figure 1-2.

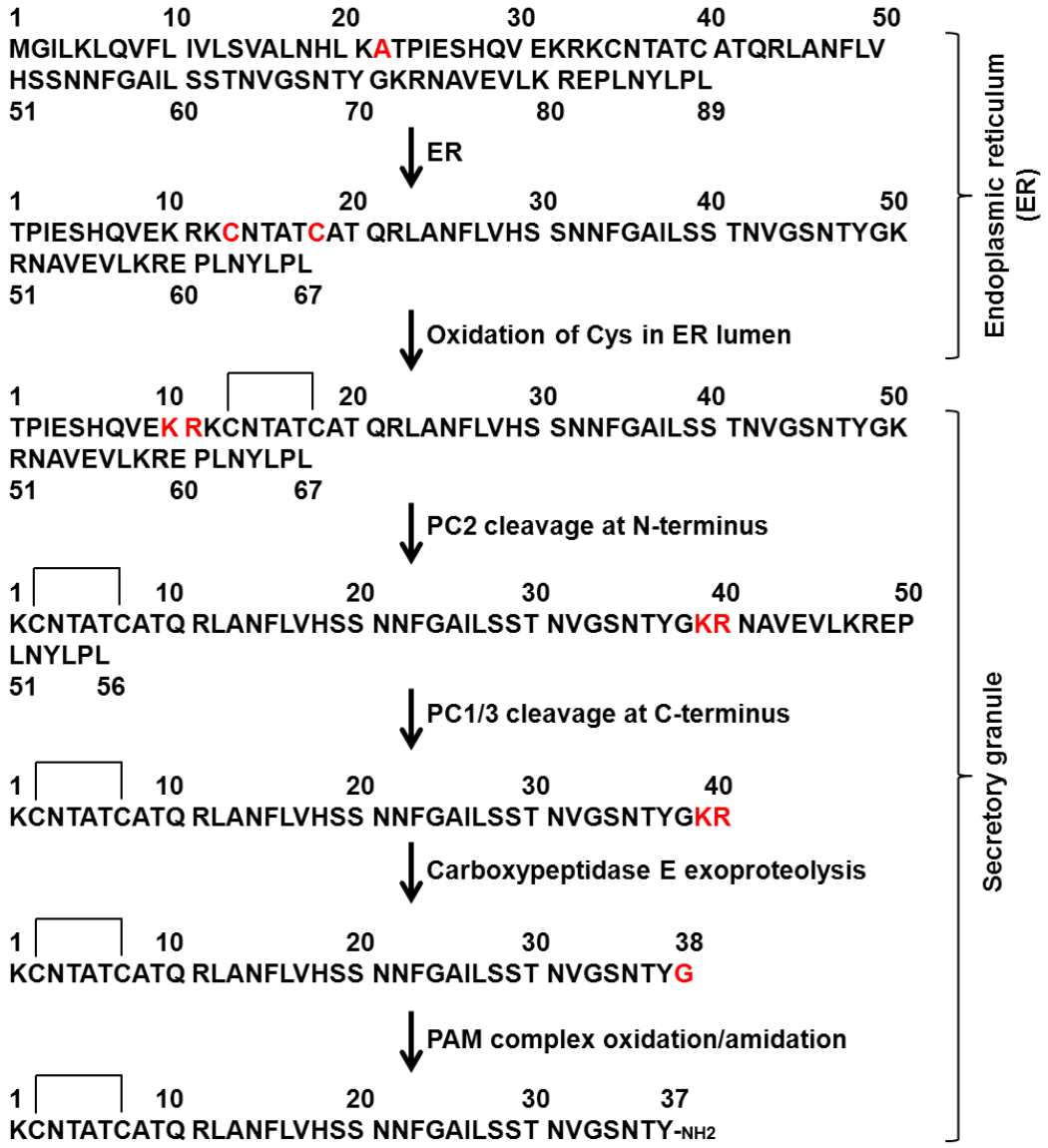

Figure 1-2. IAPP processing scheme from its precursor protein. Please note that the oxidation of cysteine residues in ER lumen and the relative timing of PC2 processing are not yet established. Targeted residues are indicated in red color.

IAPP is co-secreted with insulin from the islet β-cells of the pancreas [*26, 27*]. In its normal physiological role, IAPP acts in concert with insulin to control plasma glucose levels and independently of insulin as an appetite suppressor [*28-30*]. Since the amyloid deposits were most observed in the pancreas of ~95% of the patients suffering with type II diabetes, much of the earlier work focused on

identifying the region of IAPP involved in fibril formation. The most amyloidogenic fragment was found out to be from residues 20-29 of hIAPP [*31-35*]. A fiber model of $hIAPP_{20-29}$ was developed with the help of six inter-carbon distance obtained from rotational resonance solid-state NMR spectroscopy. One face of the $hIAPP_{20-29}$ amyloid β-sheet contains the side chains of G24, I26 and S28 and the other face the side chains of F23, A25, L27 and S29 [*36*]. The orientation of the beta sheet of the fibrils of $hIAPP_{20-29}$ with respect to each other was found out to be antiparallel from Fourier transform infrared spectrum [*37*]. Another solid state ^{2}H and ^{19}F NMR study on the fibrils of $hIAPP_{20-29}$ suggested a side-by-side arrangement of the sheet with the phenyl rings facing towards the inter-sheet space within a hydrophobic core [*38*]. Peptide based inhibitors were designed to target the 20-29 region of hIAPP in order to inhibit amyloidogenesis [*39-43*]. But later studies have shown that there are other amyloidogenic segments in hIAPP that can also independently form fibrils apart from the segment 20-29, one being located at the C-terminus from residues T30-Y37 and the other at the N-terminus from residues A8-S20 [*44-49*].

While the focus was on these amyliodogenic segments, an important breakthrough came in 1999, when Janson, J., et al showed that intermediate sized amyloid particles were toxic to human islets cells, whereas matured hIAPP containing large amyloid deposits did not cause cytotoxicity [*50*]. Voltage-clamped planar bilayer experiments in the same study showed that membrane damage was induced by early aggregates of hIAPP rather than matured hIAPP aggregates [*50*]. From light scattering experiments, the number of hIAPP

molecules involved in membrane toxicity was determined to be between 25 to 6000 IAPP molecules [*50*]. This membrane disruption activity by early hIAPP aggregates was supported by other studies on protofibrils of hIAPP which showed the permeabilization into synthetic vesicles by a pore-like mechanism [*51, 52*]. Extraction of the lipids from the membrane by growing amyloid deposits but not preformed fibrils was also observed by fluorescence confocal microscopy on lipid vesicles [*53*]. Other studies that followed supported the role of the hIAPP oligomers in the disruption of the cell membranes [*54-56*].

In one of the studies on the interaction of hIAPP with lipid membranes consisting of DOPG/DOPC, formation of preamyloid states were observed at the N-terminus but not with the C-terminus of the peptide [*57*]. This observation of N-terminus interaction with the membrane was further supported by the studies on the fragments of the hIAPP where the N-terminal 1-19 fragment of hIAPP efficiently inserted into the phospholipid monolayers as a monomer while the insertion into the membrane could not be observed with the 20-29 fragment of hIAPP [*58*].

A weakly stable hIAPP α-helix of approximately 15-19 residues in length was observed, when hIAPP was added to membranes containing PS by CD and fluorescence studies [*59*]. This study established a role for the α-helical intermediates in hIAPP aggregation when bound to membranes. Emerging evidence supports this hypothesis of the role of membrane bound α-helical intermediates of hIAPP in aggregation and toxicity to the β cells [*60, 61*]. It was also shown that $hIAPP_{1-19}$, like full length hIAPP, undergoes a transition from

random coil to α-helical intermediate state upon binding to the vesicles and causes dye leakage from POPG liposomes but unlike full length hIAPP, $hIAPP_{1-19}$ do not form fibrils [*62*]. A similar result was later obtained by measuring the calcium influx into β-cells induced by hIAPP and $hIAPP_{1-19}$. In the same study, the fibril forming $hIAPP_{20-29}$ peptide did not cause any dye leakage from POPG liposomes. Therefore, it was concluded that membrane disruption can occur independently from amyloid formation in hIAPP, and the sequences responsible for these processess are located in two different regions on the hIAPP peptide [*62*].

Rat IAPP (rIAPP) which has around ~84% sequence similarity and differs from hIAPP by six different substitutions in its sequence as shown in Figure 1-3. In this context, it is significant that rats do not develop type II diabetes. While rat IAPP has been shown to sample transient α-helical states like hIAPP, it importantly does not progress to form amyloid fibrils [*63-65*].

But the structural insights into these transient α-helices which have been implicated in membrane disruption activity has been limited so far owing to problems involved in sample solubility and aggregation. To overcome these problems, we have employed micelles in order to trap the α-helical intermediate state of the peptide in a stable form. This micelle system was further optimized for structural studies of the truncated (1-19) and full length rat and human IAPP by solution NMR spectroscopy, which could provide insights into the mechanism involved in varying activities of membrane disruption exhibited by these peptides on pancreatic β-islet cells.

Figure 1-3. Primary amino acid sequences of human and rat amylin. Both the peptides have disulfide-bridge from residues Cys2-Cys7 and are amidated at the C-terminus. Residues in rat amylin that differs from human amylin are colored in red.

1.3 HUMAN IMMUNODEFICIENCY VIRUS (HIV)

HIV infects around 0.6% of population worldwide. From its discovery in 1981 to 2007, AIDS has killed more than 25 million people [*66*]. In 2008 alone, AIDS has claimed an estimated 1.7-2.4 million lives of which more than 280000 were children [*67*]. Even though AIDS is pandemic, HIV is surprisingly weak pathogen *in vitro* with only <0.1% of the virus particles succeeding in infecting a host cell [*68, 69*]. Emerging evidences suggest that the viral attachment to the host cell membranes for its entry is the limiting factor *in vitro* [*70-72*]. Since semen is the main vector in the transmission of the HIV worldwide, a recent study on screening the components of the human semen resulted in a peptide fragment known as $PAP_{248-286}$, the fibril form of which is known as SEVI (serum-derived enhancer of viral infection), that showed a potent enhancement of the HIV infection over a broad range of HIV phenotypes [*73-75*]. $PAP_{248-286}$ is a 39 residue amino acid peptide fragment, as shown in Figure 1-4, and is part of a protein called prostatic acid phosphatase (PAP) found in the semen of humans. How $PAP_{248-286}$ is cleaved from PAP, is not yet established but is thought to be cleaved by lysozyme. Since the structures of $PAP_{248-286}$ are not known in any form, it is difficult to make predictions about the interactions of this peptide with the cell membrane that facilitate HIV viral attachment. So, the minor part of my

thesis involves the structural studies of $PAP_{248-286}$ in micelle environment by solution NMR spectroscopy, in order to understand the mechanism by which it promotes the bridging of viral and host cell membranes.

Figure 1-4. Primary amino acid sequence of $PAP_{248-286}$.

1.4 STRUCTURAL STUDIES USING NUCLEAR MAGNETIC RESONANCE SPECTROSCOPY

NMR techniques to solve 3D structures of water-soluble peptides and proteins are well-established. On the other hand, NMR techniques to study membrane-associated proteins are continued to be developed as these systems pose tremendous challenges to existing techniques. In this study, we used synthetic peptides of IAPP and SEVI for structural studies in model membranes using NMR spectroscopy. The intermediate helical structures of these peptides were stabilized in detergent micelles. Recombinant isotopically enriched peptides were not available for this study. SEVI has not been successfully biologically expressed, while the recombinant IAPP peptide is non-amidated at the C-terminal, unlike the naturally occurring peptide. Since the peptides were not enriched with isotopes of ^{13}C or ^{15}N, 2D ^{1}H-^{1}H experiments were utilized to solve the structures of the peptides embedded in micelles. After optimization of micelle sample conditions, 1D ^{1}H NMR experiments were performed to optimize the experimental conditions for structural studies. 2D ^{1}H-^{1}H TOCSY and 2D ^{1}H-^{1}H NOESY experiments were performed to assign resonances and measure NOE constraints.

The 2D ^{1}H-^{1}H TOCSY (TOtal Correlation SpectroscopY) or HOHAHA (HOmonuclear HArtmann-HAnn) correlates the chemical shifts of all protons within each amino acid residue of the peptide or protein via scalar coupling [*76, 77*]. Unlike in a 2D COSY experiment, the rotating-frame based TOCSY experiment renders *in phase* transfer of magnetization which result in *in phase* scalar coupled multiplets both in diagonal and cross peaks of the 2D spectrum. More details about the TOCSY experiment and the details of the spin dynamics can be found in the literature [*76-78*]. This experiment is equally important to that of 2D ^{1}H-^{1}H NOESY, as it helps in distinguishing the intra-residual peaks from the inter-residual peaks in a NOESY spectrum.

High resolution structures of the amyloid peptides in my thesis involves the utilization of the NOE derived distance restraints obtained from a 2D ^{1}H-^{1}H NOESY (Nuclear Overhauser Enhancement SpectroscopY) experiment. Nuclear Overhauser Effect (NOE) [*79*], which states the transfer of spin polarization from one nucleus to another by cross-relaxation or through space interaction, was named after the scientist Albert W. Overhauser who developed the hypothesis of Overhauser effect for the transfer of spin polarization from electron to nuclear spins by cross-relaxation [*80*]. For two nuclei close in proximity in space, the strength of NOE depends on the distance between the two interacting nuclear spin in a $1/r^{6}$ manner. This distance dependence limit the observation of NOEs to distances less than or equal to 6 Å. A two-dimensional NOESY experiment is therefore important, in providing all the NOEs of the peptide system, which can be converted into the distance restraints used to calculate the structures by

different simulated annealing softwares available. Therefore, NOEs provide important information about the secondary structure or the fold of a peptide/protein. More details about the NOESY experiment can be found in the literature [*81*].

While these 2D experiments are commonly used to investigate the atomic-level structures of polypeptides without the need for isotopic enrichment, solving the high-resolution structures of amyloid peptides is a tedious problem. Since an amyloid peptide aggregates rapidly in the NMR timescale and the aggregated species do not tumble rapidly to contribute to the observed signal, applying multidimensional NMR experiments has been a major challenge. For this reason, solid-state NMR experiments have been utilized in solving the high-resolution structures of end products namely the amyloid fibers. While these structures are interesting, our main objective of this study was to solve the high-resolution structures of helical intermediates present in the misfolding pathways of IAPP and SEVI. To accomplish this goal, we trapped the helical intermediates in a micellar environment using detergents and applied solution NMR experiments as mentioned above. By optimizing the concentrations of the peptide and detergent and other conditions like pH and temperature, well behaved samples were obtained for both IAPP and SEVI. These samples were quite stable for NMR experiments and provided high-resolution spectral lines that enabled us the structure determination as reported in the following chapters of the thesis. Though we aimed at solving the structures of helical intermediates in the misfolding pathway, the structure of the amyloid peptide upon interaction with the

cell membrane is also important to understand the mechanism of cell toxicity in the case of IAPP and the mecanism of membrane fusion in the case of SEVI. Therefore, the structures determined from this study could be important to address the membrane behavior of these peptides even though detergent micelles may not be the best membrane mimetic. The use of micelles is even more important as structural studies of an amyloid peptide embedded in a lipid bilayer (a better model membrane than a micelle) are tedious due to the lipid-induced aggregation of the peptide.

REFERENCES

[1] Hensley, K., Carney, J. M., Mattson, M. P., Aksenova, M., Harris, M., Wu J. F., Floyd, R. A., and Butterfield, D. A. (1994) A model for β-amyloid aggregation and neurotoxicity based on free radical generation by the peptide: relevance to Alzheimer disease. *Proc. Natl. Acad. Sci. 91*, 3270-3274.

[2] Mirzabekov, T. A., Lin, M. C., and Kagan, B. L. (1996) Pore formation by the cytotoxic islet amyloid peptide amylin. *J. Biol. Chem. 271*, 1988-1992.

[3] Tabner, B. J., Turnbull, S., El-Agnaf, O., and Allsop, D. (2001) Production of reactive oxygen species from aggregating proteins implicated in Alzheimer's disease, Parkinson's disease and other neurodegenrative diseases. *Curr. Top. Med. Chem. 1*, 507-517.

[4] Rubinsztein, D., and Carmichael, J. (2003) Huntington's disease: molecular basis of neurodegeneration. *Expert Rev. Mol. Med. 5*, 1-21.

[5] Dobson, C. M. (2001) The structural basis of protein folding and its links with human disease. *Philos. Trans. R. Soc. Lond. B. Biol. Sci. 356*, 133-145.

[6] Munch, J., Rucker, E., Standker, L., Adermann, K., Goffinet, C., Schindler, M., Wildum, S., Chinnadurai, R., Rajan, D., Specht, A., Gimenez-Gallego, G., Sanchez, P. C., Fowler, D. M., Koulov, A., Kelly, J. W., Mothes, W., Grivel, J. C., Margolis, L., Keppler, O. T., Forssmann, W. G., and Kirchhoff, F. (2007) Semen-derived amyloid fibrils drastically enhance HIV infection. *Cell 131*, 1059-1071.

[7] Centers for Disease Control and Prevention. National Diabetes Fact Sheet. United States. 2005. Available at http://www.cdc.gov/diabetes/pubs/pdf/ndfs_2005.pdf.

[8] Ludwig, G., Heitner, H. (1967) Zur Haufigkeit der Inselamyloidose des Pankreas beim Diabetes mellitus. *Zschr. Inn. Med. 22*, 814-818.

[9] Westermark, P., Wilander, E. (1978) The influence of amyloid deposits on the islet volume in maturity onset diabetes mellitus. *Diabetologia 15*, 417-421.

[10] Bell, E. T. (1959) Hyalinization of the islets of Langerhans in nondiabetic individuals. *Am. J. Pathol. 35*, 801-805.

[11] Opie E. (1901) The relation of diabetes mellitus to lesions of the pancreas: hyaline degeneration of the islands of Langerhans. *J. Exp. Med. 5*, 527-540.

[12] Westermark, P., Wernstedt, C., Wilander, E., Sletten, K. (1986) A novel peptide in the calcitonin gene-related family as an amyloid fibril protein in the endocrine pancreas. *Biochem Biophys Res Commun 140*, 827-831.

[13] Westermark, P., Wernstedt, C., O'Brien, T. D., Hayden, D. W., and Johnson, K. H. (1987) Islet Amyloid in Type 2 Human Diabetes Mellitus and Adult Diabetic Cats Contains a Novel Putative Polypeptide Hormone. *Am. J. Pathol. 127*, 414-417.

[14] Von Heijne, G. (1983) Patterns of amino acids near signal-sequence

cleavage sites. *Eur. J. Biochem. 133*, 17-21.

[15] Perlman, D., and Halvorson, H. O. (1983) A putative signal peptidase recognition site and sequence in eukaryotic and prokaryotic signal peptides. *J. Mol. Biol. 167*, 391-409.

[16] Yonemoto, I. T., Kroon, G. J., Dyson, H. J., Balch, W. E., and Kelly, J. W. (2008) Amylin Proprotein Processing Generates Progressively More Amyloidogenic Peptides that Initially Sample the Helical State. *Biochemistry 47,* 9900-9910.

[17] Sanke, T., Bell, G. I., Sample, C., Rubenstein, A. H., and Steiner, D. F. (1988) An islet amyloid peptide is derived from an 89-amino acid precursor by proteolytic processing. *J. Biol. Chem. 263*, 17243-17246.

[18] Badman, M. K., Shennan, K. I., Jermany, J. L., Docherty, K., and Clark, A. (1996) Processing of pro-islet amyloid polypeptide (proIAPP) by the prohormone convertase PC2. *FEBS Lett. 378*, 227-231.

[19] Higham, C. E., Hull, R. L., Lawrie, L., Shennan, K. I., Morris, J. F., Birch, N. P., Docherty, K., and Clark, A. (2000) Processing of synthetic pro-islet amyloid polypeptide (proIAPP) ‘amylin’ by recombinant prohormone convertase enzymes, PC2 and PC3, in vitro. *Eur. J. Biochem. 267*, 4998-5004.

[20] Marzban, L., Trigo-Gonzalez, G., Zhu, X., Rhodes, C. J., Halban, P. A., Steiner, D. F., and Verchere, C. B. (2004) Role of betacell prohormone convertase (PC)1/3 in processing of pro-islet amyloid polypeptide. *Diabetes 53*, 141-148.

[21] Docherty, K., and Hutton, J. C. (1983) Carboxypeptidase activity in the

insulin secretory granule. *FEBS Lett. 162*, 137-141.

[22] Marzban, L., Soukhatcheva, G., and Verchere, C. (2005) Role of carboxypeptidase E in processing of pro-islet amyloid polypeptide in beta-cells. *Endocrinology 146*, 1808-1817.

[23] Milgram, S., Kho, S., Martin, G., Mains, R., and Eipper, B. (1997) Localization of integral membrane peptidylglycine alpha-amidating monooxygenase in neuroendocrine cells. *J. Cell Sci. 110*, 695-706.

[24] Roberts, A. N., Leighton, B., Todd, J. A., Cockburn, D., Schofield, P. N., Sutton, R., Holt, S., Boyd, Y., Day, A. J., Foot, E. A., Willis, A. C., Reid, K. B. M., and Cooper, G. J. S. (1989) Molecular and functional characterization of amylin, a peptide associated with type 2 diabetes mellitus. *Proc. Natl. Acad. Sci. USA 86*, 9662-9666.

[25] Yonemoto, I. T., Gerard J. A. Kroon, G. J. A., Dyson, H. J., Balch, W. E., and Kelly, J. W. (2008) Amylin proprotein processing generates progressively more amyloidogenic peptides that initially sample the helical state. *Biochemistry 47*, 9900-9910.

[26] Kanatsuka, A., Makino, H., Ohsawa, H., Tokuyama, Y., Yamaguchi, T., Yoshida, S., and Adachi, M. (1989) Secretion of islet amyloid polypeptide in response to glucose. *FEBS 259*, 199-201.

[27] Khan, S. E., D'Alessio, D. A., Schwartz, M. W., Fujimoto, W. Y., Ensinck, J. W., Taborsky, G. J. J., and Porte, D. J. J. (1990) Evidence of cosecretion of islet amyloid polypeptide and insulin by beta-cells. *Diabetes 5*, 634-638.

[28] Bailey, C. J. (1999) New pharmacological approaches to glycemic control.

Diabetes Rev. 7, 94-113.

[29] Cooper, G. J. S. (1994) Amylin compared with calcitonin-gene-related peptides-Structure, biology, and relevance to metabolic disease. *Endocr. Rev. 15*, 163-201.

[30] Reda, T. K., Geliebter, A., and Pi-Sunyer, F. X. (2002) Amylin, food intake, and obesity. *Obes. Res. 10*, 1087-1091.

[31] Betsholtz, C., Svensson, V., Rorsman, F., Engstrom, U., Westermark, G. T., Wilander, E., Johnson, K., and Westermark, P. (1989) Islet amyloid polypeptide (IAPP): cDNA cloning and identification of an amyloidogenic region associated with the species-specific occurrence of age-related diabetes mellitus. *Exp. Cell Res. 183*, 484-493.

[32] Westermark, P., Engstrom, U., Johnson, K. H., Westermark, G. T., and Betsholtz, C. (1990) Islet amyloid polypeptide: Pinpointing amino acid residues linked to amyloid fibril formation. *Proc. Natl. Acad. Sci. USA 87*, 5036-5040.

[33] Moriarty, D. F., and Raleigh, D. P. (1999) Effects of sequential proline substitutions on amyloid formation by human amylin20-29. *Biochemistry 38*, 1811-1818.

[34] Tenidis, K., Waldner, M., Bernhagen, J., Fischle, W., Bergmann, M., Weber, M., Merkle, M-L., Voelter, W., Brunner, H., and Kapurniotu, A. (2000) Identification of a penta- and hexapeptide of islet amyloid polypeptide (IAPP) with amyloidogenic and cytotoxic Properties. *J. Mol. Biol. 295*, 1055-1071.

[35] Azriel, R., and Gazit, E. (2001) Analysis of the minimal amyloid-forming fragment of the islet amyloid polypeptide: An experimental support for the key

role of the phenylalanine residue in amyloid formation. *J. Biol. Chem. 276*, 34156-34161.

[36] Griffiths, J. M., Ashburn, T. T., Auger, M., Costa, P. R., Griffin, R. G., and Lansbury, P. T. Jr. (1995) Rotational resonance solid-state NMR elucidates a structural model of pancreatic amyloid. *J. Am. Chem. Soc. 117*, 3539-3546.

[37] Ashburn, T. T.; Auger, M.; Lansbury, P. T., Jr. (1992) The structural basis of pancreatic amyloid formation: isotope-edited spectroscopy in the solid state. *J. Am. Chem. Soc. 114*, 790-791.

[38] Jack, E., Newsome, M., Stockley, P. G., Radford, S. E., and Middleton, D. A. (2006) The organization of aromatic side groups in an amyloid fibril probed by solid-state ^{2}H and ^{19}F NMR spectroscopy. *J. Am. Chem. Soc. 128*, 8098-8099.

[39] Scrocchi, L. A., Chen, Y., Waschuk, S., Wang, F., Cheung, S., Darabie, A. A., McLaurin, J., and Fraser. P. E. (2002) Design of peptide-based inhibitors of human islet amyloid polypeptide fibrillogenesis. *J. Mol. Biol. 318*, 697-706.

[40] Kapurniotu, A., Schmauder, A., and Tenidis, K. (2002) Structure-based design and study of non-amyloidogenic, double N-methylated IAPP amyloid core sequences as inhibitors of IAPP amyloid formation and cytotoxicity. *J. Mol. Biol. 315*, 339-350.

[41] Tatarek-Nossol, M., Yan, L-M., Schmauder, A., Tenidis, K., Westermark, G., and Kapurniotu, A. (2005) Inhibition of hIAPP amyloid-fibril formation and apoptotic cell death by a designed hIAPP amyloid-core-containing hexapeptide. *Biol. Chem. 12*, 797-809.

[42] Yan, L-M., Tatrek-Nossol, M., Velkova, A., Kazantzis, A., and Kapurniotu, A.

(2006) Design of a mimic of nonamyloidogenic and bioactive human islet amyloid polypeptide (IAPP) as nanomolar affinity inhibitor of IAPP cytotoxic fibrillogenesis. *Proc. Natl. Acad. Sci. USA 103*, 2046-2051.

[43] Abedini, A., Meng, F., and Raleigh, D. P. (2007) A single-point mutation converts the highly amyloidogenic human islet amyloid polypeptide into a potent fibrillization inhibitor. *J. Am. Chem. Soc. 129*, 11300-11301.

[44] Nilsson, M. R., and Raleigh, D. P. (1999) Analysis of amylin cleavage products provides new insights into the amyloidogenic region of human amylin. *J. Mol. Biol. 294*, 1375-1385.

[45] Jaikaran, E. T. A. S., Higham, C. E., Serpell, L. C., Zurdo, J., Gross, M., Clark, A., and Fraser, P. E. (2001) Identification of a novel human islet amyloid polypeptide β-sheet domain and factors influencing fibrillogenesis. *J. Mol. Biol. 308*, 515-525.

[46] Mazor, Y., Gilead, S., Benhar, I., and Gazit, E. (2002) Identification and characterization of a novel molecular-recognition and self-assembly domain within the islet amyloid polypeptide. *J. Mol. Biol. 322*, 1013-1024.

[47] Scrocchi, L. A., Ha, K., Chen, Y., Wu, L., Wang, F., and Fraser, P. E. (2003) Identification of minimal peptide sequences in the (8-20) domain of human islet amyloid polypeptide involved in fibrillogenesis. *J. Struct. Biol. 141*, 218-227.

[48] Abedini, A., and Raleigh, D. P. (2006) Destabilization of Human IAPP Amyloid Fibrils by Proline Mutations Outside of the Putative Amyloidogenic Domain: Is There a Critical Amyloidogenic Domain in Human IAPP? *J. Mol. Biol. 355*, 274-281.

[49] Fox, A., Snollaerts, T., Casanova, C. E., Calciano, A., Nogaj, L. A., and Moffet, D. A. (2010) Selection for Nonamyloidogenic Mutants of Islet Amyloid Polypeptide (IAPP) Identifies an Extended Region for Amyloidogenicity. *Biochemistry 49*, 7783-7789.

[50] Janson, J., Ashley, R. H., Harrison, D., McIntyre, S., and Butler, P. C. (1999) The mechanism of islet amyloid polypeptide toxicity is membrane disruption by intermediate-sized toxic amyloid particles. *Diabetes 48*, 491-498.

[51] Anguiano, M., Nowak, R. J., and Lansbury, P. T. J. (2002) Protofibrillar islet amyloid polypeptide permeabilizes synthetic vesicles by a pore-like mechanism that may be relevant to type II diabetes. *Biochemistry 41*, 11338-11343.

[52] Balali-Mood, K., Ashley, R. H., Haub, T., and Bradshaw, J. P. (2005) Neutron diffraction reveals sequence-specific membrane insertion of prefibrillar islet amyloid polypeptide and inhibition by rifampicin. *FEBS Lett. 579*, 1143-1148.

[53] Sparr, E., Engel, M. F. M., Sakharov, D. V., Sprong, M., Jacobs, J., Kruijff, B. D., Hoppener, J. W. M., and Killian, J. A. (2004) Islet amyloid polypeptide-induced membrane leakage involves uptake of lipids by forming amyloid fibers. *FEBS Lett. 577*, 117-120.

[54] Konarkowska, B., Aitken, J. F., Kistler, J., Zhang, S., and Cooper, G. J. S. (2006) The aggregation potential of human amylin determines its cytotoxicity towards islet β-cells. *FEBS J. 273*, 3614-3624.

[55] Ritzel, R. A., Meier, J. J., Lin, C-Y., Veldhuis, J. D., and Butler, P. C. (2007) Human islet amyloid polypeptide oligomers disrupt cell coupling, induce apoptosis, and impair insulin secretion in isolated human islets. *Diabetes 56*, 65-

71.

[56] Gurlo, T., Ryazantsey, S., Huang, C-J., Yeh, M. W., Reber, H. A., Hines, O. J., O'Brien, T. D., Glabe, C. G., and Butler, P. C. (2010) Evidence for proteotoxicity in β cells in type II diabetes: Toxic islet amyloid polypeptide oligomers form intracellularly in the secretory pathway. *Am. J. Pathol. 176*, 861-869.

[57] Knight, J. D., and Miranker, A. D. (2004) Phospholipid catalysis of diabetic amyloid assembly. *J. Mol. Biol. 341*, 1175-1187.

[58] Engel, M. F. M., Yigittop, H., Elgersma, R. C., Rijkers, D. T. S., Liskamp, R. M. J., Kruijff, B. D., Hoppener, J. W. M., and Killian, A. (2006) Islet amyloid polypeptide inserts into phospholipid monolayers as monomer. *J. Mol. Biol. 356*, 783-789.

[59] Jayasinghe, S. A. and Langen, R. (2005) Lipid membranes modulate the structure of islet amyloid polypeptide. *Biochemistry 44*, 12113-12119.

[60] Knight, J. D., Hebda, J. A., and Miranker, A. D. (2006) Conserved and cooperative assembly of membrane-bound α-helical states of islet amyloid polypeptide. *Biochemistry 45*, 9496-9508.

[61] Lopes, D. H. J., Meister, A., Gohlke, A., Hauser, A., Blume, A., and Winter, R. (2007) Mechanism of islet amyloid polypeptide fibrillation at lipid interfaces studied by infrared reflection absorption spectroscopy. *Biophys. J. 93*, 3132-3141.

[62] Brender, J. R., Lee, E. L., Cavitt, M. A., Gafni, A., Steel, D. G., and Ramamoorthy, A. (2008) Amyloid fiber formation and membrane disruption are

separate processes localized in two distinct regions of IAPP, the type-2-diabetes-related peptide. *J. Am. Chem. Soc. 130*, 6424-6429.

[63] Asai, J., Nakazato, M., Kangawa, K., Matsukura, S., and Matsuo, H. (1989) Isolation and sequence determination of rat islet amyloid polypeptide. *Biochim. Biophys. Acta 164*, 400-405.

[64] Huang, C. J., Haataja, L., Gurlo, T., Butler, A. E., Wu, X., Soeller, W. C., and Butler, P. C. (2007) Induction of endoplasmic reticulum stress-induced beta-cell apoptosis and accumulation of polyubiquitinated proteins by human islet amyloid polypeptide. *Am. J. Physiol. Endocrinol Metab. 293*, E1656-E1662.

[65] Williamson, J. A., and Miranker, A. D. (2007) Direct detection of transient α-helical states in islet amyloid polypeptide. *Prot. Sci. 16*, 110-117.

[66] Joint United Nations Programme on HIV/AIDS (UNAIDS). Report on the Global HIV/AIDS Epidemic 2008. Available at http://www.unaids.org/en/dataanalysis/epidemiology/2008reportontheglobalaidsepidemic/

[67] Joint United Nations Programme on HIV/AIDS (UNAIDS). AIDS Epidemic Update. 2009. Available at http://www.unaids.org/en/media/unaids/contentassets/dataimport/pub/report/2009/jc1700_epi_update_2009_en.pdf

[68] Dimitrov, D. S., Willey, R. L., Sato, H., Chang, L. J., Blumenthal, R., and Martin, M. A. (1993) Quantitation of human immunodeficiency virus type 1 infection kinetics. *J. Virol. 67*, 2182-2190.

[69] Rusert, P., Fischer, M., Joos, B., Leemann, C., Kuster, H., Flepp, M., Bonhoeffer, S., Gunthard, H. F., and Trkola, A. (2004) Quantification of infectious HIV-1 plasma viral load using a boosted in vitro infection protocol. *Virology 326*, 113-129.

[70] Perelson, A. S., Neumann, A. U., Markowitz, M., Leonard, J. M., and Ho, D. D. (1996) HIV-1 dynamic in vivo: virion clearance rate, infected cell life-span, and viral generation time. *Science 271*, 1582-1586.

[71] Berg, H. C., and Purcell, E. M. (1977) Physics of chemoreception. *Biophys. J. 20*, 193-219.

[72] Eckert, D. M., and Kim, P. S. (2001) Mechanism of viral membrane fusion and its inhibition. *Annu. Rev. Biochem. 70*, 777-810.

[73] Munch, J., Rucker, E., Standker, L., Adermann, K., Goffinet, C., Schindler, M., Wildum, S., Chinnadurai, R., Rajan, D., Specht, A., Giménez-Gallego, G., Sánchez, P. C., Fowler, D. M., Koulov, A., Kelly, J. W., Mothes, W., Grivel, J. C., Margolis, L., Keppler, O. T., Forssmann, W. G., Kirchhoff, F. (2007) Semen-derived amyloid fibrils drastically enhance HIV infection. *Cell 131*, 1059-1071.

[74] Roan, N. R., Munch, J., Arhel, N., Mothes, W., Neidleman, J., Kobayashi, A., Smith-McCune, K., Kirchhoff, F., and Greene, W. C. (2009) The cationic properties of SEVI underlie its ability to enhance immunodeficiency virus infection. *J. Virol. 83*, 73-80.

[75] Hauber, I., Hohenberg, H., Holstermann, B., Hunstein, W., and Hauber, J. (2009) The main green tea polyphenol epigallocatechin-3-gallate counteracts semen-mediated enhancement of HIV infection. *Proc. Natl. Acad. Sci. U.S.A. 106*, 9033-9038.

[76] Braunschweiler, L., and Ernst, R. R. (1969) Coherence transfer by isotropic mixing: Application to proton correlation spectroscopy. *J. Magn. Reson. 53*, 521-528.

[77] Bax, A., and Davis, D. G. (1985) MLEV-17-based two-dimensional homonuclear magnetization transfer spectroscopy. *J. Magn. Reson. 65*, 355-360.

[78] Ramamoorthy, A., Chandrakumar, N. (1992) Comparision of the coherence-transfer efficiencies of laboratory- and rotating-frame experiments. *J. Magn. Reson. 100*, 60-68.

[79] Slichter, C. P. (1996) Principles of magnetic resonance (3rd edition). Berlin and New York: Springer.

[80] Overhauser, A. W. (1953) Polarization of nuclei in metals. *Phys. Rev. 92*, 411-415.

[81] Wuthrich, K. (1986) NMR of proteins and nucleic acids. New York: John Wiley & Sons.

CHAPTER 2. STRUCTURES OF RAT AND HUMAN ISLET AMYLOID POLYPEPTIDE $IAPP_{1-19}$ IN MICELLES BY NMR SPECTROSCOPY

This chapter is a version of a manuscript published in Biochemistry (2008) 47, 12689-12697.[1]

2.1 ABSTRACT

Disruption of the cellular membrane by the amyloidogenic peptide IAPP (or amylin) has been implicated in *β*-cell death during type II diabetes. While the structure of the mostly inert fibrillar form of IAPP has been investigated, the structural details of the highly toxic prefibrillar membrane-bound states of IAPP have been elusive. A recent study showed that a fragment of IAPP (residues 1-19) induces membrane disruption to a similar extent as the full-length peptide. However, unlike the full-length IAPP peptide, $IAPP_{1-19}$ is conformationally stable in an α-helical conformation when bound to the membrane. *In vivo* and *in vitro* measurements of membrane disruption indicate the rat version of $IAPP_{1-19}$, despite differing from $hIAPP_{1-19}$ by the single substitution of Arg18 for His18, is significantly less toxic than $hIAPP_{1-19}$, in agreement with the low toxicity of the full-length rat IAPP peptide. To investigate the origin of this difference at the atomic level, we have solved the structures of the human and rat $IAPP_{1-19}$ peptides in DPC micelles. While both rat and human $IAPP_{1-19}$ fold into similar mostly α-helical structures in micelles, paramagnetic quenching NMR

[1] Jiadi Xu helped with NMR experiments and data processing. Jeffrey Brender helped in writing the manuscript. This study was supported by the funds from NIH (DK 078885 to A.R.).

experiments indicate a significant difference in the membrane orientation of $hIAPP_{1-19}$ and $rIAPP_{1-19}$. At pH 7.3, the more toxic $hIAPP_{1-19}$ peptide is buried deeper within the micelle, while the less toxic $rIAPP_{1-19}$ peptide is located at the surface of the micelle. Protonating H18 in $hIAPP_{1-19}$ reorients the peptide to the surface of the micelle. This change in orientation is in agreement with the significantly reduced ability of $hIAPP_{1-19}$ to cause membrane disruption at pH 6.0. This difference in peptide topology in the membrane may correspond to similar topology differences for the full-length human and rat IAPP peptides, with the toxic human IAPP peptide adopting a transmembrane orientation and the nontoxic rat IAPP peptide bound to the surface of the membrane.

2.2 INTRODUCTION

Islet amyloid polypeptide (IAPP, also known as amylin) is one of an increasing number of proteins in which the propensity to form a misfolded state is correlated with pathologies in tissue functioning. Physiologically, IAPP is one of a family of peptides related to calcitonin that act in the control of metabolic functions. Specifically, IAPP acts in concert with insulin to control plasma glucose levels and acts independently of insulin to slow gastric emptying and therefore food intake [*1-3*]. For reasons that are currently poorly understood, IAPP aggregates in the pancreatic *β*-cells of type II diabetics to form highly ordered and extremely stable long protein fibers (amyloid deposits). Similarly, other tissue-specific amyloid deposits have also been identified in a growing list as possible pathological features in other common and devastating diseases such as Parkinson's, Alzheimer's, Creutzfeld-Jacob's, and Huntington's diseases. All

of these proteins, despite the differences in amino acid sequences and in the structures of the monomeric protein, adopt a common cross-*β*-sheet structure consisting of parallel association of *β*-strands to form protofibril units and lateral association of protofibril units to form amyloid fibers [*4*]. Amyloid deposition is generally correlated with the severity of the disease, increasing over time as the disease progresses and *β*-cell function decreases [*5*].

Amyloidogenic proteins commonly exhibit a strong interaction with negatively charged membranes, forming oligomeric structures within the membrane that act as largely nonselective ion channels [*6-9*]. Atomic force microscopy images show pentameric structures with a small central cavity suggestive of a well-defined ion channel when IAPP is bound to supported lipid bilayers [*6*]. The formation of these ion channels has been proposed to disrupt calcium homeostasis and lead to mitochondrial oxidative stress [*7*]. However, other studies have shown direct disruption of the membrane by the uptake of lipid molecules during fibrillogenesis into protofibril units [*10, 11*]. In order to better understand the membrane interaction and function of IAPP, it is important to determine the high-resolution structure of IAPP in a membrane environment. However, the rapid aggregation of IAPP to form amyloid fibers has been a great challenge to overcome in solving the atomistic-level resolution structures of these peptides using NMR spectroscopy. In addition, the oligomeric species of IAPP that form during the aggregation process can interact with the membrane in different ways, further complicating structural studies of IAPP. To overcome the difficulties associated with IAPP, we have recently shown that the N-terminal 1-

19 fragment of IAPP (the amino acid sequence is given in Figure 2-1) is a useful model system for the study of the IAPP-induced membrane disruption [*12*]. The full-length IAPP peptide can be divided into three regions: an N-terminal region from residues 1 to 19 that largely determines the membrane binding [*13, 14*], a primary amyloidogenic region from residues 20 to 29, and a C-terminal region from residues 30 to 37 that enhances amyloid formation [*13, 15, 16*]. Peptide array binding studies have shown that the N-terminal region of IAPP is also strongly involved in the self-association of the peptide. Using an array of decamer peptides made from hIAPP, Mazor et al. measured the binding of full-length IAPP to truncated versions of the peptide immobilized on a cellulose membrane matrix [*17*]. The strongest peptide-peptide interactions in this study were found to extend from C7 to N21, which substantially overlaps with the 1-19 region. It is noteworthy that the binding of full-length hIAPP to truncated peptides containing the main amyloidogenic region (residues 20-29) was significantly less. The preferential affinity of full-length IAPP for truncated peptides made from the N-terminal region over those made from the amyloidogenic region suggests self-association in full-length IAPP may be initiated first by interactions in the 1-19 region before any interactions within the 20-29 region can occur. This is significant because IAPP-induced toxicity and membrane damage can occur prior to amyloid formation as reported in the literature [*7, 18*]. The 1-19 fragment of IAPP may therefore serve as an excellent structural model to investigate the early aggregation and membrane disrupting activity of IAPP that is observed before the formation of amyloid fibers.

In an effort to determine the amino acid residues responsible for the toxicity of IAPP, we recently found that the N-terminal 1-19 region of human IAPP both disrupts POPG vesicles similarly to full-length human IAPP and also disrupts β-cell homeostasis like full-length human IAPP [*12, 19*]. Significantly, $hIAPP_{1-19}$ exhibits greatly reduced amyloidogenicity, forming fibers only at very high concentrations in solution [*20*]. While binding to membranes accelerates amyloid formation for full-length hIAPP, human $IAPP_{1-19}$ is conformationally stable when bound to POPG membranes, maintaining the same α-helical conformation for at least 13 days [*12*]. A similar effect has been noted for a longer fragment of the hIAPP ($hIAPP_{1-24}$) that also contains part of the amyloidogenic region [*21*].

A comparison of amino acid sequences of IAPP of different species yields some interesting information in this context. Full-length rat IAPP is both nontoxic and nonamyloidogenic, and more significantly, rats do not develop type II diabetes. However, the human and rat versions differ in only one amino acid residue within the 1-19 sequence (Figure 2-1) with the majority of the differences between human and rat IAPP being in the amyloidogenic 20-29 region.

Figure 2-1. Amino acid sequences of rat and human IAPP. The 1-19 region is shown in blue, and differences between the sequences are shown in red. A disulfide bond connects residues 2 and 7. The C-termini of the peptides used in this study are amidated like the naturally-occuring peptides.

Despite the fact that it differs from human $IAPP_{1-19}$ by only a single residue, rat $IAPP_{1-19}$ is significantly less toxic than $hIAPP_{1-19}$ [*19*]. Since the 1-19

fragments of human and rat IAPP are quite stable in a membrane environment [*12*], it would be useful to determine the high-resolution structures and folding of these peptides using NMR spectroscopy. In this study, we have solved the high-resolution structures of both human and rat $IAPP_{1-19}$ peptides using solution NMR experiments on well-behaved dodecylphosphocholine (DPC) detergent micelles. In most respects, DPC micelles are a better model to mimic the phospholipid membrane than organic solvents, such as trifluoroethanol and hexafluoro-2-proponal, which have been used in some previous studies of amyloid peptides [*22*]. Organic solvents lack the hydrophobic/hydrophilic interface that is present in lipid membranes. Furthermore, the difference in solvation structure and hydrogen bonding between organic solvents and lipid membranes tends to bias the structure toward non-native helical structures [*23-25*]. The headgroup of DPC is identical to phosphatidylcholine, the most common lipid in animal cell membranes, and is expected to be less denaturing than sodium dodecyl sulfate (SDS) due to the zwitterionic nature of the detergent. Previous studies have shown that DPC preserves the native conformations of membrane associated peptides and enzyme activity of membrane proteins in some cases [*25-30*].

2.3 MATERIALS AND METHODS

2.3.1 ***NMR Sample Preparation.*** Rat and human $IAPP_{1-19}$ were synthesized and purified by Genscript. The formation of an intramolecular disulfide bond was determined by electrospray mass spectroscopy. The absence of intermolecular disulfide bonds was confirmed by nonreducing SDS-PAGE electrophoresis, which showed a single band corresponding to the monomeric peptide. Both

peptides were first dissolved in hexafluoro-2-propanol at a concentration of 10 mg/mL and then lyophilized overnight at 1 mTorr vacuum to completely remove the solvent. The NMR sample was prepared by dissolving the lyophilized peptide to a final concentration of 1.625 mM in 20 mM phosphate buffer at pH ~7.3 containing 10% D_2O, 200 mM perdeuterated DPC, and 120 mM NaCl.

2.3.2 ***NMR Experiments.*** All NMR experiments except the paramagnetic quenching experiments were performed at 30°C on a Bruker Avance 900 MHz spectrometer equipped with a cryoprobe. Complete assignments of the side chain and backbone resonances were obtained using 2D ^{1}H-^{1}H TOCSY (with a 70 ms mixing time) and 2D ^{1}H-^{1}H NOESY (with 100 and 300 ms mixing times) experiments with 2056 complex points in the direct dimension and 512 points in the indirect dimension [*31, 32*]. Proton chemical shifts were referenced to the water proton signal at the carrier frequency. All 2D spectra were processed using Bruker TopSpin software and analyzed using SPARKY [*33, 34*]. Resonance assignment was carried out using a standard approach reported elsewhere [*35*].

2.3.3 ***Structure Calculations.*** The $rIAPP_{1-19}$ and $hIAPP_{1-19}$ structural ensembles were calculated starting from an extended structure using the simulated annealing protocol available in the NIH-XPLOR software package to generate 100 conformers. An initial temperature of 3000 K was used with 18000 high temperature steps, 9000 cooling steps, and a step size of 2 fs [*36, 37*]. A total of 180 and 208 NOEs from $rIAPP_{1-19}$ and $hIAPP_{1-19}$, respectively, were classified as strong (1.8-2.9 Å), medium (1.8-4.5 Å), or weak (1.8-6.0 Å) and utilized as structural constraints. Dihedral angle restraints were obtained from the empirical

correlation between α proton chemical shifts and dihedral angles using the TALOS module in NMRPIPE [*38*]. Final refinement of the structure ensemble was calculated using simulated annealing at an initial temperature of 500 K with 20000 cooling steps and a step size of 3 fs.

The analysis was carried out using the “accept.inp” routine included in the NIH-XPLOR software package with the requirements that NOE violations should not exceed 0.5 Å, dihedral angle restraint violations should not exceed 5°, the RMS difference for bond deviations should not exceed 0.01 Å from ideality, and the RMS difference for angle deviations should not exceed 2° from ideality. The 20 lowest energy conformers for each of the rat and human $IAPP_{1-19}$ peptides were selected for further analysis. The analysis of Ramachandran angles for the 20 lowest energy structures was carried out using PROCHECK-NMR (*39*). Peptide structures were analyzed using the program MOLMOL (*40*).

2.3.4 ***Paramagnetic Quenching***. One-dimensional ^{1}H chemical shift spectra of $IAPP_{1-19}$ in DPC micelles at a concentration of 0.4, 0.8, and 1.2 mM $MnCl_2$ at pH 7.3 and pH 6.0 were obtained. 2D ^{1}H-^{1}H NOESY spectra of $hIAPP_{1-19}$ in DPC micelles at pH 6.0 with and without 1.2 mM $MnCl_2$ were also obtained on Bruker Avance 600 MHz spectrometer. All other experimental conditions were the same as described above.

2.4 RESULTS

2.4.1 ***Assignments, Constraints and NMR Structures.*** A combination of 2D ^{1}H-^{1}H TOCSY and ^{1}H-^{1}H NOESY spectra obtained at different mixing times was used for the assignment of backbone and side chain resonances. The sequential

assignments were accomplished using the amide proton to α proton region of the 2D ^{1}H-^{1}H NOESY spectra obtained at a 300 ms mixing time. The α-proton chemical shift index plots for both peptides are given in Figure 2-2. Due to chemical exchange, the chemical shift values for the α protons of K1-T4 and T6

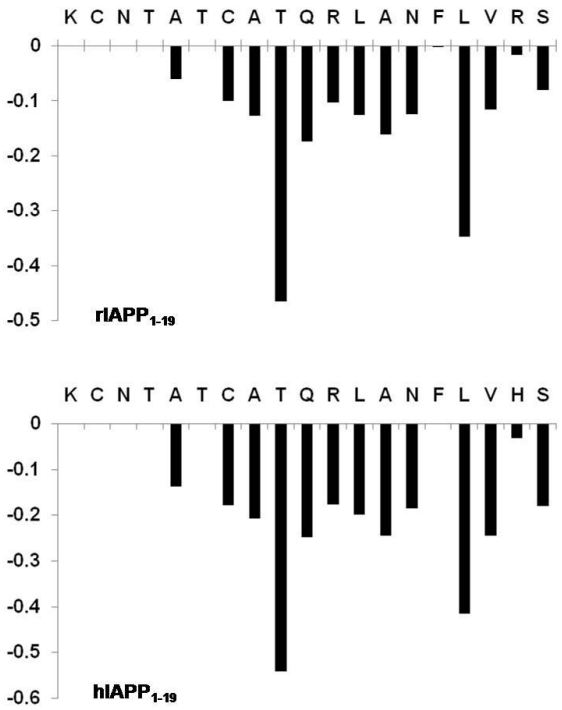

Figure 2-2. α-Proton chemical shift index of micelle bound rat (top) and human (bottom) $IAPP_{1-19}$ measured from solution NMR experiments.

of both peptides could not be observed. The fingerprint regions of NOESY spectra obtained at a 300 ms mixing time are shown in Figure 2-3. From the analysis of the 2D NOESY spectra, we have identified and assigned a total of 180 (73 intraresidue and 107 interresidue) NOEs for $rIAPP_{1-19}$ and 208 (79 intraresidue and 129 interresidue) NOEs for $hIAPP_{1-19}$. Figure 2-4 shows a summary of backbone NOEs for the secondary structure assignment with a histogram indicating the number of NOEs per residue.

The NMR spectra of $rIAPP_{1-19}$ and $hIAPP_{1-19}$ embedded in detergent

micelles are sufficiently resolved to assign most of the resonances but not to measure the *J* coupling constants. All assigned NOEs were then converted into distances and modeled using the classical simulated annealing protocol built in XPLOR-NIH [*6*]. Out of the 100 refined structures, 41 of the rat $IAPP_{1-19}$ and 60 of

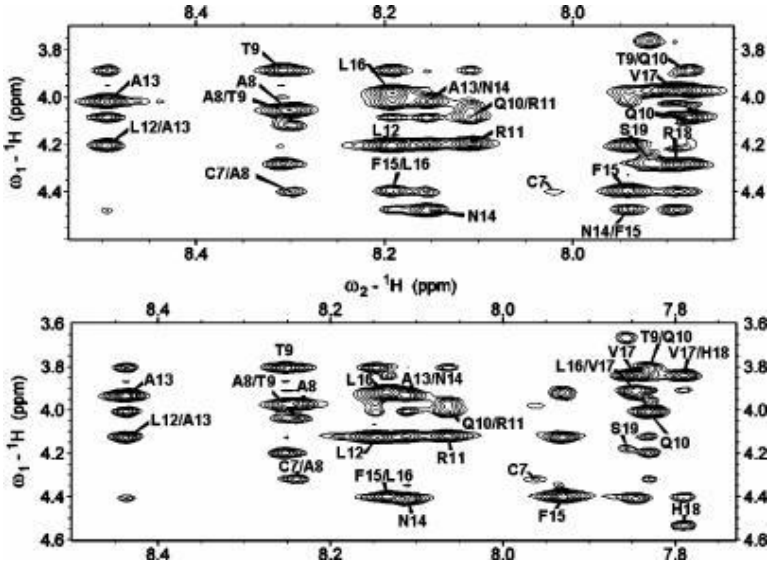

Figure 2-3. Fingerprint regions of 2D ^{1}H-^{1}H NOESY spectra of rat (top) and human (bottom) $IAPP_{1-19}$ embedded in DPC micelles at pH 7.3 showing sequential α proton NOE connectivities.

the human $IAPP_{1-19}$ did not have NOE violations >0.5 Å, dihedral angle restraint violations >5°, RMS difference for bond deviations from ideality >0.01 Å, and RMS difference for angle deviations from ideality >2°. Of the structures that passed the acceptance criteria, 20 structures were further selected for the final analysis. The superposition of backbone atoms from residues 1 to 19 gives an RMSD of 0.58 ± 0.12 and 0.57 ± 0.13 Å for $rIAPP_{1-19}$ and $hIAPP_{1-19}$ respectively, while the superposition of all heavy atoms gives an RMSD of 1.69 ± 0.28 and 1.51 ± 0.27 Å. The overlays of the backbone and side chain heavy atoms for the final selected conformers are shown in Figure 2-5. Analysis of the Ramachandran plot for the final conformers shows that 93.8% and 81.8% of the

residues fall in the most favored region while the rest of the residues fall in the additionally allowed regions for $rIAPP_{1-19}$ and $hIAPP_{1-19}$, respectively (more details are given in Table 2-1).The secondary structure representations of $rIAPP_{1-19}$ and $hIAPP_{1-19}$ are shown in Figure 2-6.

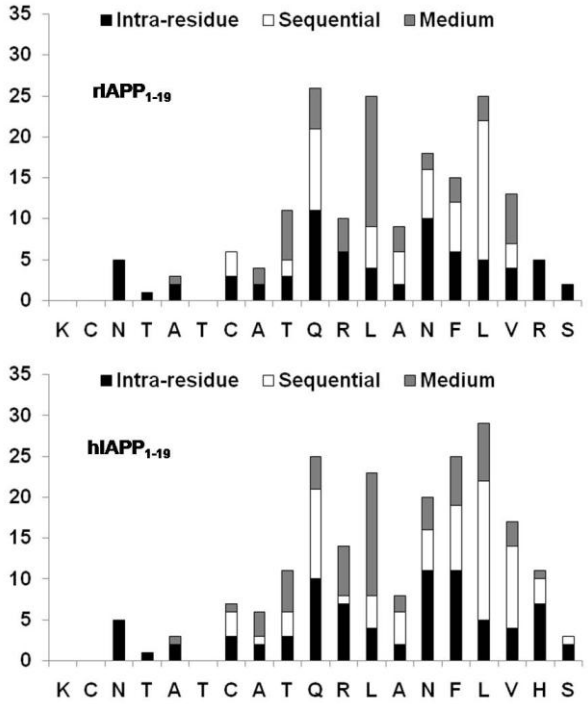

Figure 2-4. Histogram of NOEs versus residues for rat (top) and human (bottom) $IAPP_{1-19}$.

2.4.2 ***Paramagnetic Quenching Studies.*** Since $rIAPP_{1-19}$ and $hIAPP_{1-19}$ differ significantly in their functions but have similar structures, it is important to determine the orientation of both peptides with respect to the membrane. As a first approximation of the membrane orientation, we have obtained the 1D ^{1}H chemical shift spectra of both peptides in DPC micelles with varying concentrations of the paramagnetic quencher $MnCl_2$. It is known that manganese ions affect the relaxation rate of nuclei that are in close proximity and therefore decrease the observed signal intensity. Because manganese ions cannot

penetrate into the interior of the micelle, the observed changes in the signal intensities reflect the exposure of the amino acid residues of the peptide to solvent. The 1D ^{1}H chemical shift spectra of DPC micelles containing $hIAPP_{1-19}$

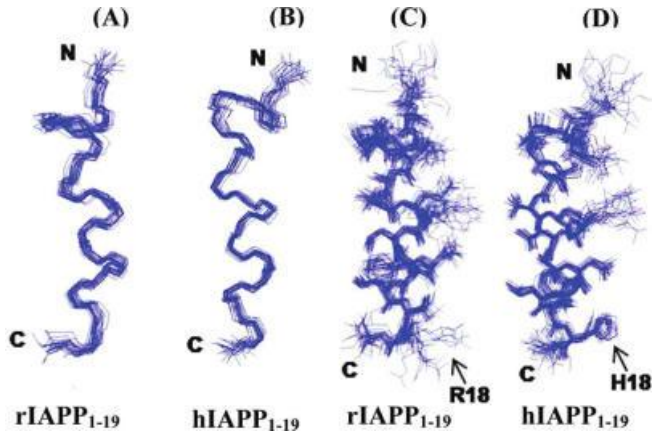

Figure 2-5. An ensemble of conformers for rat (A and C) and human (B and D) $IAPP_{1-19}$ showing the convergence of the conformers for backbone atoms (A and B) and side chain atoms (C and D).

and $rIAPP_{1-19}$ at pH 7.3 are given in Figure 2-7. The considerable decrease in the signal intensities and broadening of spectral lines observed for micelles containing $rIAPP_{1-19}$ even at the relatively low concentration of 0.4 mM $MnCl_2$ suggest that the peptide is well-exposed to the water phase and not in the hydrophobic core of the micelle.

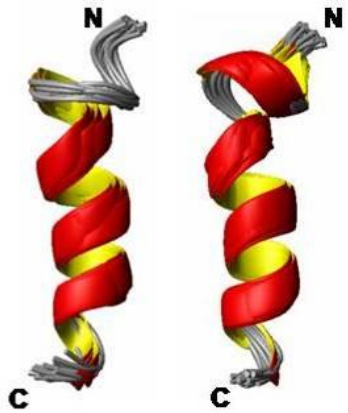

Figure 2-6. Secondary structure representations of an overlaid ensemble of conformers for rat (left) and human (right) $IAPP_{1-19}$.

On the other hand, a significant reduction in signal intensities and an increase in line broadening is observed only at a high concentration of $MnCl_2$ (1.2 mM) for micelles containing $hIAPP_{1-19}$ at pH 7.3, which suggests that the peptide is inserted into the hydrophobic core of the micelle.

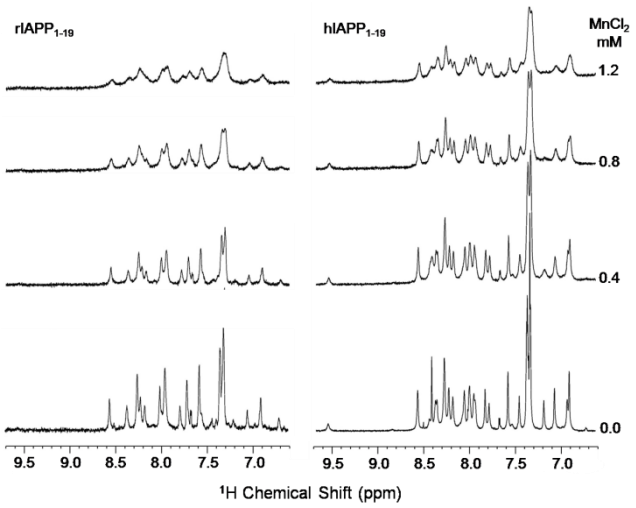

Figure 2-7. The amide-proton chemical shift region of ^1H NMR spectra of rat (left) and human (right) $IAPP_{1-19}$ in DPC micelles at pH 7.3 with and without $MnCl_2$.

Overall, these results suggest that $hIAPP_{1-19}$ is inserted into the micelle at pH 7.3 while $rIAPP_{1-19}$ binds closer to the surface. The only difference between $hIAPP_{1-19}$ and $rIAPP_{1-19}$ is the H18R mutation. Histidine is likely to be neutral at pH 7.3; therefore, if the origin of this effect is the difference in charge at residue 18, $hIAPP_{1-19}$ should adopt a surface-associated binding mode at a lower pH where H18 is protonated. Accordingly, we have measured both the 1D ^1H chemical shift (Figure 2-8) and 2D ^1H-^1H NOESY (Figure 2-9) spectra of $hIAPP_{1-19}$ in DPC micelles at pH 6.0 in the presence of $MnCl_2$. In contrast to the modest decrease in signal observed at pH 7.3 when $MnCl_2$ is added (Figure 2-7), there is a significant decrease in signal intensity at pH 6.0 with the addition of $MnCl_2$ (Figures 2-8 and 2-9). The strong effect of $MnCl_2$ on the proton spectrum of

$hIAPP_{1-19}$ in DPC micelles at pH 6.0, but not at pH 7.3, indicates $hIAPP_{1-19}$ is significantly closer to the surface of the micelle when H18 is protonated.

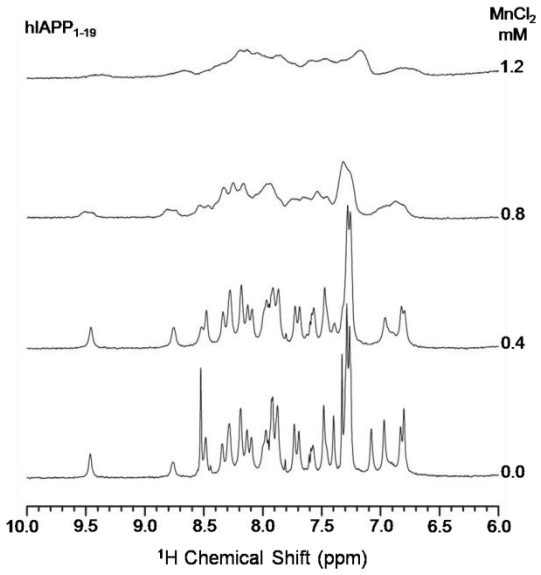

Figure 2-8. The amide-proton chemical shift region of ^1H NMR spectra of $hIAPP_{1-19}$ in DPC micelles at pH 6.0 with and without $MnCl_2$. A comparison of these ^1H spectra with those given in Figure 2-7 for $hIAPP_{1-19}$ in DPC micelles at pH 7.3 suggests that the peptide is relatively more exposed to the water phase at pH 6.0 and therefore peaks are considerably broadened even at 0.8 mM $MnCl_2$.

2.5 DISCUSSION

Since the toxicity of amyloid peptides to cells is correlated with the role of amyloid peptides in aging-related diseases [*9, 41, 42*], there is considerable current interest in solving high-resolution structures of amyloid peptides in a membrane environment. Several studies have reported global changes in the secondary structures of amyloid peptides upon binding to membrane and their significance in the conversion of nontoxic to toxic amyloids [*18, 43-45*]. While the importance of IAPP/lipid interactions is well documented, the only available high-resolution structure of membrane IAPP is for the 20-29 fragment in sodium dodecyl sulfate (SDS) micelles [*46*]. However, the toxicity of the 20-29 fragment

is significantly lower than that of the full-length IAPP peptide [*47*]. In this study, we report the first atomic-level resolution structures of a membrane-bound IAPP peptide that exhibits significant toxicity [*12, 19*]. A previous NMR study has reported the low-resolution structure of nontoxic rat IAPP in water [*48*]. While this study was in progress, a recent study reported the structure of IAPP using distance constraints measured from EPR experiments on liposomes containing selectively spin-labeled IAPP peptides [*21*].

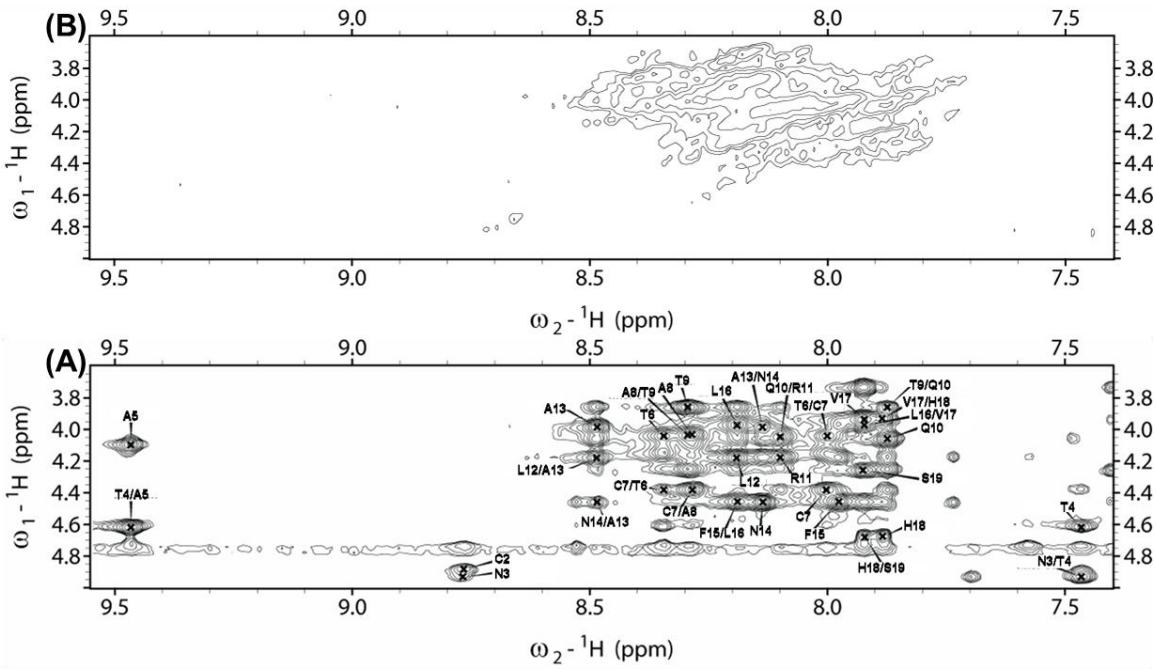

Figure 2-9. Fingerprint region of 2D ^{1}H-^{1}H NOESY spectra of hIAPP$_{1-19}$ in DPC micelles at pH 6.0 in the absence (A) and presence (B) of 1.2 mM $MnCl_2$.

The structures of hIAPP$_{1-19}$ and rIAPP$_{1-19}$ in DPC micelles are similar, consisting of a single helix extending from C7 to V17 and a distorted helical turn from C7 to the N-terminus (Figure 2-10). The N-terminal region is prevented from adopting a canonical α-helix conformation by the disulfide bridge from C2 to C7. Residues 2-5 are likely to be dynamic and poorly structured in both peptides, as

shown by the lack of NOE restraints in this region (Figure 2-4). This region may be more structured in $hIAPP_{1-19}$, as HA-NH connectivity was seen from C7 to Q10 and A8 to Q10 for $hIAPP_{1-19}$ but not in $rIAPP_{1-19}$. As these residues border the disulfide bridge from residues 2 to 7, a change in the dynamics at one end of the disulfide bridge is likely to be transmitted throughout the ring from residues 2 to 7.

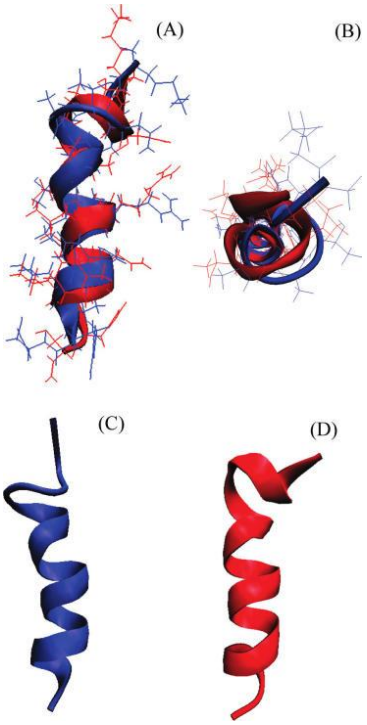

Figure 2-10. (A) Overlay of the average structures of $rIAPP_{1-19}$ (blue) and $hIAPP_{1-19}$ (red). The average of the 20 structures of each peptide was aligned using the STAMP algorithm present in the Multiseq utility in VMD [*54, 55*]. (B) Top view of $rIAPP_{1-19}$ and $hIAPP_{1-19}$ from the N-terminus. (C) View of $rIAPP_{1-19}$ showing the curve in the helical region. (D) View of $hIAPP_{1-19}$ showing the absence of a curve in the helical region.

This finding is supported by recent NMR data on full length rat and human IAPP in solution [*48, 49*]. While both rat and human IAPP are predominantly unstructured in solution, both peptides transiently sample α-helical states in solution [*48, 49*]. In agreement with the additional restraints found here for

$hIAPP_{1-19}$, full-length hIAPP in solution has a greater α-helical propensity at the N-terminus than rIAPP [*49*]. Yonemoto et al. reported the presence of strong (*i*, *i* +1) amide-amide NOEs and negative Hα chemical shift deviations across the entire sequence of hIAPP, indicating all residues of hIAPP sample α-helical dihedral angles [*49*]. Analysis of temperature coefficients and chemical shift deviations show that the corresponding stretch of rat IAPP with a propensity to form α-helical states is shorter, stretching only from A5 to S19 [*48*]. Notably, the chemical shift deviations in the α-helical forming region are larger for full length hIAPP than rIAPP in solution [*48, 49*].

Table 2-1. Statistical information for the structural ensembles of $rIAPP_{1-19}$ and $hIAPP_{1-19}$.

		$rIAPP_{1-19}$	**$hIAPP_{1-19}$**
Distance constraints			
	Total	180	208
	Intra-residual	73	79
	Inter-residual	107	129
	Sequential (i - j = 1)	56	71
	Medium (i – j = 2, 3, 4)	51	58
Structural statistics			
	NOE violations (Å)	0.059 ± 0.0007	0.056 ± 0.0014
	Dihedral angle restraint violations (º)	1.034 ± 0.104	1.589 ± 0.138
	RMSD for bond deviations (Å)	0.005 ± 0.0001	0.005 ± 0.0002
	RMSD for angle deviations (º)	0.755 ± 0.009	0.643 ± 0.021
	RMSD of all backbone atoms (Å)	0.58 ± 0.12	0.57 ± 0.13
	RMSD of all heavy atoms (Å)	1.69 ± 0.28	1.51 ± 0.27
Ramachandran plot			
	Residues in most favored region (%)	93.8	81.8
	Residues in additionally allowed region (%)	6.2	18.2

Although high-resolution structures of membrane-bound full-length IAPP are not available, both lower resolution studies on full-length IAPP in liposomes and in solution suggest the conformation determined here may represent the structured part of the full-length protein. The majority of the remaining residues on the C-terminal end of the full length protein are likely to be unstructured both in solution and when bound to the membrane. A recent EPR study using spin-

labeled full-length hIAPP has indicated that residues 9-22 form a helix when bound to anionic liposomes, while the surrounding N-terminal and C-terminal regions are less ordered without a defined secondary structure [*21*]. In accordance with these data, circular dichroism has shown that approximately 40% of full-length human IAPP and 35% of full-length rIAPP are in a helical conformation when bound to the membrane [*18, 43*]. The NMR studies mentioned above on full-length IAPP in solution also support the model of a C-terminal region with weaker helix propensity than the N-terminal region [*48, 49*].

While the structures of $rIAPP_{1-19}$ and $hIAPP_{1-19}$ are quite similar, the H18R substitution has a strong effect on the orientation of the peptide with respect to the membrane. The difference in the location of $hIAPP_{1-19}$ and $rIAPP_{1-19}$ in the membrane can be seen in Figure 2-7. The signal for $rIAPP_{1-19}$ is diminished substantially upon the addition of the paramagnetic quencher $MnCl_2$ even at low concentrations, while the signal for $hIAPP_{1-19}$ is hardly affected. Since the Mn^{2+} ion cannot penetrate into the hydrophobic core of the micelle, the absence of quenching by Mn^{2+} for $hIAPP_{1-19}$ indicates $rIAPP_{1-19}$ is located closer to the surface of the membrane than hIAPP1-19 [*50*]. The structural basis for this difference is most likely due to the anchoring of R18 in $rIAPP_{1-19}$ to the phosphate group of the DPC molecule by a charge-charge interaction. The anchoring of $rIAPP_{1-19}$ to the surface of the membrane at two points by the charges on K1 and R18 would likely fix the position of the peptide within the micelle [*51*]. The effect of anchoring of $rIAPP_{1-19}$ to the surface of the micelle can be seen in the structure of $rIAPP_{1-19}$. The helix in the $rIAPP_{1-19}$ structure has a noticeable curve with the

hydrophobic residues of the amphipathic helix on the concave side and the polar and charged residues on the opposite side that is absent in the corresponding helix of the $hIAPP_{1-19}$ structure (Figure 2-10C). Distorted helices usually occur when the peptide binds near the surface of the micelle, with the structure adopting some of the curvature of the micelle surface. Because $hIAPP_{1-19}$ at pH 7.3 lacks the C-terminal charge of R18 in $rIAPP_{1-19}$, it possesses a greater degree of orientational flexibility. Without the requirement that residue 18 must be anchored to the surface, $hIAPP_{1-19}$ can adopt an orientation that buries it deeper within the micelle. The importance of charge in determining the binding topology of $hIAPP_{1-19}$ can be clearly seen by comparing the effect of $MnCl_2$ on the proton spectrum of $hIAPP_{1-19}$ at pH 7.3 and at pH 6.0. In contrast to the modest quenching observed at pH 7.3 (Figure 2-7), $MnCl_2$ strongly quenches the signal at pH 6.0 (Figures 2-8 and 2-9). This is a strong indication that $hIAPP_{1-19}$ adopts a surface-associated binding mode similar to $rIAPP_{1-19}$ when H18 is protonated.

Interestingly, neutron diffraction experiments have suggested a similar difference in topologies for the full-length rat and human IAPP peptides [*52*]. A surface-associated peptide is expected to strongly disorder the packing of the bilayer by creating a void beneath the peptide that must be filled by the acyl chains of nearby phospholipids; such effects have been reported for membrane-disrupting antimicrobial peptides based on solid-state NMR studies in lipid bilayers [*56, 57*]. A transmembrane peptide, on the other hand, does not create a void volume in the membrane and can be expected to have little effect on the packing of the bilayer if it does not alter the thickness of the membrane. The

density profile of the bilayer measured by neutron diffraction in the presence of full-length hIAPP is remarkably similar to that of the bilayer in the absence of the peptide [*52*]. The density profile of bilayers containing full-length rIAPP, on the other hand, showed a significant reduction in density in the hydrophobic core of the bilayer, consistent with the splaying of acyl chains to occupy the void volume created with a surface-associated peptide [*52*]. Critically, water was detected in the interior of the bilayer in this experiment when human but not rat IAPP was added, indicating that a transmembrane orientation is related to the membrane disruption induced by human IAPP but not rat IAPP [*52*]. The importance of peptide binding topology for membrane disruption is in agreement with our results reported in the companion paper, which show that the membrane disruption by $hIAPP_{1-19}$ is reduced at pH 6.0 and is approximately equal to that of $rIAPP_{1-19}$ at pH 6.0 [*19*].

An alternative topology for full-length hIAPP has been proposed by Apostolidou et al. in studies using spin-labeled IAPP bound to anionic liposomes in the presence of quenchers with different lipid penetration profiles [*21*]. They found that full-length human IAPP was oriented parallel to the membrane surface in these conditions with the center of the helix located 6-9 Å below the phosphate group. In this EPR study, a very low (1:1000) peptide-to-lipid ratio was used, and it is therefore likely the peptide was in the monomeric state. It can clearly be seen from Figure 2-5 that a monomeric IAPP peptide in a transmembrane orientation would have unfavorable electrostatic interactions due to the presence of the charged R11 residue in the hydrophobic core of the membrane. The small size of

the spherical micelle used in this study allows the charged side chain of R11 to easily extend outside/near the surface of the micelle regardless of the overall orientation of the peptide. In larger liposomes, a correct orientation of the peptide is necessary to stabilize this charge. In the surface-associated orientation, the charge on a monomeric peptide can be stabilized by interactions with either the headgroups or phosphates of the interfacial region [*21*]. In order to avoid this unfavorable interaction in a transmembrane orientation, oligomerization of the peptide is necessary. The binding of hIAPP to the membrane and the membrane disruption induced by hIAPP are both strongly cooperative, and saturation of IAPP binding occurs at a higher density than is possible with a surface associated orientation [*18*]. This suggests a model in which IAPP first binds to the membrane in a monomeric form, recruits other IAPP monomers to the surface, and then inserts into the membrane as an oligomer with a water-filled channel that stabilizes the unfavorable charge [*18*]. It should be noted that a transmembrane orientation would imply a hydrophobic mismatch for both $hIAPP_{1-19}$ and full-length hIAPP if the remaining residues in full-length hIAPP are unfolded as suggested by EPR, CD, and NMR studies on homologous peptides [*18, 21, 43, 53*].

2.6 CONCLUSION

In conclusion, we have solved the high-resolution structures and found the membrane orientations of human and rat $IAPP_{1-19}$ using NMR experiments on dodecylphosphocholine micelles in an effort to understand the functional differences between these two peptides. The 1-19 fragment was chosen because

evidence suggests this region is responsible for most of the membrane damage induced by hIAPP [*12-14, 19*]. The structure determined here may hold insights into both the normal physiological action of IAPP and the damage to *β*-cell membranes caused by the pathological aggregation of IAPP. Future studies are needed to determine the structure of the oligomeric forms of IAPP at high resolution and to understand the role of membrane composition in the structural folding of oligomeric IAPP.

REFERENCES

[1] Bailey, C. J. (1999) New pharmacological approaches to glycemic control. *Diabetes Rev. 7*, 94-113.

[2] Cooper, G. J. S. (1994) Amylin compared with calcitonin-gene-related peptide-Structure, biology, and relevance to metabolic disease. *Endocr. Rev. 15*, 163-201.

[3] Reda, T. K., Geliebter, A., and Pi-Sunyer, F. X. (2002) Amylin, food intake, and obesity. *Obes. Res. 10*, 1087-1091.

[4] Makin, O. S., and Serpell, L. C. (2005) Structures for amyloid fibrils. *FEBS J. 272*, 5950-5961.

[5] Clark, A., and Nilsson, M. R. (2004) Islet amyloid: a complication of islet dysfunction or an aetiological factor in type 2 diabetes? *Diabetologia 47*, 157-169.

[6] Quist, A., Doudevski, L., Lin, H., Azimova, R., Ng, D., Frangione, B., Kagan, B., Ghiso, J., and Lal, R. (2005) Amyloid ion channels: A common structural link for protein-misfolding disease. *Proc. Natl. Acad. Sci. U.S.A. 102*, 10427-10432.

[7] Demuro, A., Mina, E., Kayed, R., Milton, S. C., Parker, I., and Glabe, C. G. (2005) Calcium dysregulation and membrane disruption as a ubiquitous neurotoxic mechanism of soluble amyloid oligomers. *J. Biol. Chem. 280*, 17294-17300.

[8] Kayed, R., Sokolov, Y., Edmonds, B., McIntire, T. M., Milton, S. C., Hall, J. E., and Glabe, C. G. (2004) Permeabilization of lipid bilayers is a common conformation-dependent activity of soluble amyloid oligomers in protein misfolding diseases. *J. Biol. Chem. 279*, 46363-46366.

[9] Ferreira, S. T., Vieira, M. N. N., and De Felice, F. G. (2007) Soluble protein oligomers as emerging toxins in Alzheimer's and other amyloid diseases. *IUBMB Life 59*, 332-345.

[10] Engel, M. F., Khemtemourian, L., Kleijer, C. C., Meeldijk, H. J., Jacobs, J., Verkleij, A. J., de Kruijff, B., Killian, J. A., and Hoppener, J. W. (2008) Membrane damage by human islet amyloid polypeptide through fibril growth at the membrane. *Proc. Natl. Acad. Sci. U.S.A. 105*, 6033-6038.

[11] Sparr, E., Engel, M. F. M., Sakharov, D. V., Sprong, M., Jacobs, J., de Kruijff, B., Hoppener, J. W. M., and Killian, J. A. (2004) Islet amyloid polypeptide-induced membrane leakage involves uptake of lipids by forming amyloid fibers. *FEBS Lett. 577*, 117-120.

[12] Brender, J. R., Lee, E. L., Cavitt, M. A., Gafni, A., Steel, D. G., and Ramamoorthy, A. (2008) Amyloid fiber formation and membrane disruption are separate processes localized in two distinct regions of IAPP. The type-2-diabetes-related peptide. *J. Am. Chem. Soc. 130*, 6424-6429.

[13] Engel, M. F. M., Yigittop, H., Elgersma, R. C., Rijkers, D. T. S., Liskamp, R. M. J., de Kruijff, B., Hoppener, J. W. M., and Killian, J. A. (2006) Islet amyloid polypelptide inserts into phospholipid monolayers as monomer. *J. Mol. Biol. 356*, 783-789.

[14] Lopes, D. H. J., Meister, A., Gohlke, A., Hauser, A., Blume, A., and Winter, R. (2007) Mechanism of islet amyloid polypeptide fibrillation at lipid interfaces studied by infrared reflection absorption spectroscopy. *Biophys. J. 93*, 3132-3141.

[15] Westermark, P., Engstrom, U., Johnson, K. H., Westermark, G. T., and Betsholtz, C. (1990) Islet amyloid polypeptides-Pinpointing amino-acid-residues linked to amyloid fibril formation. *Proc. Natl. Acad. Sci. U.S.A. 87*, 5036-5040.

[16] Jaikaran, E., Higham, C. E., Serpell, L. C., Zurdo, J., Gross, M., Clark, A., and Fraser, P. E. (2001) Identification of a novel human islet amyloid polypeptide beta-sheet domain and factors influencing fibrillogenesis. *J. Mol. Biol. 308*, 515-525.

[17] Mazor, Y., Gilead, S., Benhar, I., and Gazit, E. (2002) Identification and characterization of a novel molecular-recognition and self-assembly domain within the islet amyloid polypeptide. *J. Mol. Biol. 322*, 1013-1024.

[18] Knight, J. D., Hebda, J. A., and Miranker, A. D. (2006) Conserved and cooperative assembly of membrane-bound α-helical states of islet amyloid polypeptide. *Biochemistry 45*, 9496-9508.

[19] Brender, J. R., Hartman, K., Reid, K. R., Kennedy, R. T., and Ramamoorthy, A. (2008) A single mutation in the nonamyloidogenic region of islet amyloid

polypeptide greatly reduces toxicity. *Biochemistry 47*, 12680-12688.

[20] Radovan, D., Smirnovas, V., and Winter, R. (2008) Effect of pressure on islet amyloid polypeptide aggregation: Revealing the polymorphic nature of the fibrillation process. *Biochemistry 47*, 6352-6360.

[21] Apostolidou, M., Jayasinghe, S. A., and Langen, R. (2008) Structure of α-helical membrane-bound hIAPP and its implications for membrane-mediated misfolding. *J. Biol. Chem. 283*, 17205-17210.

[22] Crescenzi, O., Tomaselli, S., Guerrini, R., Salvadori, S., D'Ursi, A. M., Temussi, P. A., and Picone, D. (2002) Solution structure of the Alzheimer amyloid beta-peptide (1-42) in an apolar microenvironment-Similarity with a virus fusion domain. *Eur. J. Biochem. 269*, 5642-5648.

[23] Buck, M. (1998) Trifluoroethanol and colleagues: cosolvents come of age. Recent studies with peptides and proteins. *Q. Rev. Biophys. 31*, 297-355.

[24] Sanders, C. R., and Sonnichsen, F. (2006) Solution NMR of membrane proteins: practice and challenges. *Magn. Reson. Chem. 44*, S24-S40.

[25] Zamoon, J., Mascioni, A., Thomas, D. D., and Veglia, G. (2003) NMR solution structure and topological orientation of monomeric phospholamban in dodecylphosphocholine micelles. *Biophys. J. 85*, 2589-2598.

[26] Traaseth, N. J., Thomas, D. D., and Veglia, G. (2006) Effects of Ser16 phosphorylation on the allosteric transitions of phospholamban/Ca2+-ATPase complex. *J. Mol. Biol. 358*, 1041-1050.

[27] Zamoon, J., Nitu, F., Karim, C., Thomas, D. D., and Veglia, G. (2005) Mapping the interaction surface of a membrane protein: Unveiling the

conformational switch of phospholamban in calcium pump regulation. *Proc. Natl. Acad. Sci. U.S.A. 102*, 4747-4752.

[28] Vinogradova, O., Sonnichsen, F., and Sanders, C. R. (1998) On choosing a detergent for solution NMR studies of membrane proteins. *J. Biomol. NMR 11*, 381-386.

[29] Porcelli, F., Buck-Koehntop, B. A., Thennarasu, S., Ramamoorthy, A., and Veglia, G. (2006) Structures of the dimeric and monomeric variants of magainin antimicrobial peptides (MSI-78 and MSI-594) in micelles and bilayers, determined by NMR spectroscopy. *Biochemistry 45*, 5793-5799.

[30] Porcelli, F., Verardi, R., Shi, L., Henzler-Wildman, K. A., Ramamoorthy, A., and Veglia, G. (2008) NMR structure of the cathelicidin-derived human antimicrobial peptide LL-37 in dodecylphosphocholine micelles. *Biochemistry 47*, 5565-5572.

[31] Bax, A., and Davis, D. G. (1985) MLEV-17-based two-dimensional homonuclear magnetization transfer spectroscopy. *J. Magn. Reson. 65*, 355-360.

[32] Kumar, A., Ernst, R. R., and Wuthrich, K. (1980) A twodimensional nuclear overhauser enhancement (2D NOE) experiment for the elucidation of complete proton-proton cross-relaxation networks in biological macromolecules. *Biochem. Biophys. Res. Commun. 95*, 1-6.

[33] Delaglio, F., Grzesiek, S., Vuister, G. W., Zhu, G., Pfeifer, J., and Bax, A. (1995) NMRpipesa multidimensional spectral processing system based on UNIX pipes. *J. Biomol. NMR 6*, 277-293.

[34] Kneller, D. G., and Kuntz, I. D. (1993) UCSF Sparky-an NMR display,

annotation and assignment tool. *J. Cell. Biochem.* 254-254.

[35] Wuthrich, K. (1986) *NMR of Proteins and Nucleic Acids*, John Wiley and Sons, New York.

[36] Nilges, M., Gronenborn, A. M., Brunger, A. T., and Clore, G. M. (1988) Determination of 3-dimensional structures of proteins by simulated annealing with interproton distance restraints-application to crambin, potato carboxypeptidase inhibitor and barley serine proteinase inhibitor-2. *Protein Eng. 2*, 27-38.

[37] Schwieters, C. D., Kuszewski, J. J., Tjandra, N., and Clore, G. M. (2003) The Xplor-NIH NMR molecular structure determination package. *J. Magn. Reson. 160*, 65-73.

[38]. Cornilescu, G., Delaglio, F., and Bax, A. (1999) Protein backbone angle restraints from searching a database for chemical shift and sequence homology. *J. Biomol. NMR 13*, 289-302.

[39] Laskowski, R. A., Rullmann, J. A. C., MacArthur, M. W., Kaptein, R., and Thornton, J. M. (1996) AQUA and PROCHECK-NMR: Programs for checking the quality of protein structures solved by NMR. *J. Biomol. NMR 8*, 477-486.

[40] Koradi, R., Billeter, M., and Wuthrich, K. (1996) MOLMOL: A program for display and analysis of macromolecular structures. *J. Mol. Graphics 14*, 51-55.

[41] Lashuel, H. A., and Lansbury, P. T. (2006) Are amyloid diseases caused by protein aggregates that mimic bacterial pore-forming toxins? *Q. Rev. Biophys. 39*, 167-201.

[42] Haataja, L., Gurlo, T., Huang, C. J., and Butler, P. C. (2008) Islet Amyloid in

type 2 diabetes, and the toxic oligomer hypothesis. *Endocr. Rev. 29*, 302-316.

[43] Jayasinghe, S. A., and Langen, R. (2005) Lipid membranes modulate the structure of islet amyloid polypeptide. *Biochemistry 44*, 12113-12119.

[44] (a) Bokvist, M., Lindstrom, F., Watts, A., and Grobner, G. (2004) Two types of Alzheimer's beta-amyloid (1-40) peptide membrane interactions: Aggregation preventing transmembrane anchoring versus accelerated surface fibril formation. *J. Mol. Biol. 335*, 1039-1049. (b) Ilangovan, U., and Ramamoorthy, A. (1998) Conformational studies of human islet amyloid peptide using molecular dynamics and simulated annealing methods. *Biopolymers 45*, 9.

[45] Davidson, W. S., Jonas, A., Clayton, D. F., and George, J. M. (1998) Stabilization of alpha-synuclein secondary structure upon binding to synthetic membranes. *J. Biol. Chem. 273*, 9443-9449.

[46] Mascioni, A., Porcelli, F., Ilangovan, U., Ramamoorthy, A., and Veglia, G. (2003) Conformational preferences of the amylin nucleation site in SDS micelles: An NMR study. *Biopolymers 69*, 29-41.

[47] Tenidis, K., Waldner, M., Bernhagen, J., Fischle, W., Bergmann, M., Weber, M., Merkle, M. L., Voelter, W., Brunner, H., and Kapurniotu, A. (2000) Identification of a penta- and hexapeptide of islet amyloid polypeptide (IAPP) with amyloidogenic and cytotoxic properties. *J. Mol. Biol. 295*, 1055-1071.

[48] Williamson, J. A., and Miranker, A. D. (2007) Direct detection of transient α-helical states in islet amyloid polypeptide. *Protein Sci. 16*, 110-117.

[49] Yonemoto, I. T., Kroon, G. J., Dyson, H. J., Balch, W. E., and Kelly, J. W. (2008) Amylin proprotein processing generates progressively more

amyloidogenic peptides that initially sample the helical state. *Biochemistry 47*, 9900-9910.

[50] Jarvet, J., Danielsson, J., Damberg, P., Oleszczuk, M., and Graeslund, A. (2007) Positioning of the Alzheimer Abeta(1-40) peptide in SDS micelles using NMR and paramagnetic probes. *J. Biomol. NMR 39*, 63-72.

[51] Daily, A. E., Greathouse, D. V., van der Wel, P. C. A., and Koeppe, R. E. (2008) Helical distortion in tryptophan- and lysine-anchored membrane-spanning alpha-helices as a function of hydrophobic mismatch: A solid-state deuterium NMR investigation using the geometric analysis of labeled alanines method. *Biophys. J. 94*, 480-491.

[52] Balali-Mood, K., Ashley, R. H., Hauss, T., and Bradshaw, J. P. (2005) Neutron diffraction reveals sequence-specific membrane insertion of pre-fibrillar islet amyloid polypeptide and inhibition by rifampicin. *FEBS Lett. 579*, 1143-1148.

[53] Motta, A., Andreotti, G., Amodeo, P., Strazzullo, G., and Morelli, M. A. C. (1998) Solution structure of human calcitonin in membrane-mimetic environment: The role of the amphipathic helix. *Proteins 32*, 314-323.

[54] Roberts, E., Eargle, J., Wright, D., and Luthey-Schulten, Z. (2006) MultiSeq: Unifying sequence and structure data for evolutionary analysis. *BMC Bioinf. 7*, 382-392.

[55] Humphrey, W., Dalke, A., and Schulten, K. (1996) VMD: Visual molecular dynamics. *J. Mol. Graphics 14*, 33-38.

[56] Henzler-Wildman, K. A., Martinez, G. V., Brown, M. F., and Ramamoorthy, A. (2004) Perturbation of the hydrophobic core of lipid bilayers by the human

antimicrobial peptide LL-37. *Biochemistry 43*, 8459-8469.

[57] Ramamoorthy, A., Thennarasu, S., Tan, A., Lee, D. K., Clayberger, C., and Krensky, A. M. (2006) Cell selectivity correlates with membrane interactions: a case study on the antimicrobial peptide G15 derived from granulysin. *Biochim. Biophys. Acta 1758*, 154-163.

CHAPTER 3. THREE-DIMENSIONAL STRUCTURE AND ORIENTATION OF RAT ISLET AMYLOID POLYPEPTIDE PROTEIN IN A MEMBRANE ENVIRONMENT BY SOLUTION NMR SPECTROSCOPY

This chapter is a version of a manuscript published in J. Am. Chem. Soc. (2009) 131, 8252-8261.[2]

3.1 ABSTRACT

Islet amyloid polypeptide (IAPP or amylin) is a 37-residue peptide hormone associated with glucose metabolism that is cosecreted with insulin by *β*-cells in the pancreas. Since human IAPP is a highly amyloidogenic peptide, it has been suggested that the formation of IAPP amyloid fibers is responsible for the death of *β*-cells during the early stages of type II diabetes. It has been hypothesized that transient membrane-bound α-helical structures of human IAPP are precursors to the formation of these amyloid deposits. On the other hand, rat IAPP forms transient α-helical structures but does not progress further to form amyloid fibrils. To understand the nature of this intermediate state and the difference in toxicity between the rat and human versions of IAPP, we have solved the high-resolution structure of rat IAPP in the membrane-mimicking detergent micelles composed of dodecylphosphocholine. The structure is characterized by a helical region spanning the residues A5 to L23 and a disordered C-terminus. A distortion in the helix is seen at R18 and S19 that may be involved in receptor binding. Paramagnetic quenching NMR experiments

[2] Jiadi Xu helped in setting up the NMR experiments. Subramanian Vivekanandan helped in structural calculations. Kevin Hartman carried out the DSC studies. Jeffrey Brender helped in writing the manuscript. This study was supported by the funds from NIH (DK 078885 to A.R.).

indicate that rat IAPP is bound on the surface of the micelle, in agreement with other nontoxic forms of IAPP. A comparison to the detergent-bound structures of other IAPP variants indicates that the N-terminal region may play a crucial role in the self-association and toxicity of IAPP by controlling access to the putative dimerization interface on the hydrophobic face of the amphipathic helix.

3.2 INTRODUCTION

Islet amyloid polypeptide (IAPP; also known as amylin) is the major component of amyloid deposits found in the pancreas of type II diabetic patients. Since amyloid deposits are observed in approximately 95% of diabetic patients but are rarely found in nondiabetic individuals, it has been hypothesized that IAPP fibrillization is involved in the pathogenic development of the disease.4-6 More specifically, aggregates of IAPP have been implicated in the loss of *β*-cell mass and a reduction in insulin production [*1*]. Disruption of the *β*-cell membrane is central to this process [*2, 3*]. IAPP oligomers, but not the mature amyloid fibers, have been shown to induce apoptosis by the disruption of calcium homeostasis and the creation of oxidative stress. The mechanism of membrane disruption by IAPP and other amyloid proteins is still a subject of considerable debate [*3-5*].

A cross-species comparison of IAPP sequences has shown an interesting correlation between the occurrence of a type II like form of diabetes and the propensity of the corresponding IAPP sequence to form amyloid fibers. Humans, nonhuman primates, and cats all have amyloidogenic forms of IAPP.

Revealingly, a type II diabetic-like syndrome has been observed in all these mammals. Out of the nonamyloidogenic forms of IAPP, the rat variant (rIAPP, sequence shown in Figure 3-1) has been the most intensively studied. In contrast to the human form of IAPP (hIAPP), rIAPP is almost completely nontoxic to *β*-cells even at high concentrations. Significantly, rats do not develop diabetes-like symptoms even when rIAPP is overexpressed [*6*].

Figure 3-1. Amino acid sequences of rat and human IAPP with non-conserved residues shown in red color in the rat IAPP sequence. Both the peptides are amidated at the C-terminus and have a disulfide bridge from Cys2 to Cys7.

The nontoxicity of rIAPP has usually been attributed to its inability to form the *β*-sheet amyloid fibers characteristic of hIAPP. However, mature amyloid fibers are relatively inert compared to the high toxicity exhibited by prefibrillar oligomeric species. Protofibrillar intermediates have been implicated in disturbing cellular homeostasis by disrupting the cellular membrane, either through the formation of ion channels or by a nonspecific general disruption of the lipid bilayer. The structure of the earlier intermediate species is unknown. The sequence of rIAPP differs from hIAPP primarily by the substitution of prolines for critical residues in the amyloidogenic region of hIAPP [*7, 8*]. Since prolines act as *β*-sheet breakers, the absence of rIAPP cytotoxicity has been interpreted as evidence for the theory that the highly toxic prefibrillar intermediates of IAPP possess a similar *β*-sheet-enriched structure as the mature hIAPP fiber. However, membrane disruption by hIAPP is a complex process with contributions from multiple conformations and multiple oligomeric states [*3*]. In particular, an

initial increase in the permeability of the membrane occurs immediately upon the addition of the peptide to the membrane [*9*]. This is followed by a larger increase in permeability, corresponding to a complete disruption of the membrane that is correlated with the formation of amyloid fibers [*4, 10-13*]. The biphasic nature of membrane disruption is mirrored by biphasic changes in the conformation of the peptide. Both rIAPP and hIAPP are predominantly α-helical when initially bound to the membrane, as shown for rIAPP in this study and by circular dichroism (CD) and electron paramagnetic resonance (EPR) data for hIAPP bound to phospholipid vesicles [*9, 14-16*]. From this α-helical intermediate state, both rIAPP and hIAPP then aggregate to form *β*-sheet fibers. The initial increase in membrane permeability after IAPP binding may be linked to the formation of pores caused by the self-association of several α-helical IAPP monomers on the membrane [*9*].

The importance of these helical intermediate states of IAPP has been shown by fragments of IAPP ($IAPP_{1-19}$) which form the helical intermediate state when bound to the membrane but do not progress from this state to form amyloid fibers [*17-19*]. The toxicity of these fragments mirrors the relative toxicity of the full-length versions of IAPP [*17, 19*]. Rat $IAPP_{1-19}$ is significantly less toxic than $hIAPP_{1-19}$, despite differing from $hIAPP_{1-19}$ by only one residue (a substitution of arginine for histidine at residue 18). Although $rIAPP_{1-19}$ is less toxic to *β*-cells than $hIAPP_{1-19}$, it is still considerably more toxic than $rIAPP_{1-37}$, which does not disrupt membranes of less than 50% anionic lipid content (the typical range for a *β*-cell is 10-20%) [*20*]. Amyloidogenic propensity of hIAPP may be seen in this sense as

sufficient, but not necessary, for membrane disruption.

To understand how structural differences in the initial helical state may affect the formation of later aggregates and the process of membrane disruption by IAPP, we have solved the high resolution structure of rIAPP in dodecylphosphocholine (DPC) micelles from two-dimensional (2D) NMR experiments. Previous studies have shown interesting differences between the transient helical conformational states in rIAPP and hIAPP; however, the transient nature of these states has prevented the collection of sufficient distant constraints to create a high resolution structure [*21, 22*]. The high-resolution structure reported here also gives insight into the interaction of IAPP with its membrane-bound G-coupled protein receptor.

3.3 MATERIALS AND METHODS

3.3.1 ***NMR Sample Preparation*.** Rat IAPP amidated at the C-terminus was synthesized and purified by GenScript. The purity of the peptide was checked by analytical HPLC. The homogeneity and purity of the peptide sample was also proved by NMR experiments. The formation of the intramolecular disulfide bond from residues 2-7 was verified by electrospray mass spectroscopy. The lyophilized peptide was dissolved in hexafluoroisopropyl alcohol at a concentration of 10 mg/mL and then lyophilized overnight under vacuum to completely remove the solvent. Samples were prepared for NMR measurements by dissolving 3 mg of lyophilized peptide in 20 mM phosphate buffer at pH ~ 7.3 containing 10% D_2O, 120 mM NaCl, and 200 mM perdeuterated DPC (Cambridge Isotopes Laboratory) to a final concentration of 2.5 mM. IAPP-DPC

samples were tested for stability before and after NMR experiments using CD experiments at different temperatures.

3.3.2 ***NMR Data Collection and Processing*****.** All NMR spectra of IAPP embedded in DPC micelles were recorded at 30 °C using a Bruker spectrometer operating at a ^{1}H resonance frequency of 900 MHz equipped with a triple-resonance *z*-gradient cryogenic probe optimized for ^{1}H detection. The 2D TOCSY (total correlation spectroscopy) spectrum of the sample was obtained for a 70 ms mixing time using 512 experiments in the indirect dimension, each with 32 scans and a recycle delay of 2 s. 2D ^{1}H-^{1}H NOESY (nuclear Overhauser enhancement spectroscopy) spectra of the same sample were obtained for 100 and 300 ms mixing times using 512 experiments in the indirect dimension, each with 64 scans and a recycle delay of 2 s. Complex data points were acquired for quadrature detection in both the frequency dimensions of these 2D experiments. All spectra were zero-filled in both dimensions to yield matrices of 2048 x 2048 points. Both TOCSY and NOESY spectra were used in the complete assignment of backbone and side-chain resonances. Proton chemical shifts were referenced to the water proton signal at 4.7 ppm (at 30 °C). All 2D spectra were processed using NMRPIPE and TopSpin software from Bruker and analyzed using SPARKY [*23, 24*]. Resonance assignment was carried out using a standard approach reported elsewhere [*25*].

3.3.3 ***Structure Calculations*****.** Structure calculations were performed using the X-PLOR-NIH program. An extended structure of rIAPP was used as a starting point for the hybrid molecular dynamics simulated annealing (SA) protocol at a

temperature of 4000 K for the generation of an initial 100 structures [*26, 27*]. Subsequently, these structures were refined using a further SA step and energy minimization. The final refinement was carried out using the refine_gentle.inp protocol, which gradually introduces the van der Waals radii. A total of 485 NOEs from the rat IAPP were classified into three distance categories according to their peak intensities obtained from SPARKY analysis-strong (1.8-2.9 Å), medium (1.8-4.5 Å), and weak (1.8-6.0 Å)-and used in the structure calculations of which 262 were intra-residue and 223 inter-residue NOEs (Table 3-1). The torsion angle restraints were obtained from the TALOS module (http://spin.niddk.nih.gov/bax/software/TALOS) in NMRPIPE using the H_α chemical shift values [*28*]. The few ambiguous angles found in the loop region were assigned an additional 60° of conformational freedom compared to their predicted values. Of the 100 structures generated, the 10 lowest energy structures were selected for further analysis. Those structures selected had no violations of (a) NOE constraints higher than 0.5 Å, (b) bond angles higher than 5°, and (c) bond lengths higher than 0.05 Å. The covalent geometry of the conformers generated was determined using PROCHECK_NMR [*29*].

3.3.4 *Paramagnetic Quenching*. One-dimensional ^1H chemical shift spectra of rat IAPP in DPC micelles at concentrations of 0.4, 0.8, and 1.2 mM $MnCl_2$ and at a pH of 7.3 were obtained. All other experimental conditions were the same as mentioned above.

3.3.5 *Differential Scanning Calorimetry*. Multilamellar vesicle samples for differential scanning calorimetry (DSC) experiments were prepared by first mixing

rIAPP in methanol with DMPC/DMPG (7:3) in chloroform. Samples were then vortexed and dried under a stream of nitrogen gas to create a lipid-peptide film. Residual solvent was removed from the film by placing the samples under high vacuum overnight. After the drying process, sodium phosphate buffer (50 mM Na_2PO_4 with 150 mM NaCl at pH 7.3) was added to the dry lipid film, followed by vortexing, several freeze-thaw cycles, and brief sonication. The total molar concentration of lipid was kept constant (5.9 mM) for each sample while the molar peptide concentration was varied as indicated. A total of four heating and four cooling scans were run with a temperature range of 5-45 °C. The heating scans were run at 0.25 °C/min, whereas the cooling scans were run at 1.0 °C/min with a 10 min equilibration period between scans.

Table 3-1. Statistical information for the structural ensemble of rat IAPP.

Distance constraints		
	Total	485
	Intra-residual	262
	Inter-residual	223
	Sequential (i - j = 1)	138
	Medium (i – j = 2, 3, 4)	85
Structural statistics		
	NOE violations (Å)	0.0554 ± 0.0008
	Dihedral angle restraint violations (º)	1.3053 ± 0.0609
	RMSD for bond deviations (Å)	0.0051 ± 0.0010
	RMSD for angle deviations (º)	0.8158 ± 0.0180
	RMSD of all backbone atoms (Å)	
	Ala 5 – Val 17	0.22 ± 0.07
	Ala 5 – Leu 23	0.52 ± 0.19
	RMSD of all heavy atoms (Å)	
	Ala 5 – Val 17	0.72 ± 0.15
	Ala 5 – Leu 23	1.24 ± 0.21
Ramachandran plot		
	Residues in most favored region (%)	75.9
	Residues in additionally allowed region (%)	20.3
	Residues in additionally allowed region (%)	1.4
	Residues in disallowed region (%)	2.4

The data was converted to molar heat capacity using the average molecular weight of the lipids, the lipid concentration, and a partial specific

volume of 0.988 mL/g for the lipid mixture. Excess heat capacity was calculated by subtracting a baseline with buffer in both the reference and sample cells at the same scanning rate.

3.4 RESULTS

3.4.1 *Assignments, Constraints and NMR Structures*. Micelles containing the detergent DPC and the rat IAPP were prepared for NMR measurements as mentioned in the previous section. As with all membrane-bound peptides, sample preparation is a key step in obtaining the high-resolution spectra of rat IAPP. In our analysis of different experimental conditions, we determined that rat IAPP behaves well with DPC, giving rise to very well-resolved and unique resonances for each of the amide sites in the 2D TOCSY spectrum. In an effort to optimize spectral resolution and sensitivity, several 1D ^{1}H spectra were acquired over a temperature range of 25-45 °C. Only marginal chemical shift changes were observed for the N- and C-termini and the more solvent-exposed residues (residues 24-37), whereas the majority of the residues did not exhibit any chemical shift variation. This demonstrates that the structure is essentially the same at all the temperatures analyzed. The best compromise between resolution and sensitivity was found to be at 30 °C, and we have chosen this temperature to carry out our NMR experiments. Since IAPP peptides are known to aggregate, the micelles were further tested for stability using CD experiments at different temperatures. The CD spectra suggested that the rIAPP-DPC micelle was quite stable even after several months and the peptide had significant helical structure in micelles, indicating that rIAPP remained bound to the DPC micelle. Therefore,

it was concluded that the sample was suitable for NMR measurements to determine the high-resolution structure and topology of the membrane-associated peptide.

A combination of 2D ^{1}H-^{1}H TOCSY and 2D ^{1}H-^{1}H NOESY spectra was used for the assignment of backbone and side-chain resonances. The 2D ^{1}H-^{1}H NOESY spectra of the rat IAPP obtained in deuterated DPC micelles at pH 7.3 displays numerous, well-resolved cross-peaks, with more than 1.00 ppm spectral dispersion in the amide region indicating that the peptide is well-folded. This spectrum demonstrates numerous NOEs such as $d_{NN}(i, i + 1)$ and $d_{\alpha N}(i, i + 3)$ that are diagnostic for α-helices as shown in Figure 3-2. The sequential assignments were accomplished using the amide proton to α-proton region of the 2D ^{1}H-^{1}H NOESY spectrum obtained at a 300 ms mixing time. Spectra obtained at mixing times of 100 and 300 ms were nearly identical, except that the longer mixing time produced relatively stronger cross-peaks. The α-proton chemical shift index (CSI) plot for the rat IAPP is given in Figure 3-3. Chemical shift values for α-protons were not observed for residues K1, C2, and P28, most likely due to fast relaxation suppressing the signal intensity for these residues. Due to high quality of the spectra, the assignment of resonances was straightforward, with the exception of residues in the flexible C-terminal region of the peptide. The fingerprint region of the assigned 2D NOESY spectrum of the peptide obtained at a 300 ms mixing time is shown in Figure 3-4.

We have identified and assigned a total of 485 (262 intraresidue and 223 inter-residue) NOEs from the analysis of the 2D ^{1}H-^{1}H NOESY spectrum. A

summary of backbone NOEs for the secondary structure assignment with a histogram indicating the number of NOEs per residue is given in Figure 3-5.

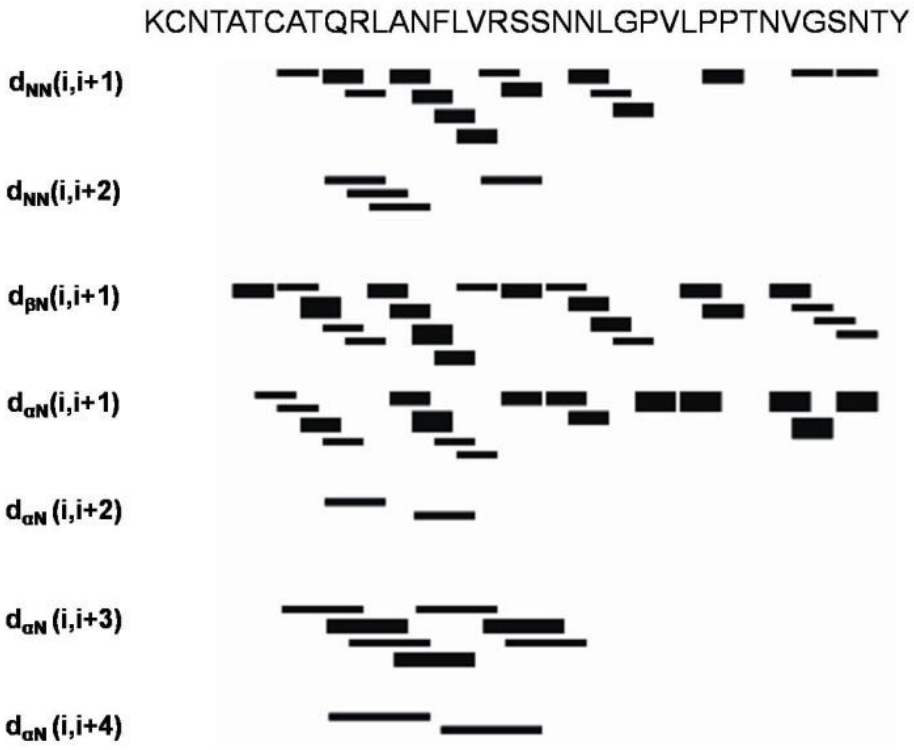

Figure 3-2. A summary of the sequential and medium-range NOE connectivities for rIAPP in DPC micelles at 30 °C, pH 7.3. The intensities of the observed NOEs are represented by the thickness of lines and are classified as strong, medium, and weak, corresponding to upper bound constraints of 2.9, 4.5, and 6 Å, respectively.

From the density of $d_{\alpha N}(i, i + 1)$, $d_{NN}(i, i + 1)$, and $d_{\beta N}(i, i+ 1)$ NOE correlations, it is possible to identify three distinct regions: an N-terminal helix encompassing Ala5-Val17, a short helix from Ser20-Leu23, and a third, long flexible loop region consisting of residues 24-37. Taken together, the NOE and CSI data support the presence of a predominantly α-helical structure within the Ala5-Leu23 region, with the stretch of residues from Ala5-Val17 and Ser20-Leu23 acting as a more stable core.

The remainder of the peptide on the C-terminal end from Gly24-Tyr37 is

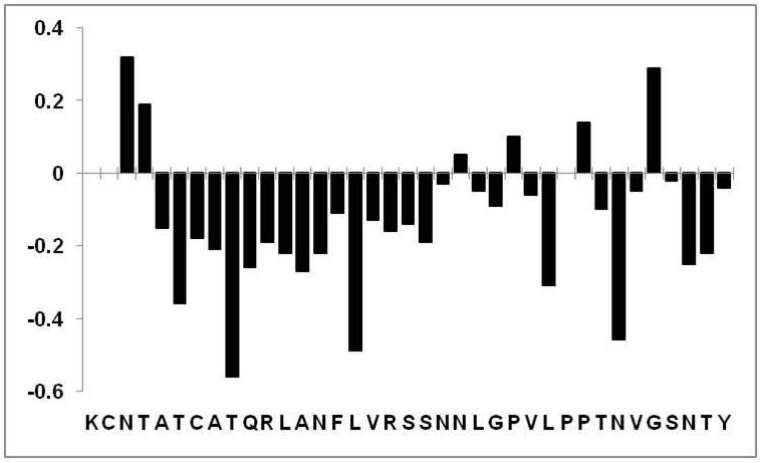

Figure 3-3. α-Proton chemical shift index (CSI) for rat IAPP showing the propensity of IAPP to form an α-helix at the N-terminal region of the peptide. The CSI was calculated by subtracting the values measured for the peptide from the random coil shifts reported in the literature [*25*].

predominantly disordered. The RMSD analysis supports the presence of higher disorder at the C-terminus of the helical region. The RMSD between structures is 0.52 ± 0.19 for the Cα backbone atoms and 1.24 ± 0.21 for all heavy atoms from residues 5-23. For the Cα atoms of N-terminal well-ordered region (residues 5-17), the calculated RMSD decreases to 0.22 ± 0.07 and 0.72 ± 0.15 for the backbone and heavy atoms, respectively. This difference in backbone RMSD clearly shows that the 5-17 region of rat IAPP is relatively stable and that the helical region from residues 18-23 is more disordered. The overlays of the backbone and side-chain heavy atoms for the final selected conformers are shown in Figure 3-6. The secondary structure representation of rIAPP is shown in Figure 3-6C.

All the measured distances and predicted dihedral angles were subsequently modeled using SA calculations with the XPLORNIH program. The Ramachandran plots generated using PROCHECK_NMR of the 10 lowest

energy structures show that residues V26, L27, T30, and S34 fall in the disallowed region of the Ramachandran plot. This is most likely due to the high mobility of the C-terminal region as well as the presence of the proline residues (P25, P28, and P29) toward the C-terminal end of the peptide.

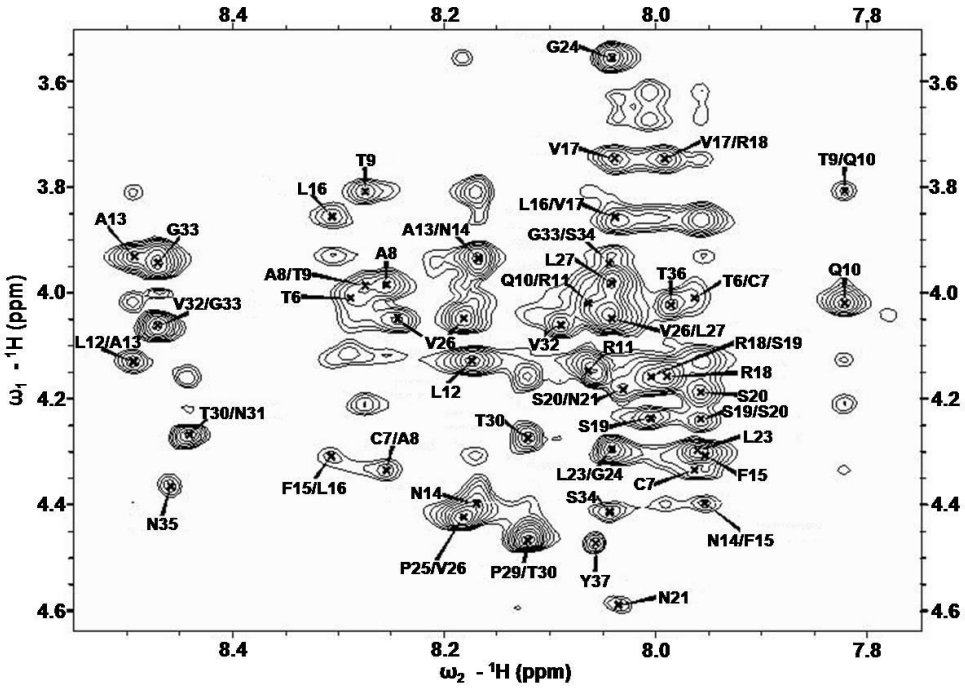

Figure 3-4. The fingerprint region of 2D ^{1}H-^{1}H NOESY spectrum of rat IAPP showing the NOE α-proton connectivities. A single resonance was detected for each residue except for Val 26, which has two resonance peaks.

3.4.2 ***Positioning of rIAPP in the Micelle*****.** A first approximation of the membrane orientation of rIAPP was obtained using the paramagnetic quencher Mn^{2+} to identify those residues of the peptide that are exposed to solvent. Paramagnetic manganese ions decrease the signal intensity of nuclei that are in close proximity to the ion by increasing the relaxation rate. Because manganese ions cannot penetrate into the hydrophobic interior of the micelle, changes in signal intensity reflect the exposure of the amino acid residues of the peptide to the solvent.

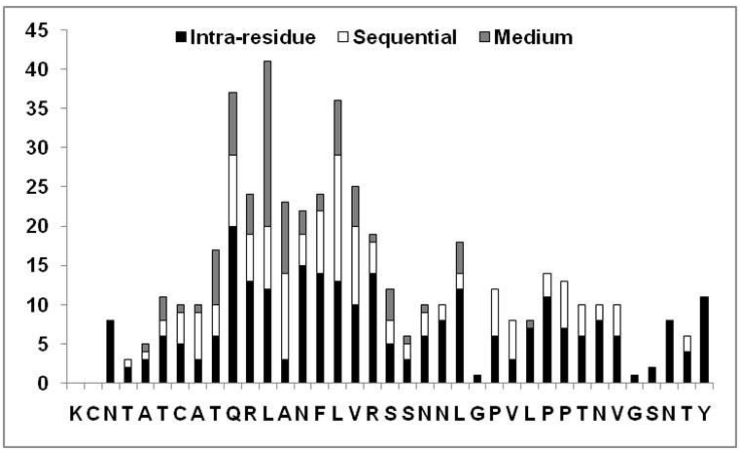

Figure 3-5. A histogram of NOEs vs the residue number for rat IAPP, showing the number of intraresidue, sequential (i - j = 1), and mediumrange (i - j = 2, 3, 4) NOEs. Long-range (i - j > 4) NOEs were not observed.

The 1D ^{1}H chemical shift spectra of DPC micelles containing rIAPP and varying concentrations of $MnCl_2$ (0.4, 0.8, and 1.2 mM) are given in Figure 3-7. The considerable shift and broadening of peaks from micelles containing rat IAPP at low concentrations of $MnCl_2$ suggest that the peptide is in general well-exposed to the water phase and not deeply buried in the hydrophobic core of the micelle.

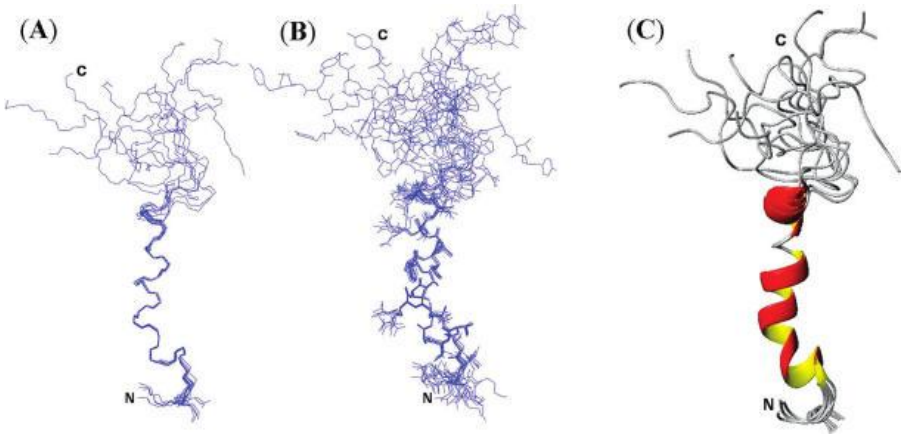

Figure 3-6. Ensemble of conformers for rat IAPP showing the convergence of conformers for backbone atoms (A) and side-chain atoms (B). (C) Secondary structure representation of an overlaid ensemble of conformers for rat IAPP. Two helices, an ordered helix (A5-V17) and a more disordered helix (S20-L23), can be seen in the structure.

To identify the exposure of specific residues to solvent more precisely, 2D ^{1}H-^{1}H TOCSY spectra were used to monitor the changes in the chemical shift and signal intensity of individual α-proton peaks after the addition of 0.8 mm $MnCl_2$. The percentage decrease in the signal intensity of the α-proton chemical shift resonances calculated from the TOCSY spectra is given in Figure 3-8.

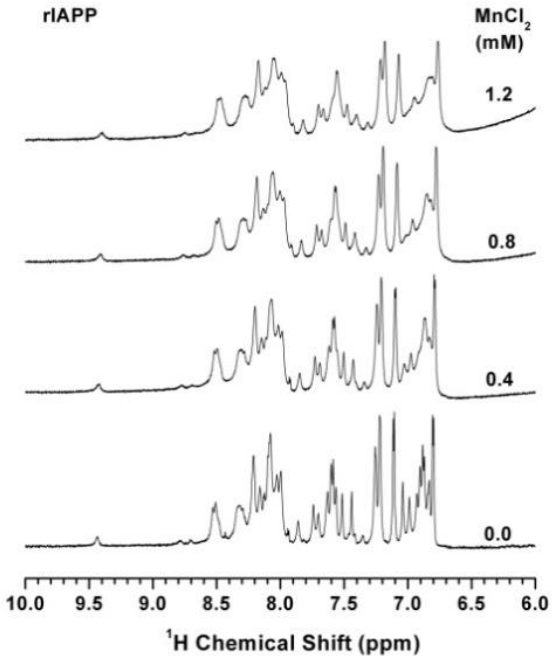

Figure 3-7. Amide-proton chemical shift region of ^{1}H NMR spectra of rat IAPP in DPC micelles at pH 7.3 with and without $MnCl_2$. The spectral intensities were normalized.

Exact intensity calculations could not be made for some residues, either due to overlapping chemical shifts (A13 with G33 and F15 with L23) or the absence of peaks in the ^{1}H-^{1}H TOCSY spectrum even without paramagnetic ions (K1, C2, R11, N22, G24, P25, P28, P29, and N35), and therefore the quenching data for these residues is not included in the plot. It is interesting to note that the decrease in the intensity of the α-proton chemical shift resonances upon the addition of the quencher is less in the stable helix located toward the N-terminal

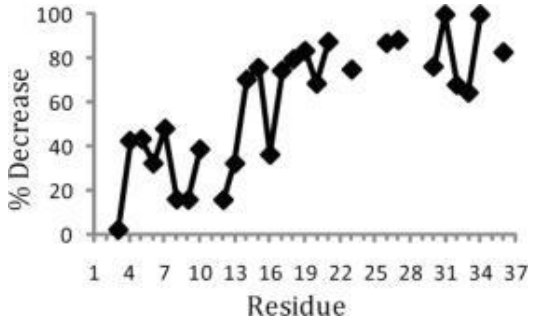

Figure 3-8. Percentage decrease in the signal intensity of α-proton chemical shift resonances of rat IAPP embedded in DPC micelles at pH 7.3 after the addition of 0.8 mM $MnCl_2$.

region (A5-V17) than in the flexible but structured helix (R18-L23) and the unstructured C-terminus (G24-Y37), indicating that the C-terminal region is significantly more exposed to the solvent. Thus, the site-specific paramagnetic quenching results clearly indicate that the N-terminal part of rat IAPP is a stable helix that is bound to the surface of the membrane, whereas the C-terminal is mobile and is exposed to the solvent, as supported by the random coil structure as well as the large decrease in signal intensity of α-proton chemical shift resonances upon exposure to paramagnetic quencher $MnCl_2$.

3.4.3 *Differential Scanning Calorimetry of rIAPP in Vesicles*. The interaction of rIAPP with phospholipid membranes was also characterized by alterations of the main phase transition as detected by differential scanning calorimetry. The main phase transition is associated with the melting of the acyl chains in the hydrophobic core of the membrane from the rigid gel phase to the more fluid liquid-crystalline phase. This phase transition is sensitive to the binding of peptides to the membrane, in particular to the depth at which the peptide penetrates into the bilayer. The degree of perturbation of the phase transition is correlated with the displacement of the acyl chains of the lipid and is strongest if

the peptide localizes in the bilayer at the glycerol region preceding the acyl chains and less for peptides that bind only at the top of the bilayer or insert into the membrane in a transmembrane orientation [*30-32*]. Rat IAPP reduces the phase transition temperature (melting temperature (Tm), enthalpy change (Δ*H*, equal to the area of the transition on the thermogram), and cooperativity of the transition (related to the width of the transition) (Figure 3-9). The transition is asymmetric at higher concentrations (>1.0% rIAPP), suggesting rIAPP may be

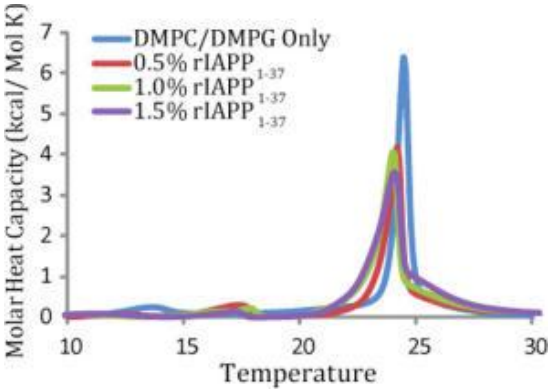

Figure 3-9. Differential scanning calorimetry of the pre-transition and the main gel to liquid-crystalline phase transition of 7:3 DMPC:DMPG vesicles at the indicated molar ratio of rIAPP to lipid. Peptide and lipids were co-dissolved in a chloroform/ethanol solution, dried, and re-suspended in sodium phosphate buffer, pH 7.3 with 150 mM NaCl.

forming peptide-rich domains or forming clusters of DMPG-rich domains [*19*]. The degree of reduction is significant, but less than that observed for peptides known to bind near the glycerol region [*33-35*]. Taken together with the paramagnetic quenching data, DSC suggests rIAPP binds at the surface of the membrane with the disordered loop extending into the solvent.

3.5 DISCUSSION

Early intermediates in the misfolding pathway have been implicated in pathogenesis of a growing number of common and devastating diseases such as

type II diabetes, Alzheimer's disease, and Parkinson's disease. Since damage to the cellular membrane has been identified as a major source of the toxicity of amyloid proteins, it has been recognized that solving the atomic-level resolution structures of amyloid peptides and proteins in a membrane environment would provide insights into their toxic properties [*36-41*]. Such atomic-level resolution structural insights will enable the design of compounds to suppress the toxicity of amyloids and will therefore aid the design of drugs to treat amyloid diseases. Unfortunately, structural studies have been difficult as these systems are not amenable for X-ray diffraction studies due to the difficulty in obtaining high-quality single crystals. In this study, we have investigated the 3D structure of rIAPP in a detergent micelle using NMR spectroscopy in order to understand the folding of intermediates of IAPP in membrane and the origin of toxicity of the hIAPP peptide by looking at its nontoxic rIAPP counterpart which forms similar folding intermediates and can disrupt membranes under certain conditions [*9, 11, 15*].

The high-resolution structure of membrane-bound rIAPP determined here resembles the transient helical forms of both rIAPP and hIAPP in solution, with some differences as outlined below [*21, 22*]. The structure of rIAPP in DPC micelles is dominated by an N-terminal helical region from residues A5 to L23 and a disordered C-terminus. In solution, the helical region of rIAPP is shorter than in the membrane-bound form, spanning residues 5-19, whereas residues 20-23 are involved in hydrogen bonding interactions with the helix but do not adopt a helical conformation [*22*]. Human IAPP, which lacks the conformational restraints imposed by the three prolines in rIAPP, has a greater helical propensity

in solution that extends throughout the entire molecule except for the N-terminal ring which is conformationally constrained by the disulfide bond between residues 2 and 7 [*21*]. The helical propensity for hIAPP in solution is greatest, however, in the N-terminal section up to residue 20 which is similar to the results presented here [*21*].

Some hypotheses about the driving force for membrane catalyzed aggregation can be directly supported by comparing the rIAPP with the very recently solved structure of unamidated hIAPP in SDS micelles [*42*]. The structure of hIAPP bound to SDS has an overall fold similar to that of rIAPP in DPC micelles, consisting of an ordered N-terminal helix, a flexible hinge region, and a less ordered helix that is followed by a disordered C-terminus. The N-terminal helical region in the rIAPP structure (5-17) corresponds to a similar stretch of helical residues in the hIAPP structure (5-17) as well as in a lower resolution EPR study of spin-labeled hIAPP bound to small unilamellar vesicles (9-22), as can be expected by the very high degree of sequence homology in this region [*14*]. A flexible region that corresponds to the center of the loop in the *β*-hairpin structure of the IAPP amyloid fiber is seen in both structures [*43-45*]. This hinge may also have implications for the binding of IAPP to its receptor as discussed below. The major difference between the two structures is in the C-terminal region, which is completely disordered in the rIAPP structure but consists of a dynamic helix (S20-L27) followed by a disordered C-terminal tail in the hIAPP structure. Membrane-catalyzed aggregation is believed to proceed first by the association of the helical regions of the peptide, followed by the

formation of *β*-sheet structure in the disordered regions [*9, 46*]. The formation of secondary structure in unstructured regions of the peptide upon self-association is believed to be a major contributor to the binding energy of hIAPP to membranes and is also thought to be responsible for the cooperativity seen in the binding of hIAPP to membranes [*9*]. Our structure confirms that a large section of the rIAPP peptide remains unstructured when bound to the membrane. The lesser degree of structure in the C-terminus of rIAPP is likely to impact the early self-association of rIAPP in several ways. First, it is probable that the additional helix present in the hIAPP structure provides an additional ordered interaction surface to nucleate self-association. Second, if the C-terminus of rIAPP cannot form ordered structures, as the DPC micelle bound peptide structure indicates, a large contribution to energy of self-association is lost. It has been shown that proline mutations outside the amyloidogenic region of IAPP (proline substitutions at positions 17, 19, and 30) result in a large inhibition of amyloid formation and the loss of amyloid fiber stability [*47*]. In light of the differences between rIAPP and hIAPP structures in the C-terminal region, it would be interesting to further investigate the effect of mutations that stabilize or destabilize secondary structure specifically in this region [*48, 49*].

In solution, the prolines of rIAPP are predominantly, but not exclusively, in the trans conformation. A small percentage of the P25 and P28 residues, but not P29, are in the cis conformation as shown by the observation of α-α NOE connectivities for P25 and P28 that are diagnostic for the cis conformation [*22*]. The prolines in the membrane-bound form have a stronger preference for the

trans conformation than those in rIAPP in solution as multiple resonances are only seen for V26, and not for G24 and L27. This indicates P28 and P29 are exclusively in the trans conformation when bound to the membrane, and only P25 is undergoing slow cis/trans isomerization. The C-terminal residues of rIAPP from T30 are in an extended, disordered conformation extending outward from the helix. The disordered C-terminus does not interact with any other part of the rIAPP molecule, as shown by the absence of long or medium-range NOEs. Rat IAPP is a monomer in the micelle as shown by the absence of long-range NOEs for the side-chain atoms.

Rat IAPP binds to the surface of the micelle in an orientation that has been associated with low cytotoxicity in other amyloid peptides. Most of the residues in rIAPP are highly quenched by the water-soluble Mn^{2+} ion. Since the Mn^{2+} ion cannot penetrate into the hydrophobic core of the micelle, this result indicates most of the residues in rIAPP are located at solvent-accessible sites in the micelle. A peptide bound to the surface of the micelle will have a periodic quenching efficiency reflective of the asymmetric solvent exposure of the two faces of the helix. On the other hand, a helix that is deeply inserted into the micelle will be largely insensitive to the presence of Mn^{2+} ions, except for residues at the ends of the helix that extend into the solvent or into the interfacial region of the micelle. In the rIAPP sample, the quenching efficiency oscillates periodically in the main helical region from T6 to approximately R18, with maximal quenching occurring approximately every $i + 4$ residues as is expected for a surface bound α-helix (Figure 3-8). The existence of highly quenched

residues also indicates rIAPP is relatively tightly bound to the micelle and not dissociating from the surface despite the neutral overall charge on DPC. The unstructured C-terminus (G24-Y37) of the peptide is almost completely quenched by Mn^{2+}, indicating this region extends out of the micelle into the solvent (Figure 3-10). Although the orientation of the N-terminal region cannot be directly determined from the quenching data due to the lack of signal in this area, it can be inferred that this region curves toward the micelle based on the hydrophobicity of these residues.

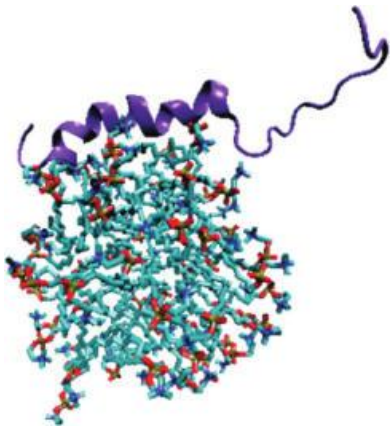

Figure 3-10. A cartoon representation of rIAPP binding to the surface of the micelle. The micelle structure was obtained from a molecular dynamics simulation of 54 DPC molecules in explicit water [*78*].

The importance of membrane binding topology in controlling the toxicity of IAPP has been illustrated by experiments on the rat and human versions of the $IAPP_{1-19}$ fragment. Human IAPP and $hIAPP_{1-19}$ have similar toxicity to *β*-cells [*17*]. The analogous $rIAPP_{1-19}$ peptide is significantly less toxic despite differing from $hIAPP_{1-19}$ only by the single substitution of Arg for His at residue 18 and can only disrupt membranes at high peptide to lipid ratios which are likely to facilitate peptide oligomerization and membrane insertion [*19*]. This difference in toxicity of

the two peptides is associated with a corresponding difference in membrane binding topologies. At neutral pH, $hIAPP_{1-19}$ is buried within the micelle, whereas $rIAPP_{1-19}$ adopts a surface associated binding mode. Protonation of H18 in $hIAPP_{1-19}$ moves the peptide to the surface of the micelle and is accompanied by a corresponding decrease in toxicity [*18, 19*]. Neutron diffraction, fluorescence anisotropy measurements, and analysis of packing density all suggest a similar, deeply inserted binding mode for the full-length human IAPP peptide [*9, 16, 50*]. Although EPR quenching experiments have shown a surface associated topology for hIAPP at low peptide-to-lipid ratios, [*14*] it is likely that this topology is associated with peptide in a monomeric form that is associated with low toxicity [*9, 19*].

Differences in the position and flexibility of the N-terminal loop contribute to differences in self-association for IAPP variants. The differences in the location of the peptides within the membrane observed are insufficient to explain the relative toxicity of IAPP variants. Although both $rIAPP_{1-19}$ and full length rIAPP adopt a surface-associated orientation, there are still significant differences in toxicity between the two peptides [*19*]. Although the full-length rIAPP peptide is almost entirely nontoxic, $rIAPP_{1-19}$ is moderately toxic to *β*-cells. Significantly, $rIAPP_{1-19}$ can disrupt membranes at high peptide-to-lipid ratios, suggesting that although membrane-mediated oligomerization is impaired in $rIAPP_{1-19}$ it is not almost entirely absent as it is in rIAPP. Membrane insertion cannot easily occur for IAPP without oligomerization, as the charged arginine (R11) in the middle of the amphipathic helix cannot be buried in the membrane

without the formation of a water-filled channel or major distortions of the bilayer. As oligomerization is essential for cooperative membrane binding and membrane disruption, structural differences in rIAPP which affect self-association may explain the lack of toxicity of this peptide. Aggregation of the IAPP peptide is believed to be mediated by favorable coiled coil interactions among the leucine residues located on the hydrophobic face of the amphipathic helix [*9*]. Blockage of this site can therefore be expected to be associated with a decrease in self-association and toxicity. Intriguingly, both properties correlate with the position and flexibility of the N-terminal loop (residues 2-7). In all the membrane-bound IAPP structures solved thus far, this region adopts a loosely coiled conformation due to the structural constraints imposed by the C2-C7 disulfide bridge. In the structure of the highly toxic hIAPP and $hIAPP_{1-19}$ peptides, the N-terminal loop is bent away from the hydrophobic interface [*18*]. In this position the hydrophobic side of the helix is exposed and can mediate hydrophobic interactions that favor the formation of a helical bundle (Figure 3-11, parts A and B, respectively). Conversely, in the structure of nontoxic rIAPP this loop is bent toward the hydrophobic face of the helix in a manner that would block binding of IAPP to the hydrophobic face of the helix (see Figure 3-11C). The N-terminus of moderately toxic $rIAPP_{1-19}$ is also tilted toward the hydrophobic face of the helical region (Figure 3-11D) [*18*]. However, the N-terminal loop of $rIAPP_{1-19}$ is considerably more flexible than that of rIAPP. The extra flexibility in the N-terminus of $rIAPP_{1-19}$ is likely to facilitate a movement of this region away from the hydrophobic face of the helix upon dimerization. The greater rigidity of the rIAPP N-terminal loop can

be seen by a comparison of the NOEs in this region. The N-terminal loops of both 1-19 fragments are only constrained in by HA-NH connectivity in the residues adjoining the disulfide bridge and not by any constraints within the N-terminal loop itself, indicating a significant degree of flexibility within the N-terminal loop. The full-length rIAPP structure, on the other hand, has several NOEs within the disulfide bridge, indicating a considerably more rigid N-terminus.

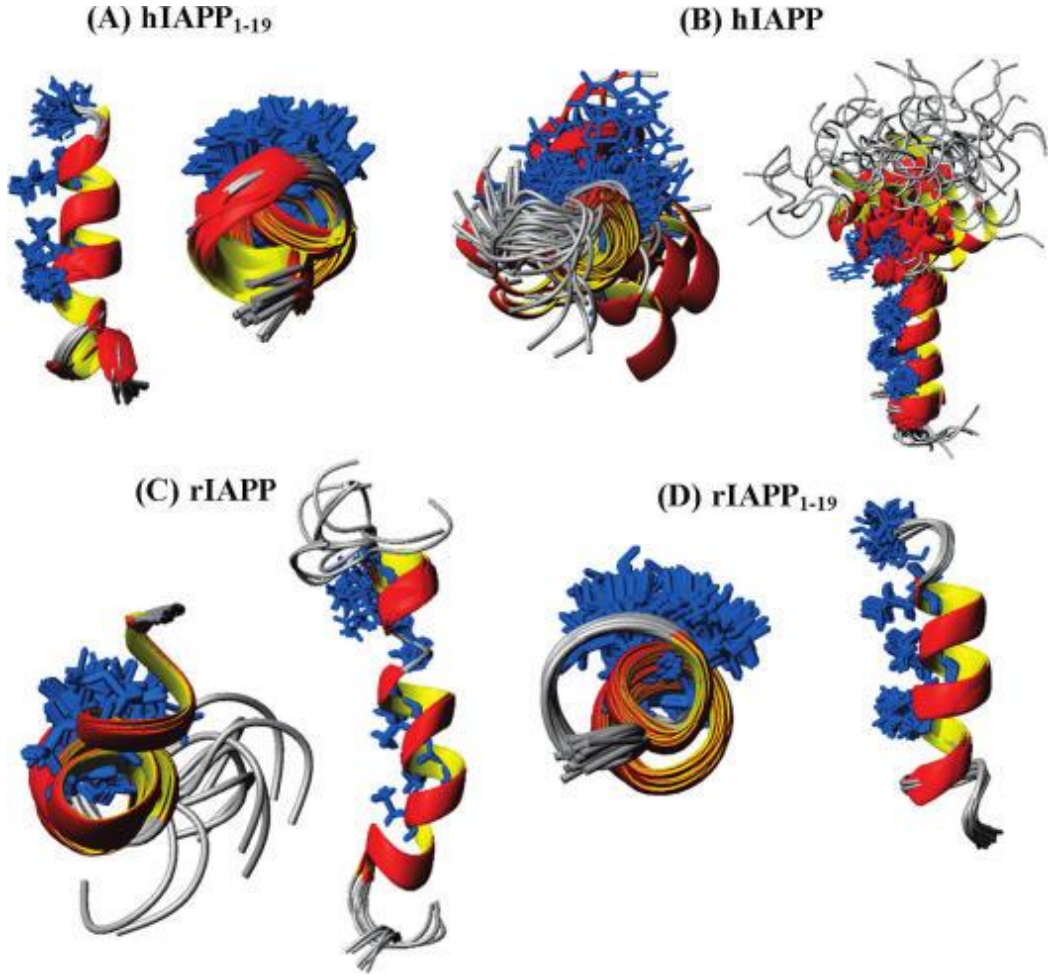

Figure 3-11. Structures of $hIAPP_{1-19}$ (A), hIAPP (B), rIAPP (C), and $rIAPP_{1-19}$ (D) showing the degree of occlusion of the putative self-association site by the N-terminal loop in each structure. The hydrophobic residues that have been implicated in coiled-coil interactions stabilizing the IAPP oligomer are colored in blue.

The sequences of all the IAPP variants discussed above are identical up

to residue 18, and it may seem paradoxical that the N-terminal regions are different in the absence of any tertiary structure in the peptides. The likely source of this difference is alterations in the peptide-membrane interactions, which also aids in explaining the differing propensities of the peptides to aggregate. In solution, rIAPP is prevented from aggregating largely by the conformational restraints imposed by the three proline residues [*7, 8*]. However, it is important to note that hIAPP with triple proline substitutions displays greatly reduced, but still detectable, aggregation [*47*]. This suggests that the charge on R18 and alterations in the N-terminus play some role in the relative aggregation propensity. Aggregation rates are greatly enhanced once the peptide is bound to the membrane due to the concentrating effect of restricting diffusion to a two dimensional surface and the restriction of angular motion [*16, 51, 52*]. Several features of the membrane-bound rIAPP act in concert to retard aggregation and the formation of toxic oligomers. First, the charge on R18 inhibits the deep insertion of the peptide into the membrane as seen for the $rIAPP_{1-19}$ peptide [*18, 19*]. Furthermore, the disordered C-terminus in rIAPP that is absent in $rIAPP_{1-19}$ compounds the difficulty of membrane insertion as hydrogen bonding of the peptide to solvent cannot be accommodated in the hydrophobic interior of an intact membrane. This difference in the C-terminal end of the peptide likely has the effect of altering the interaction of rIAPP with the membrane compared to $rIAPP_{1-19}$. The likely result of this difference in the interactions of rIAPP, $rIAPP_{1-19}$, $hIAPP_{1-19}$, and most likely hIAPP with the membrane are alterations of the structure and dynamics at the N-terminus, which could impact the self-

association of IAPP as discussed above.

Significance of the structure for the normal biological activity of IAPP. IAPP belongs to the CGRP family of peptides that includes calcitonin-gene-related peptide (CGRP), calcitonin, adrenomodulin, and IAPP [*53*]. Although the sequences of these peptides are somewhat dissimilar, all the peptides in this family bind to common G-coupled protein receptors and produce similar effects in many tissues [*54, 55*]. Many of the peptides in this family such as human CGRP and calcitonin are also amyloidogenic and aggregate to form membrane-disruptive oligomeric structures [*56-59*]. NMR studies on these peptides in detergent micelles have shown that these properties are apparently linked to common structural elements held among the family. All of the peptides in this family possess an amidated C-terminus, an amphipathic helix near the N-terminus, a largely disordered C-terminus, and an N-terminal ring connected by a disulfide bond [*60-63*]. Two binding sites have been proposed for the binding of peptides of this family to the membrane-bound receptor: one near the membrane surface that would be consistent with the orientation found in this study for rIAPP and another requiring a more deeply inserted membrane orientation as found for $hIAPP_{1-19}$ and hypothesized for hIAPP [*60, 64, 65*]. Relatively little is known about structure activity relationships for IAPP's normal biological action in comparison to its pathological aggregation. Experiments on truncated versions of calcitonin and CGRP (the closest homologue of IAPP) have shown that the formation of the amphipathic helix is sufficient for receptor binding but activation of the receptor requires the N-terminal ring [*66*]. Removal of the N-terminal ring

or reduction of the disulfide bridge results in CGRP binding to its receptor in an inactive conformation. A similar N-truncated rIAPP construct ($rIAPP_{8-37}$) has been shown to act as an antagonist for rIAPP's effects on insulin secretion and carbohydrate and lipid metabolism [*67-69*]. Given the importance of the N-terminal ring for the biological activity of IAPP, it would be interesting to further study the biological activity of IAPP in light of the structural differences in the N-terminal ring shown here for rIAPP and $IAPP_{1-19}$ and is hypothesized for hIAPP [*70*].

Several structural features that have been shown to be important for other members of this family are absent in the rIAPP structure. A *β*-turn centered on P34 has been shown to be important for the activity of the related calcitonin [*60, 71, 72*] and CGRP peptides [*62, 73, 74*]. Similar *β*-turns have been shown to be a common feature for the activation of other peptide-activated G-coupled protein receptors [*75*]. This turn is absent in both the rIAPP and hIAPP structures, although the 20-29 fragment of hIAPP adopts a similar distorted type I *β*-turn that has been implicated in the binding of IAPP to glycolipids [*42, 76, 77*]. However, since considerable flexibility exists at this site it is possible that IAPP adopts the *β*-turn conformation in this region seen in its homologues upon binding to the IAPP receptor. A significant degree of mobility has also been detected by EPR at residues 21 and 22 for hIAPP bound to small unilamellar vesicles [*14*]. An interaction of the disordered C-terminus with the N-terminus has been invoked as contributing to the higher potency of salmon calcitonin over human calcitonin [*60, 61*]. This interaction is also absent in rIAPP. The C-terminus of rIAPP is folded

away from the helix as in the human calcitonin structure, as indicated by the absence of medium- or long-range NOEs in this region [*60*].

3.6 CONCLUSION

We have solved the first structure of rat IAPP in a membrane environment. By comparing the rIAPP structure with other toxic and nontoxic variants of IAPP, we have identified two structural features that correlate with the toxicity of the peptide. Rat IAPP is bound to the surface in a manner similar to the nontoxic $rIAPP_{1-19}$ and low-pH $hIAPP_{1-19}$ peptides and does not penetrate deeply into the micelle like the toxic neutral pH $hIAPP_{1-19}$ peptide. The position of the N-terminal disulfide bridge has been identified as another factor that may modulate aggregation and toxicity. The nontoxic rIAPP structure has a relatively rigid N-terminus that is bent toward the hydrophobic face of the amphipathic helix, whereas more toxic forms of IAPP have a more flexible N-terminus that is positioned away from the amphipathic helix. A comparison of the rIAPP structure to other homologous peptides that share the same receptors, hIAPP, and also fragments from hIAPP shows rIAPP does not possess the *β*-turn seen in these peptides that is required to activate the receptor, but this region is flexible and may form a *β*-turn upon binding to the receptor. Further structural studies on IAPP, in particular with respect to its normal biological activity, will be particularly useful in understanding the effects of this peptide.

REFERENCES

[1] Haataja, L., Gurlo, T., Huang, C. J., Butler, P. C. (2008) Islet amyloid in type 2 diabetes and the toxic oligomer hypothesis. *Endocr. Rev. 29*, 302-316.

[2] Jayasinghe, S. A., Langen, R. (2007) Membrane interaction of islet amyloid polypeptide. *Biochim. Biophys. Acta 1768*, 2002-2009.

[3] Khemtemourian, L., Killian, J. A., Hoppener, J. W., Engel, M. F. (2008) Recent insights in islet amyloid polypeptide-induced membrane disruption and its role in beta-cell deathin type 2 diabetes mellitus. *Exp. Diabetes Res. 2008*, 421287.

[4] Engel, M. F., Khemtemourian, L., Kleijer, C. C., Meeldijk, H. J., Jacobs, J., Verkleij, A. J., de Kruijff, B., Killian, J. A., Hoppener, J. W. (2008) Membrane damage by human islet amyloid polypeptide through fibril growth at the membrane. *Proc. Natl. Acad. Sci. U.S.A. 105*, 6033-6038.

[5] Quist, A., Doudevski, L., Lin, H., Azimova, R., Ng, D., Frangione, B., Kagan, B., Ghiso, J., Lal, R. (2005) Amyloid ion channels: a common structural link for protein-misfolding disease. *Proc. Natl. Acad. Sci. U.S.A. 102*, 10427-10432.

[6] Huang, C. J., Haataja, L., Gurlo, T., Butler, A. E., Wu, X. J., Soeller, W. C., Butler, P. C. (2007) Induction of endoplasmic reticulum stress-induced beta-cell apoptosis and accumulation of polyubiquitinated proteins by human islet amyloid polypeptide. *Am. J. Physiol. 293*, E1656-E1662.

[7] Westermark, P., Engstrom, U., Johnson, K. H., Westermark, G. T., Betsholtz, C. (1990) Islet amyloid polypeptide: pinpointing amino acid residues linked to amyloid fibril formation. *Proc. Natl. Acad. Sci. U.S.A. 87*, 5036-5040.

[8] Moriarty, D. F., Raleigh, D. P. (1999) Effects of sequential proline substitutions on amyloid formation by human amylin 20-29. *Biochemistry 38*, 1811-1818.

[9] Knight, J. D., Hebda, J. A., Miranker, A. D. (2006) Conserved and cooperative

assembly of membrane-bound alpha-helical states of islet amyloid polypeptide. *Biochemistry 45*, 9496-9508.

[10] Brender, J. R., Durr, U. H. N., Heyl, D., Budarapu, M. B., Ramamoorthy, A. (2007) Membrane fragmentation by an amyloidogenic fragment of human islet amyloid polypeptide detected by solid-state NMR spectroscopy of membrane nanotubes. *Biochim. Biophys. Acta 1768*, 2026-2029.

[11] Green, J. D., Kreplak, L., Goldsbury, C., Blatter, X. L., Stolz, M., Cooper, G. S., Seelig, A., Kist-Ler, J., Aebi, U. (2004) Atomic force microscopy reveals defects within mica supported lipid bilayers induced by the amyloidogenic human amylin peptide. *J. Mol. Biol. 342*, 877-887.

[12] Sparr, E., Engel, M. F. M., Sakharov, D. V., Sprong, M., Jacobs, J., de Kruijff, B., Hoppener, J. W. M., Killian, J. A. (2004) Islet amyloid polypeptide-induced membrane leakage involves uptake of lipids by forming amyloid fibers. *FEBS Lett. 577*, 117-120.

[13] Domanov, Y. A., Kinnunen, P. K. J. (2008) Islet amyloid polypeptide forms rigid lipid-protein amyloid fibrils on supported phospholipid bilayers. *J. Mol. Biol. 376*, 42-54.

[14] Apostolidou, M., Jayasinghe, S. A., Langen, R. (2008) Structure of alpha-helical membrane-bound human islet amyloid polypeptide and its implications for membrane-mediated misfolding. *J. Biol. Chem. 283*, 17205-17210.

[15] Jayasinghe, S. A., Langen, R. (2005) Lipid membranes modulate the structure of islet amyloid polypeptide. *Biochemistry 44*, 12113-12119.

[16] Knight, J. D., Miranker, A. D. (2004) Phospholipid catalysis of diabetic

amyloid assembly. *J. Mol. Biol. 341*, 1175-1187.

[17] Brender, J. R., Lee, E. L., Cavitt, M. A., Gafni, A., Steel, D. G., Ramamoorthy, A. (2008) Amyloid fiber formation and membrane disruption are separate processes localized in two distinct regions of IAPP, the type-2-diabetes-related peptide. *J. Am. Chem. Soc. 130*, 6424-6429.

[18] Nanga, R. P. R., Brender, J. R., Xu, J., Veglia, G., Ramamoorthy, A. (2008) Structures of rat and human islet amyloid polypeptide IAPP(1-19) in micelles by NMR spectroscopy. *Biochemistry 47*, 12689-12697.

[19] Brender, J. R., Hartman, K., Reid, K. R., Kennedy, R. T., Ramamoorthy, A. (2008) A single mutation in the nonamyloidogenic region of islet amyloid polypeptide greatly reduces toxicity. *Biochemistry 47*, 12680-12689.

[20] Rustenbeck, I., Matthies, A., Lenzen, S. (1994) Lipid composition of glucose-stimulated pancreatic islets and insulin-secreting tumor cells. *Lipids 29*, 685-692.

[21] Yonemoto, I. T., Kroon, G. J., Dyson, H. J., Balch, W. E., Kelly, J. W. (2008) Amylin proprotein processing generates progressively more amyloidogenic peptides that initially sample the helical state. *Biochemistry 47*, 9900-9910.

[22] Williamson, J. A., Miranker, A. D. (2007) Direct detection of transient alpha-helical states in islet amyloid polypeptide. *Protein Sci. 16*, 110-117.

[23] Delaglio, F., Grzesiek, S., Vuister, G. W., Zhu, G., Pfeifer, J., Bax, A. (1995) NMRPipe: a multidimensional spectral processing system based on UNIX pipes. *J. Biomol. NMR 6*, 277-293.

[24] Goddard, T. D., Kneller, D. G. (1999) SPARKY 3; University of California, San Francisco, California.

[25] Wuthrich, K. (1986) *NMR of Proteins and Nucleic Acids*. John Wiley and Sons: New York.

[26] Nilges, M., Gronenborn, A. M., Brunger, A. T., Clore, G. M. (1988) Determination of three-dimensional structures of proteins by simulated annealing with interproton distance restraints. Application to crambin, potato carboxypeptidase inhibitor and barley serine proteinase inhibitor 2. *Protein Eng. 2*, 27-38.

[27] Stein, E. G., Rice, L. M., Brunger, A. T. (1997) Torsion-angle molecular dynamics as a new efficient tool for NMR structure calculation. *J. Magn. Reson. 124*, 154-164.

[28] Cornilescu, G., Delaglio, F., Bax, A. (1999) Protein backbone angle restraints from searching a database for chemical shift and sequence homology. *J. Biomol. NMR 13*, 289-302.

[29] Laskowski, R. A., Rullman, J. A. C., MacArther, M. W., Kaptein, R., Thornton, J. M. (1996) AQUA and PROCHECK-NMR: programs for checking the quality of protein structures solved by NMR. *J. Biomol. NMR 8*, 477-486.

[30] Pappalardo, G., Milardi, D., Magri, A., Attanasio, F., Impellizzeri, G., La Rosa, C., Grasso, D., Rizzarelli, E. (2007) Environmental factors differently affect human and rat IAPP: conformational preferences and membrane interactions of IAPP17-29 peptide derivatives. *Chem. Eur. J. 13*, 10204-10215.

[31] Grasso, D., Milardi, D., La Rosa, C., Rizzarelli, E. (2001) DSC study of the interaction of the prion peptide PrP106-126 with artificial membranes. *New J. Chem. 25*, 1543-1548.

[32] Sciacca, M. F. M., Pappalardo, M., Milardi, D., Grasso, D. M., La Rosa, C. (2008) Calcium-activated membrane interaction of the islet amyloid polypeptide: implications in the pathogenesis of type II diabetes mellitus. *Arch. Biochem. Biophys. 477*, 291-298.

[33] Thennarasu, S., Lee, D. K., Poon, A., Kawulka, K. E., Vederas, J. C., Ramamoorthy, A. (2005) Membrane permeabilization, orientation, and antimicrobial mechanism of subtilosin A. *Chem. Phys. Lipids 137*, 38-51.

[34] Hallock, K. J., Lee, D. K., Omnaas, J., Mosberg, H. I., Ramamoorthy, A. (2002) Membrane composition determines pardaxin's mechanism of lipid bilayer disruption. *Biophys. J. 83*, 1004-1013.

[35] Henzler-Wildman, K. A., Martinez, G. V., Brown, M. F., Ramamoorthy, A. (2004) Perturbation of the hydrophobic core of lipid bilayers by the human antimicrobial peptide LL-37. *Biochemistry 43*, 8459-8469.

[36] Coles, M., Bicknell, W., Watson, A. A., Fairlie, D. P., Craik, D. J. (1998) Solution structure of amyloid beta-peptide(1-40) in a water-micelle environment. Is the membrane-spanning domain where we think it is? *Biochemistry 37*, 11064-11077.

[37] Mandal, P. K., Pettegrew, J. W. (2004) Alzheimer's disease: soluble oligomeric Abeta(1-40) peptide in membrane mimic environment from solution NMR and circular dichroism studies. *Neurochem. Res. 29*, 2267-2272.

[38] Ulmer, T. S., Bax, A. (2005) Comparison of structure and dynamics of micelle-bound human alpha-synuclein and Parkinson disease variants. *J. Biol. Chem. 280*, 43179-43187.

[39] Ulmer, T. S., Bax, A., Cole, N. B., Nussbaum, R. L. (2005) Structure and dynamics of micelle-bound human alpha-synuclein. *J. Biol. Chem. 280*, 9595-9603.

[40] Jarvet, J., Danielsson, J., Damberg, P., Oleszczuk, M., Graeslund, A. (2007) Positioning of the Alzheimer Abeta(1-40) peptide in SDS micelles using NMR and paramagnetic probes. *J. Biomol. NMR 39*, 63-72.

[41] Shao, H. Y., Jao, S. C., Ma, K., Zagorski, M. G. (1999) Solution structures of micelle-bound amyloid beta-(1-40) and beta-(1-42) peptides of Alzheimer's disease. *J. Mol. Biol. 285*, 755-773.

[42] Patil, S. M., Xu, S., Sheftic, S. R., Alexandrescu, A. T. (2009) Dynamic alpha-helix structure of micelle-bound human amylin. *J. Biol. Chem. 284*, 11982-11991.

[43] Luca, S., Yau, W. M., Leapman, R., Tycko, R. (2007) Peptide conformation and supramolecular organization in amylin fibrils: constraints from solid-state NMR. *Biochemistry 46*, 13505-13522.

[44] Wiltzius, J. J. W., Sievers, S. A., Sawaya, M. R., Cascio, D., Popov, D., Riekel, C., Eisenberg, D. (2008) Atomic structure of the cross-beta spine of islet amyloid polypeptide (amylin). *Protein Sci. 17*, 1467-1474.

[45] Kajava, A. V., Aebi, U., Steven, A. C. (2005) The parallel superpleated beta-structure as a model for amyloid fibrils of human amylin. *J. Mol. Biol. 348*, 247-252.

[46] Abedini, A., Raleigh, D. P. (2009) A role for helical intermediates in amyloid formation by natively unfolded polypeptides? *Phys. Biol. 6*, 15005.

[47] Abedini, A., Raleigh, D. P. (2006) Destabilization of human IAPP amyloid fibrils by proline mutations outside of the putative amyloidogenic domain: is there a critical amyloidogenic domain in human IAPP? *J. Mol. Biol. 355*, 274-281.

[48] Koo, B. W., Hebda, J. A., Miranker, A. D. (2008) Amide inequivalence in the fibrillar assembly of islet amyloid polypeptide. *Protein Eng., Des. Sel. 21*, 147-154.

[49] Green, J., Goldsbury, C., Min, T., Sunderji, S., Frey, P., Kistler, J., Cooper, G., Aebi, U. (2003) Full-length rat amylin forms fibrils following substitution of single residues from human amylin. *J. Mol. Biol. 326*, 1147-1156.

[50] Balali-Mood, K., Ashley, R. H., Hauss, T., Bradshaw, J. P. (2005) Neutron diffraction reveals sequence-specific membrane insertion of pre-fibrillar islet amyloid polypeptide and inhibition by rifampicin. *FEBS Lett. 579*, 1143-1148.

[51] Bokvist, M., Grobner, G. (2007) Misfolding of amyloidogenic proteins at membrane surfaces: the impact of macromolecular crowding. *J. Am. Chem. Soc. 129*, 14848.

[52] Aisenbrey, C., Borowik, T., Bystrom, R., Bokvist, M., Lindstrom, F., Misiak, H., Sani, M. A., Grobner, G. (2008) How is protein aggregation in amyloidogenic diseases modulated by biological membranes? *Eur. Biophys. J. Biophys. Lett. 37*, 247-255.

[53] Wimalawansa, S. J. (1997) Amylin, calcitonin gene-related peptide, calcitonin, and adrenomedullin: a peptide superfamily. *Crit. Rev. Neurobiol. 11*, 167-239.

[54] Lutz, T. A., Tschudy, S., Rushing, P. A., Scharrer, E. (2000) Amylin

receptors mediate the anorectic action of salmon calcitonin (sCT). *Peptides 21*, 233-238.

[55] Christopoulos, G., Perry, K. J., Morfis, M., Tilakaratne, N., Gao, Y. Y., Fraser, N. J., Main, M. J., Foord, S. M., Sexton, P. M. (1999) Multiple amylin receptors arise from receptor activity-modifying protein interaction with the calcitonin receptor gene product. *Mol. Pharmacol. 56*, 235-242.

[56] Diociaiuti, M., Polzi, L. Z., Valvo, L., Malchiodi-Albedi, F., Bombelli, C. Guadiano, M. C. (2006) Calcitonin forms oligomeric pore-like structures in lipid membranes *Biophys. J. 91*, 2275-2281.

[57] Fowler, S. B., Poon, S., Muff, R., Chiti, F., Dobson, C. M., Zurdo, J. (2005) Rational design of aggregation-resistant bioactive peptides: reengineering human calcitonin. *Proc. Natl. Acad. Sci. U.S.A. 102*, 10105-10110.

[58] Micelli, S., Meleleo, D., Picciarelli, V., Gallucci, E. (2006) Effect of pH-variation on insertion and ion channel formation of human calcitonin into planar lipid bilayers. *Front. Biosci. 11*, 2035-2044.

[59] Stipani, V., Gallucci, E., Micelli, S., Picciarelli, V., Benz, R. (2001) Channel formation by salmon and human calcitonin in black lipid membranes. *Biophys. J. 81*, 3332-3338.

[60] Motta, A., Andreotti, G., Amodeo, P., Strazzullo, G., Morelli, M. A. C. (1998) Solution structure of human calcitonin in membrane-mimetic environment: the role of the amphipathic helix. *Proteins 32*, 314-323.

[61] Motta, A., Pastore, A., Goud, N. A., Morelli, M. A. C. (1991) Solution conformation of salmon calcitonin in sodium dodecyl sulfate micelles as

determined by two-dimensional NMR and distance geometry calculations. *Biochemistry 30*, 10444-10450.

[62] Carpenter, K. A., Schmidt, R., von Mentzer, B., Haglund, U., Roberts, E., Walpole, C. (2001) Turn structures in CGRP C-terminal analogues promote stable arrangements of key residue side chains. *Biochemistry 40*, 8317-8325.

[63] Oconnell, J. P., Kelly, S. M., Raleigh, D. P., Hubbard, J. A. M., Price, N. C., Dobson, C. M., Smith, B. J. (1993) On the role of the C-terminus of alpha-calcitonin-gene-related peptide (alpha CGRP). The structure of des-phenylalaninamide 37-alpha CGRP and its interaction with the CGRP receptor. *Biochem. J. 291*, 205-210.

[64] Morelli, M. A. C., Pastore, A., Motta, A. (1992) Dynamic properties of salmon calcitonin bound to sodium dodecyl sulfate micelles: a restrained molecular dynamics study from NMR data. *J. Biomol. NMR 2*, 335-348.

[65] Nakamuta, H., Orlowski, R. C., Epand, R. M. (1990) Evidence for calcitonin receptor heterogeneity: binding studies with nonhelical analogs. *Endocrinology 127*, 163-169.

[66] Kapurniotu, A. (2004) Contribution of conformationally constrained calcitonin (Ct) analogs to the understanding of the structural and conformational requirements of calcitonin bioactivity and to the design of potent agonists. *Curr. Med. Chem. 11*, 2845-2865.

[67] Hettiarachchi, M., Chalkley, S., Furler, S. M., Choong, Y. S., Heller, M., Cooper, G. J. S., Kraegen, E. W. (1997) Rat amylin-(8-37) enhances insulin action and alters lipid metabolism in normal and insulin-resistant rats. *Am. J.*

Physiol. 36, E859-E867.

[68] Wang, M. W., Young, A. A., Rink, T. J., Cooper, G. J. S. (1991) 8-37h-CGRP antagonizes actions of amylin on carbohydrate metabolism in vitro and in vivo. *FEBS Lett. 291*, 195-198.

[69] Ye, J. M., Lim-Fraser, M., Cooney, G. J., Cooper, G. J. S., Iglesias, M. A., Watson, D. G., Choong, B., Kraegen, E. W. (2001) Evidence that amylin stimulates lipolysis in vivo: a possible mediator of induced insulin resistance. *Am. J. Physiol. 280*, E562-E569.

[70] Neumann, J. M., Couvineau, A., Murail, S., Lacapere, J. J., Jamin, N., Laburthe, M. (2008) Class-B GPCR activation: is ligand helix-capping the key? *Trends Biochem. Sci. 33*, 314-319.

[71] Kazantzis, A., Waldner, M., Taylor, J. W., Kapurniotu, A. (2002) Conformationally constrained human calcitonin (hCt) analogues reveal a critical role of sequence 17-21 for the oligomerization state and bioactivity of hCt. *Eur. J. Biochem. 269*, 780-791.

[72] Kapurniotu, A., Kayed, R., Taylor, J. W., Voelter, W. (1999) Rational design, conformational studies and bioactivity of highly potent conformationally constrained calcitonin analogues. *Eur. J. Biochem. 265*, 606-618.

[73] Lang, M., De Pol, S., Baldauf, C., Hofmann, H. J., Reiser, O., Beck-Sickinger, A. G. (2006) Identification of the key residue of calcitonin gene related peptide (CGRP) 27-37 to obtain antagonists with picomolar affinity at the CGRP receptor. *J. Med. Chem. 49*, 616-624.

[74] Wisskirchen, F. M., Doyle, P. M., Gough, S. L., Harris, C. J., Marshall, I.

(1999) Conformational restraints revealing bioactive beta-bend structures for halpha CGRP8-37 at the CGRP2 receptor of the rat prostatic vas deferens. *Br. J. Pharmacol. 126*, 1163-1170.

[75] Tyndall, J. D. A., Pfeiffer, B., Abbenante, G., Fairlie, D. P. (2005) Over one hundred peptide-activated G protein-coupled receptors recognize ligands with turn structure. *Chem. Rev. 105*, 793-826.

[76] Levy, M., Garmy, N., Gazit, E., Fantini, J. (2006) The minimal amyloid-forming fragment of the islet amyloid polypeptide is a glycolipid-binding domain. *FEBS J. 273*, 5724-5735.

[77] (a) Mascioni, A., Porcelli, F., Ilangovan, U., Ramamoorthy, A., Veglia, G. (2003) Conformational preferences of the amylin nucleation site in SDS micelles: an NMR study. *Biopolymers 69*, 29-41. (b) Ilangovan, U., Ramamoorthy, A. (1998) Conformational studies of human islet amyloid peptide using molecular dynamics and simulated annealing methods. *Biopolymers 45*, 9-20.

[78] Tieleman, D. P., van der Spoel, D., Berendsen, H. J. C. (2000) Molecular dynamics simulations of dodecylphosphocholine micelles at three different aggregate sizes: micellar structure and lipid chain relaxation. *J. Phys. Chem. B 104*, 6380-6388.

CHAPTER 4. THE C-TERMINUS OF AMIDATED IAPP IS LARGELY HELICAL AT PHYSIOLOGICAL pH IN A MEMBRANE ENVIRONMENT : AN NMR STUDY

This chapter is a version of a manuscript submitted to Biophys. J.[3]

4.1 ABSTRACT

Human islet amyloid polypeptide is a hormone coexpressed with insulin by pancreatic beta-cells. For reasons not clearly understood, hIAPP aggregates in type II diabetics to form oligomers that interfere with beta-cell function, eventually leading to the loss of insulin production. The cellular membrane catalyzes the formation of amyloid deposits and is a target of amyloid toxicity through disruption of the membrane's structural integrity. Previously, the structure of recombinant hIAPP has been solved in SDS micelles at acidic pH. However, the naturally expressed peptide has an amidated C-terminus not present in the recombinant form and aggregation into the fibrillar form primarily occurs at a neutral pH. Since the aggregation of hIAPP is highly influenced by electrostatic interactions, we determined the structure of hIAPP with an amidated C-terminus in SDS micelles at pH 7.3. Both structures have an overall kinked helix motif, with residues 7-17 and 21-28 in a helical conformation in both structures. However, unlike the previously solved structure, the C-terminus of amidated hIAPP is also structured, with a 3_{10} dynamic helix from Gly33-Asn35. In addition, the angle between the N- and C-terminal helices is constrained to 85º instead of the free

[3] Subramanian Vivekanandan helped in structural calculations. Jeffrey Brender helped in writing the manuscript. This study was supported by the funds from NIH (DK 078885 to A.R.).

rotation present in the structure of recombinant hIAPP. These changes allow a greater penetration of the peptide into the micelle surface, as shown by paramagnetic quenching studies, and are likely to play a role in its aggregation.

4.2 INTRODUCTION

Human Islet Amyloid Polypeptide (also known as amylin) is a 37 residue peptide hormone secreted from pancreatic β-cells (Figure 4-1). In its normal physiological role, hIAPP is associated with appetite suppression and, in conjunction with insulin, in maintaining proper glycemic levels [*1*]. However, a change in the cellular environment in the early stages of type II diabetes, poorly understood at present, causes it to aggregate into dense, insoluble fibrillar deposits that accumulate in the pancreas [*2*]. These proteinaceous deposits, known as amyloid, have a characteristic β-sheet secondary structure similar to those found in Alzheimer's, Parkinson's, Huntington's, and a variety of other degenerative disorders [*3*]. Like the amyloid deposits found in these diseases, hIAPP aggregates of various forms have been linked to cellular death and impairment of normal tissue functioning [*4-6*].

Figure 4-1. Primary sequence of the C-terminus-amidated human IAPP including the disulfide bridge between Cys2 and Cys7.

One of the primary mechanisms by which hIAPP and amyloidogenic peptides in general cause cellular death is the disruption of the integrity of the cellular membrane [*7*]. Human islet amyloid polypeptide, but not the non-amyloidogenic rat variant, has been shown to cause significant impairment of the

integrity of the phospholipid membrane in both model membranes and in cells [*8-13*]. The exact mechanism of membrane disruption is unknown but has been linked to peptide aggregation on the membrane surface [*8, 11, 12*]. Binding of hIAPP to lipid membranes also markedly accelerates the aggregation to fibril formation, a factor that is likely to be important in determining the final amount of amyloid deposition [*14-16*].

Human IAPP initially binds to the membrane in an α-helical state. Once bound to the membrane, aggregation of the peptide causes a cooperative conformational change from the helical conformation to the β-sheet amyloid form [*17-20*]. In order to gain a better insight in to this process, the structure of hIAPP bound to SDS micelles was recently solved [*21*]. In this system, hIAPP is monomeric and adopts a largely α-helical conformation, [*21*] in general agreement with the initial membrane-bound conformation of the peptide in other membrane types [*18, 19*]. More specifically, the structure was a single helix from residues 5-28, with the helix kinked near residues 18-22 and the stability of the helix decreasing towards the C-terminal end [*21*]. The peptide was found to be bound to the micelle surface with a slight penetration of the N-terminal helix into the detergent headgroup region [*21*].

However, several differences exist between the conditions used to solve this structure and those likely to be encountered by hIAPP in the physiological setting. First, the studies were performed at an acidic pH of 4.6 [*21*]. A recent NMR study on a truncated version of hIAPP ($hIAPP_{1-19}$) showed that protonation of His18 causes a change in its membrane binding topology from a buried to a

surface associated state [*22*]. This observed change in membrane topology with pH was linked with a greatly reduced potential of $hIAPP_{1-19}$ to disrupt phospholipid vesicles, a phenomenon that was also observed for β-cell membranes as demonstrated by a H18R $hIAPP_{1-19}$ mutant [*9*]. Further, the aggregation of hIAPP is strongly pH dependent [*23, 24*], with protonation of H18 slowing the aggregation by a factor of ~4 [*24*]. The decrease in the aggregation potential of hIAPP at acidic pH is one factor that allows hIAPP to be safely stored in the secretory granule (pH ~5.5) in a presumably non-aggregated form [*25*].

Second, hIAPP is normally expressed with an amidated C-terminus that is essential for proper biological function [*26*]. The NMR study used a recombinant form of the peptide with a non-amidated C-terminus, altering the electrostatic interactions at the C-terminal end of the peptide [*21*]. This small change is significant for hIAPP as studies have shown that the free acid of hIAPP is significantly less amyloidogenic than the amidated version [*27*]. In addition, a recent study has shown relatively strong interactions between protonated His18 and Tyr37, [*28*] which may partly be attributable to a salt bridge formation between His 18 and the C-terminus, an interaction that will not occur in the amidated peptide. Therefore, it is important to determine the structure of membrane-bound hIAPP under conditions more close to the physiological state. In this study, we have solved the high-resolution structure of C-terminus-amidated hIAPP in SDS micelles and determined the membrane-binding topology with respect to the micelle at physiological pH. Our results indicate a substantial structural difference in the C-terminus of the peptide, which is

disordered in the previous hIAPP structure but is ordered under the conditions employed in this study.

4.3 MATERIALS AND METHODS

4.3.1 *Sample preparation*. Human IAPP (hIAPP) was synthesized and purified by SynBioSci (Toronto, ON) with a disulfide bridge from residues Cys2-Cys7 and an amidated C-terminus. The peptide was dissolved in hexafluoroisopropanol to monomerize the preformed aggregates of hIAPP, and then lyophilized to remove the solvent. For NMR experiments, the sample was prepared by dissolving a 3 mg of lyophilized peptide in 20 mM sodium phosphate buffer at pH ~7.3 containing 10% D_2O, 120 mM NaCl and 200 mM perdeuterated SDS (Cambridge Isotopes Laboratory) to a final peptide concentration of 2.5 mM.

4.3.2 *NMR Data Collection and Processing.* All NMR experiments on SDS micelles containing hIAPP were performed at 25 °C using a 900 MHz Bruker Avance NMR spectrometer equipped with a triple-resonance cryogenic probe. After optimizing the experimental parameters using 1D ^{1}H NMR spectrum of the sample, a 2D ^{1}H-^{1}H TOCSY spectrum was recorded with an 80 ms mixing time and 2D ^{1}H-^{1}H NOESY spectra were recorded at 100 ms and 300 ms mixing times in order to assign backbone and side-chain resonances. Complex data points were acquired for quadrature detection in both frequency dimensions of the 2D experiments. For all the spectra, zero-filling was applied in both dimensions to yield matrices of 2048 x 2048 points. Proton chemical shifts were referenced by setting the water peak at 4.7 ppm. All 2D spectra were processed using TopSpin 2.1 software (from Bruker) and analyzed using SPARKY [29].

Resonance assignments were done using a standard approach as reported elsewhere [30].

4.3.3 ***Structure Calculations.*** The final structural calculations were carried out with the CYANA 2.1 program package using simulated annealing in combination with molecular dynamics in torsion angle space.(*31*) NOE connectivities were used for the calculation of dihedral angle restraints [32]. Unambiguous long-range NOE constraints were used during the first round of structural calculations to generate an initial low-resolution structure. The remaining ambiguous NOE cross-peaks were assigned in an iterative fashion by applying a structure-aided filtering strategy in repeated rounds of structure calculations [33]. A total of 500 conformers were calculated using 8000 annealing steps for each conformer after complete assignment of resonances. The lowest 20 energy conformers were selected and visualized using MOLMOL [34].

4.3.4 ***Paramagnetic Quenching.*** 2D ^{1}H-^{1}H TOCSY spectra of hIAPP embedded in SDS micelles were recorded in the absence and in the presence of 0.8 mM $MnCl_2$. All the other experimental conditions were the same as mentioned above.

4.4 RESULTS

4.4.1 ***3D Structure of hIAPP in SDS micelles****.* 2D ^{1}H-^{1}H TOCSY and NOESY spectra of hIAPP embedded in SDS micelles were used to assign the backbone and side chain resonances of the peptide. The deviation of the H_α chemical shifts from the corresponding values for a random coil structure (H_α chemical shift index) was used as an indicator of the secondary structure of the peptide. In an

α-helical structure, H_α protons experience a shift to higher field corresponding to a negative deviation in the CSI plot. A negative deviation spanning 3 or more residues indicates the propensity for an α-helical conformation. The CSI plot shows the propensity for a helix formation in two regions of the hIAPP, a longer helix in the region from Ala5 to Ser28 and a shorter helix from Ser34 to Tyr37 as shown in Figure 4-2. The chemical shift value for the H_α proton of Cys2 was not observed in the spectra, most likely due to a chemical exchange process.

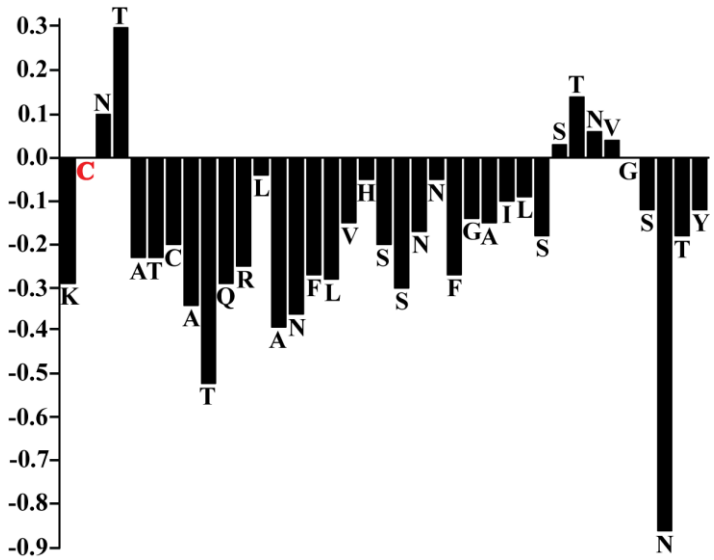

Figure 4-2. α-Proton chemical shift index measured from hIAPP embedded in SDS micelles. The CSI was calculated by subtracting the appropriate random coil chemical shifts reported in the literature. A CSI ≤ -0.1 is considered indicative of a helical conformation.

The fingerprint region of the NOESY spectra obtained at a 300 ms mixing time is shown in Figure 4-3 with sequential assignment of residues. From the analysis of 2D NOESY spectra, we have assigned a total of 568 (446 short, 119 medium and 3 long range) NOEs for hIAPP (Figure 4-4). The final 3D structure of the peptide is presented in Figure 4-5 (pdb id 2L86). The superposition of backbone atoms from residues 7 to 37 gives an RMSD of 0.46 ± 0.15 Å as

shown in Figure 4-5, while the superposition of all heavy atoms gives an RMSD of 1.09 ± 0.23 Å (see Table 4-1 for more structure statistics). Three helical domains are evident from the numerous $d_{NN}(i,i+1)$, $d_{NN}(i,i+2)$, $d_{\alpha\beta}(i,i+3)$, $d_{\alpha N}(i,i+3)$ and $d_{\alpha N}$ (i,i+4) NOE connectivities that are diagnostic of an α-helix as shown in Figure 4-5. Two of the helical domains extending from residues Cys7-Val17

Table 4-1. Statistical information for the hIAPP structural ensemble.

Distance constraints		
	Total	568
	Short (i – j ≤ 1)	446
	Medium (i – j = 2, 3, 4)	119
	Long (i – j ≥ 5)	3
Structural statistics		
	Violated distance constrains	0
	Violated angle constrains	0
	RMSD of all backbone atoms (Å)	
	Cys 7 – Tyr 37	0.49 ± 0.17
	RMSD of all heavy atoms (Å)	
	Cys 7 – Tyr 37	1.32 ± 0.27
Ramachandran plot		
	Residues in most favored region (%)	86.6
	Residues in additionally allowed region (%)	10.8
	Residues in additionally allowed region (%)	2.6

and Asn21-Ser28 are stable α-helices, while the third is a short dynamic 3_{10}-helix extending from Gly33 to Asn35. The two stable helices are separated by a turn from residues His18-Ser20. The break in the N-terminal α-helix at His18, also present in the previous NMR structure of the recombinant hIAPP [*21*], is confirmed by the absence of $d_{\alpha\beta}(i,i+3)$, $d_{\alpha N}(i,i+3)$ NOEs from Leu16-Ser19 and His18-Ser20 that would be present if Leu16-Ser19 were in a helical conformation (Figure 4-4). Unlike the structure of the recombinant hIAPP, the second helix does not rotate freely about the first helix but is constrained in a bent conformation with an inter-helical angle determined by MOLMOL to be 85º ± 5º.

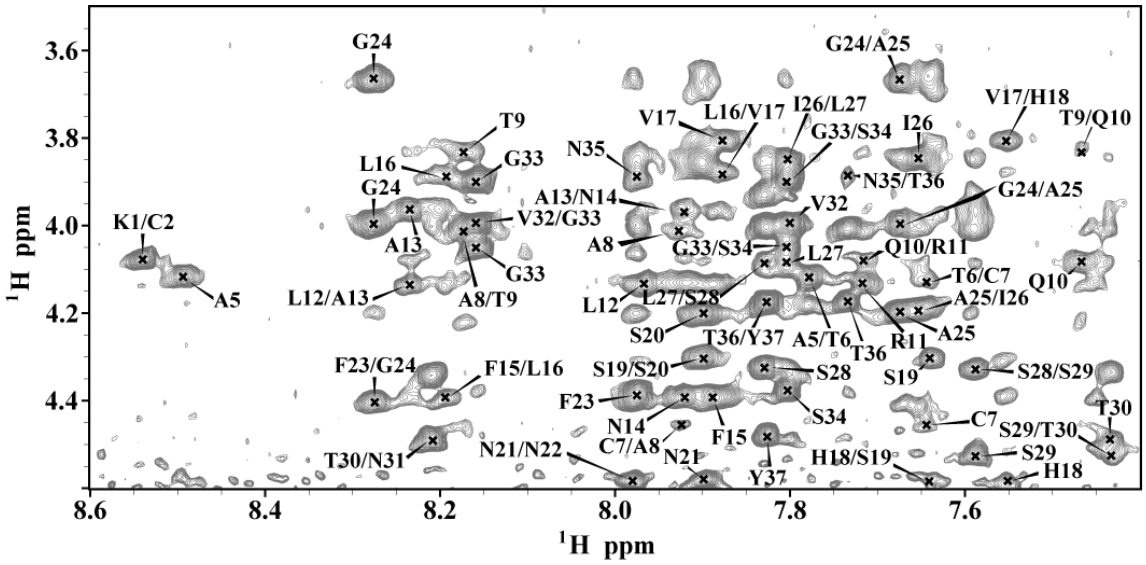

Figure 4-3. The fingerprint region of 2D ^{1}H-^{1}H NOESY spectrum of hIAPP in SDS micelles showing sequential H_α - H_N NOE connectivities.

This constraint between the two helices can be attributed to the presence of $d_{\alpha N}(i,i+2)$ and $d_{\alpha N}(i,i+3)$ NOEs from V17 to S19 and also from V17 to S20 which limit the conformational space to the bent conformation observed in the structure (Figure 4-4).

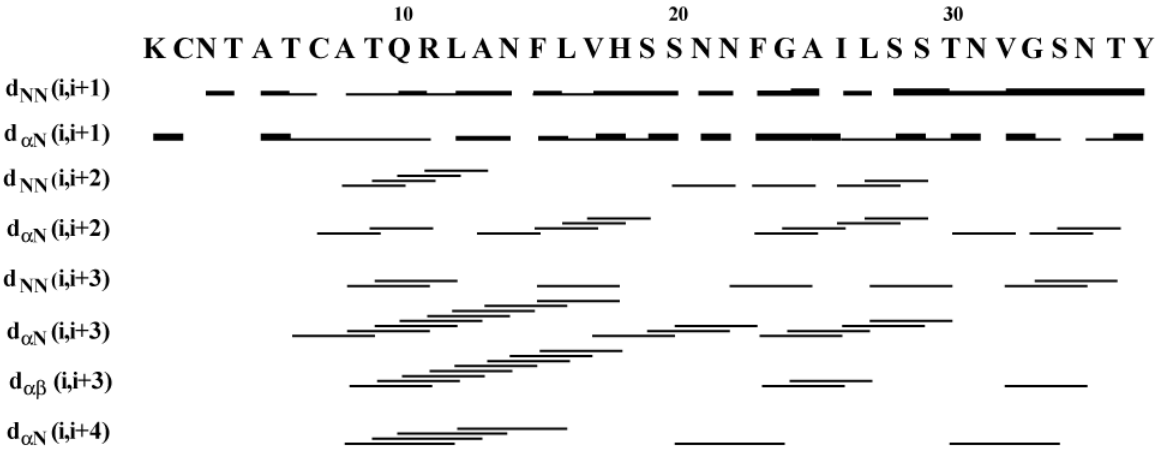

Figure 4-4. A summary of the sequential and medium range NOE connectivities for hIAPP in SDS micelles. The intensities of the observed NOEs are represented by the thickness of lines and are classified as strong, medium, and weak.

The dynamic 3_{10}-helix from Gly33 to Asn35 found in this study was not

observed in the structure of the recombinant hIAPP. The absence of $d_{NN}(i,i+3)$, $d_{\alpha\beta}(i,i+3)$, and $d_{\alpha N}$ (i,i+4) NOEs in the spectra of recombinant hIAPP in this region,[*21*] as well as their presence in the current study, support this difference between the two structures. In particular, $d_{NN}(i,i+3)$ NOEs from Val32-Asn35 and Gly33-Thr36, a $d_{\alpha\beta}(i,i+3)$ NOE from Val32-Asn35, and a $d_{\alpha N}$ (i,i+4) NOE from Thr30-Ser34 (Figure 4-4) indicate the existence of a helical conformation from Gly 33 to Asn 35, none of which were observed in the spectra of recombinant hIAPP [*21*]. The presence of $d_{\alpha N}(i,i+2)$ NOEs spanning Thr30-Val32, Gly33-Asn35, and Ser34-Thr36 indicates the formation of a 3_{10}-, rather than α-, helix (Figure 4-4). This contention is further supported by the observation of hydrogen bonds in the final structure between the backbone of Gly33 to Thr36 and Ser34 and the C-terminal amide, an i to to i+3 pattern typical for 3_{10} helices.

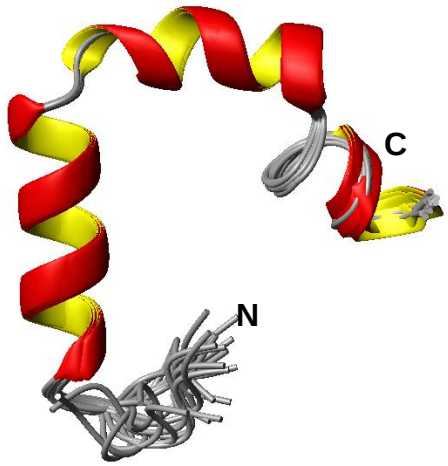

Figure 4-5. High-resolution NMR structures of hIAPP in SDS micelles at physiological pH. Note that the N-terminal helix from C7-V17 is separated from the other helix from N21-S28 by a turn comprising of residues H18-S20 and the C-terminus has a short 3_{10}-helix comprising of residues G33-N35.

4.4.2 *Localization of hIAPP in SDS micelles.* In order to find the orientation of the peptide with respect to the SDS micelle, we have performed paramagnetic

quenching experiments using $MnCl_2$ as a paramagnetic ion. Since Mn^{2+} ions are less likely to penetrate into the hydrophobic interior of the micelle, only residues exposed to solvent experience the paramagnetic induced relaxation effect that results in broadening of the corresponding peaks. In the 2D TOCSY spectrum recorded in the presence of 0.8 mM $MnCl_2$, most of the resonances in the finger print region disappeared as shown in Figure 4-6, indicating most of the residues of hIAPP are exposed to the solvent and the peptide is located close to the surface of the micelle. However, the Hα protons of T9, R11 and L12, the side chain peaks of K1, N3, Q10, R11, N14, and the amide protons of C2, A5-A13, F15-L16, S20, A25, S29, V32, T36 and Y37 are still observable but with a reduced intensity. These results indicate that the side chains of residues in the stable helical region Cys7-Val17, as well as some of the residues in the dynamic 3_{10}-helical region Gly33-Asn 35, are most likely embedded into the head group region of the detergent.

4.5 DISCUSSION

The structure of hIAPP in the physiological amidated form at neutral pH resembles that of the recombinant free acid at an acidic pH with two important differences (Figure 4-7). In the structure of Patil et al., IAPP is folded into a dynamic helix, kinked between residues 18-22, with a conformationally unconstrained C-terminal end from residues 30-37 [*21*]. Paramagnetic quenching data suggests the hIAPP free acid is partially immersed into the SDS micelle at acidic pH, with the folded N-terminal helix (residues 2-16) immersed to a greater depth than the 21-29 helix and the conformationally free C-terminus [*21*].

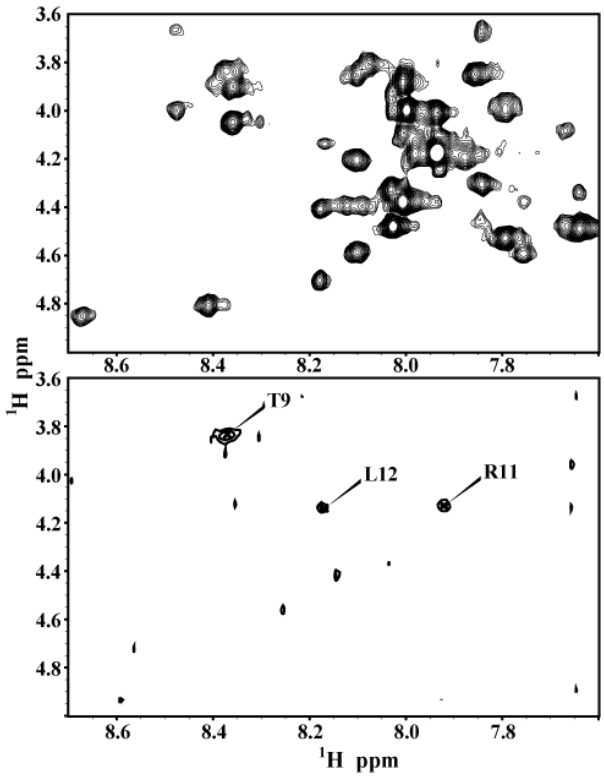

Figure 4-6. 2D ^{1}H-^{1}H TOCSY spectra of hIAPP in SDS micelles at physiological pH in the absence (top) and presence (bottom) of 0.8 mM $MnCl_2$.

The helix-turn-helix conformation found in both structures is a common motif found in many of the high-resolution structures of amyloids bound to the detergent micelles, where an amphipathic helix is separated from a more polar helix by a short flexible region. In all these high-resolution structures there is a variable degree of conformational flexibility, as the location of the linker as well as length of the helical regions vary depending upon the experimental conditions [*21, 35-38*]. The location of the kinks in the structure in detergent micelles largely correlates with the location of the turns in the structure of the amyloid fiber [*39-43*].

Although the overall helix-turn-helix motif of the previous structure is preserved, the kink is much more pronounced in the new structure of hIAPP determined in

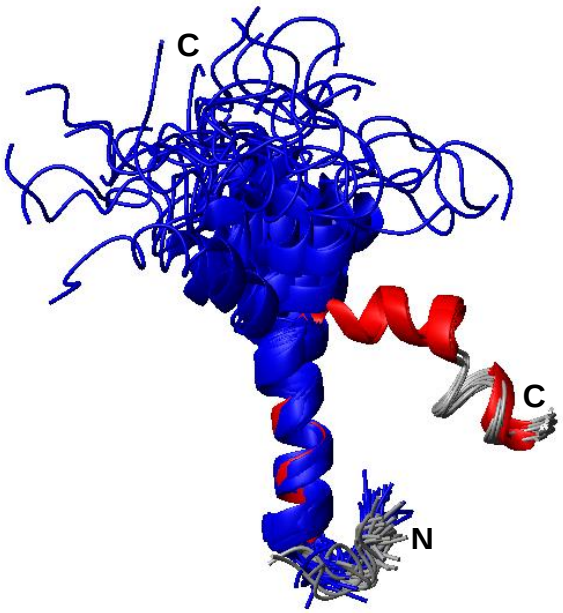

Figure 4-7. Overlay of the ensemble of NMR structures of hIAPP in SDS micelles solved at acidic pH (blue) and physiological pH (red). Note that the N-terminal helix (residues to 7 to 17) overlays quite well, while a substantial deviation is observed for the second helix from 21 to 28.

this study. While the N-terminal α-helix of both the structures overlays well from Cys7-Val17 with a backbone RMSD of 0.48 ± 0.25 Å as shown in Figure 4-7, the second helix deviates significantly from each other. At acidic pH, the helix from Asn22-Ser28 in the the hIAPP free acid wobbles about the N-terminal helix with an inter-helical angle of 30°C [*21*]. By contrast, the Asn21-Ser28 helix of C-amidated-hIAPP at neutral pH is constrained to lie at an interhelical angle of 85°. The strongly bent aspect of the structure resembles those of hIAPP and the related pramlintide construct determined at neutral pH in fluorinated organic solvents, [*24, 44*] suggesting the kink in the helix is not enforced by membrane binding. In both structures the region of the peptide constrained by the disulfide ring is partially unstructured and pointing away from the hydrophobic side of the N-terminal helix [*21*].

In addition to the differences observed in the kink region of the peptide, a substantial difference exists at the C-terminal end. In our structure residues Gly33 to Asn35 at the C-terminal end of the peptide are in a 3_{10} helical conformation, in comparison to the conformationally unconstrained C-terminus found in the structure of Patil et al [*21*]. The CD spectra of hIAPP at pH 4.6 and 10.8 are similar, suggesting that the change in the protonation state of His18 is not responsible for the observed differences [*21*]. The formation of the 3_{10} helix from Gly33 to Asn35 is therefore most likely due to the change from an unprotected, negatively charged C-terminus to the amidated, uncharged variant present in the physiologically expressed peptide. The negatively charged free acid will unfavorably interact with the headgroup of SDS and negatively charged lipids, while the amidated version not only lacks this unfavorable interaction but also has the potential for favorable hydrogen bonding interactions with the detergent or lipid headgroup. As a consequence, the C-terminus interacts more strongly with the SDS micelle, penetrating deeper into the micelle as shown by the larger number of NOEs that survive paramagnetic quenching, particularly at the C-terminal end (see Figure 4-6). The change in the protonation state of His18 may assist in this process, as His18 once deprotonated loses its electrostatic interactions with the negatively charged head group of SDS micelles. The loss of this anchoring point may allow a greater penetration into the membrane, as was observed with the 1-19 fragment of hIAPP [*9, 22*].

Several lines of evidence point to the importance of the C-terminal end of hIAPP in amyloid formation. First, as a peptide fragment, residues 30-37

independently form amyloid deposits [*45*]. Second, mutations at the C-terminal can adversely affect the kinetics of amyloid formation. For instance, mutation of Asn31 to Leu or Asn35 to Leu is sufficient for a three-fold decrease in the fibrillogenesis rate, [*46*] while mutations of Asn31 to Ser or Val32 to Ala abolish amyloid formation [*47*]. Third, the hIAPP free acid aggregates significantly slower (1/9 the rate) than the amidated variant, suggesting electrostatics at the C-terminal end plays a key role in aggregation [*27*]. Fourth, the entire C-terminus is incorporated into the amyloid fiber in the current structural model of hIAPP amyloid fibers, indicating interactions of the C-terminal with the N-terminal stabilize the final structure [*41*]. Finally, the N-terminal regions of hIAPP and the nonamyloidogenic and nontoxic rat IAPP variant are similar, with most of the differences in the structure concentrated at the C-terminal end [*22, 48*]. Taken together, these findings raise the possibility that, while the C-terminus is not strictly essential for amyloid formation by hIAPP, [*49*] its conformation can significantly modulate the kinetics of amyloid formation (see Figure 4-8 for a possible model).

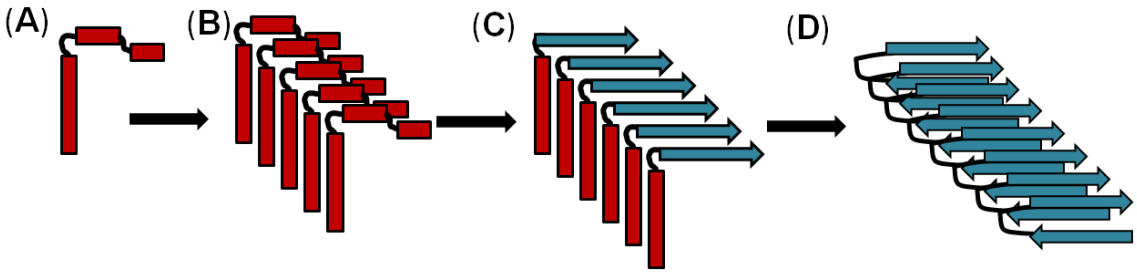

Figure 4-8. A possible schematic model for the aggregation of hIAPP in the presence of lipid membranes. (A) hIAPP initially binds to the membrane in a helical conformation. (B) Once bound to the membrane, hIAPP aggregates on the membrane surface to form helical bundles (C) Aggregation of the peptide causes a conformational change in the less structured C-terminus to the β-sheet conformation of the amyloid form. (D) Formation of β-sheets at the C-terminus

triggers a corresponding conformational change at the N-terminus, producing the final amyloid fiber.

The existence of a structured C-terminus is significant for a structural interpretation of both membrane-mediated and membrane-free aggregation of hIAPP. The transition from a conformationally unconstrained monomeric peptide to the highly ordered amyloid supermolecular complex is entropically disfavored. For this reason, amyloid formation from conformationally unconstrained monomers is frequently kinetically inaccessible, despite the overall favorable free energy change associated with amyloid formation for hydrophobic sequences [*50*]. Partially structured intermediates can reduce the entropic cost of the highly disfavored initial step of amyloid formation by favorably positioning aggregation prone regions to interact with each other. In particular, there is evidence for a mechanistic role for helical intermediates in amyloid aggregation [*3, 51*]. Helical intermediates have been directly observed for some amyloidogenic proteins and have been indirectly inferred for others from mutational analysis and solvent perturbation studies [*52, 53*]. Utilizing this fact, inhibitors have been constructed to prevent amyloid formation by either excessively destabilizing or overstabilizing the helical state [*54, 55*]. 3_{10} helices are particularly suited for undergoing a helix to beta sheet transition due to the relative similarities in the phi/psi torsion angles between the beta-sheet and 3_{10} helix conformations and the relative ease of partially unfolding a 3_{10} helix compared to the α-helix conformation [*3*].

4.6 CONCLUSION

In conclusion, we have solved the structure of hIAPP with an amidated C-terminus in SDS micelles at pH 7.3. When compared with the nonamidated C-

terminus hIAPP solved at pH 4.9, both the structures have an overall kinked helix motif, with residues 7-17 and 21-28 in a helical conformation in both structures. However, the C-terminus of amidated hIAPP is structured, with a 3_{10} dynamic helix from Gly33-Asn35, which was not observed in the structure of recombinant hIAPP solved at an acidic pH. In addition, the angle between the N- and C-terminal helices is constrained to 85º instead of the free rotation present in the structure of recombinant hIAPP. These differences observed in our structure might play an important role in the aggregation process of hIAPP.

REFERENCES

[1] Scherbaum, W. A. (1998) The role of amylin in the physiology of glycemic control. *Exp. Clin. Endocrinol. Diabet. 106*, 97-102.

[2] Haataja, L., Gurlo, T., Huang, C. J., and Butler, P. C. (2008) Islet Amyloid in Type 2 Diabetes, and the Toxic Oligomer Hypothesis. *Endocr. Rev. 29*, 302-316.

[3] Harrison, R. S., Sharpe, P. C., Singh, Y., and Fairlie, D. P. (2007) Amyloid peptides and proteins in review. *Rev. Physiol. Biochem. P. 159*, 1-77.

[4] Butler, A. E., Janson, J., Ritzel, R., Sultana, C., Soeller, W. C., and Butler, P. C. (2002) Accelerated apoptosis overcomes increased replication to cause beta-cell loss in diabetes in mice transgenic for h-IAPP. *Diabetes 51*, A7-A7.

[5] Henson, M. S., Buman, B. L., Jordan, K., Rahrmann, E. P., Hardy, R. M., Johnson, K. H., and O'Brien, T. D. (2006) An in vitro model of early islet amyloid polypeptide (IAPP) fibrillogenesis using human IAPP-transgenic mouse islets. *Amyloid 13*, 250-259.

[6] Ritzel, R. A., Meier, J. J., Lin, C. Y., Veldhuis, J. D., and Butler, P. C. (2007)

Human islet amyloid polypeptide oligomers disrupt cell coupling, induce apoptosis, and impair insulin secretion in isolated human islets. *Diabetes 56*, 65-71.

[7] Butterfield, S. M., and Lashuel, H. A. (2010) Amyloidogenic Protein Membrane Interactions: Mechanistic Insight from Model Systems, *Angew. Chem. Int. Ed. Engl. 49*, 5628-5654.

[8] Brender, J. R., Durr, U. H. N., Heyl, D., Budarapu, M. B., and Ramamoorthy, A. (2007) Membrane fragmentation by an amyloidogenic fragment of human Islet Amyloid Polypeptide detected by solid-state NMR spectroscopy of membrane nanotubes, *Biochim. Biophys. Acta 1768*, 2026-2029.

[9] Brender, J. R., Hartman, K., Reid, K. R., Kennedy, R. T., and Ramamoorthy, A. (2008) A Single Mutation in the Nonamyloidogenic Region of Islet Amyloid Polypeptide Greatly Reduces Toxicity, *Biochemistry 47*, 12680-12688.

[10] Smith, P. E. S., Brender, J. R., and Ramamoorthy, A. (2009) Induction of Negative Curvature as a Mechanism of Cell Toxicity by Amyloidogenic Peptides: The Case of Islet Amyloid Polypeptide, *J. Am. Chem. Soc. 131*, 4470-4478.

[11] Sparr, E., Engel, M. F. M., Sakharov, D. V., Sprong, M., Jacobs, J., de Kruijff, B., Hoppener, J. W. M., and Killian, J. A. (2004) Islet amyloid polypeptide-induced membrane leakage involves uptake of lipids by forming amyloid fibers, *FEBS Lett. 577*, 117-120.

[12] Engel, M. F., Khemtemourian, L., Kleijer, C. C., Meeldijk, H. J., Jacobs, J., Verkleij, A. J., de Kruijff, B., Killian, J. A., and Hoppener, J. W. (2008) Membrane damage by human islet amyloid polypeptide through fibril growth at the

membrane, *Proc. Natl. Acad. Sci. U. S. A. 105*, 6033-6038.

[13] Janson, J., Ashley, R. H., Harrison, D., McIntyre, S., and Butler, P. C. (1999) The mechanism of islet amyloid polypeptide toxicity is membrane disruption by intermediate-sized toxic amyloid particles, *Diabetes 48*, 491-498.

[14] Knight, J. D., and Miranker, A. D. (2004) Phospholipid catalysis of diabetic amyloid assembly, *J. Mol. Biol. 341*, 1175-1187.

[15] Brender, J. R., Lee, E. L., Cavitt, M. A., Gafni, A., Steel, D. G., and Ramamoorthy, A. (2008) Amyloid Fiber Formation and Membrane Disruption are Separate Processes Localized in Two Distinct Regions of IAPP, the Type-2-Diabetes-Related Peptide, *J. Am. Chem. Soc. 130*, 6424-6429.

[16] Jayasinghe, S. A., and Langen, R. (2007) Membrane interaction of islet amyloid polypeptide, *Biochim. Biophys. Acta 1768*, 2002-2009.

[17] Knight, J. D., Hebda, J. A., and Miranker, A. D. (2006) Conserved and cooperative assembly of membrane-bound alpha-helical states of islet amyloid polypeptide, *Biochemistry 45*, 9496-9508.

[18] Apostolidou, M., Jayasinghe, S. A., and Langen, R. (2008) Structure of alpha -Helical membrane-bound hIAPP and its implications for membrane-mediated misfolding, *J. Biol. Chem. 283*, 17205-17210.

[19] Jayasinghe, S. A., and Langen, R. (2005) Lipid membranes modulate the structure of islet amyloid polypeptide, *Biochemistry 44*, 12113-12119.

[20] Williamson, J. A., Loria, J. P., and Miranker, A. D. (2009) Helix stabilization precedes aqueous and bilayer-catalyzed fiber formation in islet amyloid polypeptide, *J. Mol. Biol. 393*, 383-396.

[21] Patil, S. M., Xu, S. H., Sheftic, S. R., and Alexandrescu, A. T. (2009) Dynamic alpha-Helix Structure of Micelle-bound Human Amylin, *J. Biol. Chem. 284*, 11982-11991.

[22] Nanga, R. P. R., Brender, J. R., Xu, J. D., Veglia, G., and Ramamoorthy, A. (2008) Structures of Rat and Human Islet Amyloid Polypeptide IAPP(1-19) in Micelles by NMR Spectroscopy, *Biochemistry 47*, 12689-12697.

[23] Mishra, R., Geyer, M., and Winter, R. (2009) NMR spectroscopic investigation of early events in IAPP amyloid fibril formation, *ChemBioChem 10*, 1769-1772.

[24] Brender, J. R., Hartman, K., Nanga, R. P., Popovych, N., de la Salud Bea, R., Vivekanandan, S., Marsh, E. N., and Ramamoorthy, A. (2010) Role of zinc in human islet amyloid polypeptide aggregation, *J. Am. Chem. Soc. 132*, 8973-8983.

[25] Hutton, J. C. (1982) The Internal Ph and Membrane-Potential of the Insulin-Secretory Granule, *Biochem. J. 204*, 171-178.

[26] Roberts, A. N., Leighton, B., Todd, J. A., Cockburn, D., Schofield, P. N., Sutton, R., Holt, S., Boyd, Y., Day, A. J., Foot, E. A., and et al. (1989) Molecular and functional characterization of amylin, a peptide associated with type 2 diabetes mellitus, *Proc. Natl. Acad. Sci. U. S. A. 86*, 9662-9666.

[27] Yonemoto, I. T., Kroon, G. J., Dyson, H. J., Balch, W. E., and Kelly, J. W. (2008) Amylin proprotein processing generates progressively more amyloidogenic peptides that initially sample the helical state, *Biochemistry 47*, 9900-9910.

[28] Wei, L., Jiang, P., Xu, W., Li, H., Zhang, H., Yan, L., Chan-Park, M. B., Liu, X. W., Tang, K., Mu, Y., and Pervushin, K. (2010) The molecular basis of distinct aggregation pathways of islet amyloid polypeptide, *J. Biol. Chem. In press*.

[29] Goddard, T. D., and Kneller, D. G. (1999) SPARKY 3, University of California, San Francisco.

[30] Wuthrich, K., (Ed.) (1986) *NMR of proteins and nucleic acids.* , John Wiley and Sons, New York.

[31] Guntert, P., Mumenthaler, C., and Wuthrich, K. (1997) Torsion angle dynamics for NMR structure calculation with the new program DYANA, *J. Mol. Biol. 273*, 283-298.

[32] Cornilescu, G., Delaglio, F., and Bax, A. (1999) Protein backbone angle restraints from searching a database for chemical shift and sequence homology, *J. Biomol. NMR 13*, 289-302.

[33] Herrmann, T., Guntert, P., and Wuthrich, K. (2002) Protein NMR structure determination with automated NOE assignment using the new software CANDID and the torsion angle dynamics algorithm DYANA, *J. Mol. Biol. 319*, 209-227.

[34] Koradi, R., Billeter, M., and Wuthrich, K. (1996) MOMOL: A program for display and analysis of macromolecular structures., *J. Mol. Graph. Model. 14*, 51-55.

[35] Coles, M., Bicknell, W., Watson, A. A., Fairlie, D. P., and Craik, D. J. (1998) Solution structure of amyloid beta-peptide(1-40) in a water-micelle environment. Is the membrane-spanning domain where we think it is?, *Biochemistry 37*, 11064-11077.

[36] Motta, A., Andreotti, G., Amodeo, P., Strazzullo, G., and Morelli, M. A. C. (1998) Solution structure of human calcitonin in membrane-mimetic environment: The role of the amphipathic helix, *Proteins 32*, 314-323.

[37] Motta, A., Pastore, A., Goud, N. A., and Morelli, M. A. C. (1991) Solution Conformation of Salmon-Calcitonin in Sodium Dodecyl-Sulfate Micelles as Determined by 2-Dimensional Nmr and Distance Geometry Calculations, *Biochemistry 30*, 10444-10450.

[38] Ulmer, T. S., Bax, A., Cole, N. B., and Nussbaum, R. L. (2005) Structure and dynamics of micelle-bound human alpha-synuclein, *J. Biol. Chem. 280*, 9595-9603.

[39] Tompa, P. (2009) Structural disorder in amyloid fibrils: its implication in dynamic interactions of proteins, *FEBS J. 276*, 5406-5415.

[40] Luhrs, T., Ritter, C., Adrian, M., Riek-Loher, D., Bohrmann, B., Doeli, H., Schubert, D., and Riek, R. (2005) 3D structure of Alzheimer's amyloid-beta(1-42) fibrils, *Proc. Natl. Acad. Sci. U. S. A. 102*, 17342-17347.

[41] Luca, S., Yau, W. M., Leapman, R., and Tycko, R. (2007) Peptide conformation and supramolecular organization in amylin fibrils: Constraints from solid-state NMR, *Biochemistry 46*, 13505-13522.

[42] Heise, H., Hoyer, W., Becker, S., Andronesi, O. C., Riedel, D., and Baldus, M. (2005) Molecular-level secondary structure, polymorphism, and dynamics of full-length alpha-synuclein fibrils studied by solid-state NMR, *Proc. Natl. Acad. Sci. U. S. A. 102*, 15871-15876.

[43] Vilar, M., Chou, H. T., Luhrs, T., Maji, S. K., Riek-Loher, D., Verel, R.,

Manning, G., Stahlberg, H., and Riek, R. (2008) The fold of alpha-synuclein fibrils, *Proc. Natl. Acad. Sci. U. S. A. 105*, 8637-8642.

[44] Cort, J. R., Liu, Z., Lee, G. M., Huggins, K. N., Janes, S., Prickett, K., and Andersen, N. H. (2009) Solution state structures of human pancreatic amylin and pramlintide, *Protein Eng. Des. Sel. 22*, 497-513.

[45] Nilsson, M. R., and Raleigh, D. P. (1999) Analysis of amylin cleavage products provides new insights into the amyloidogenic region of human amylin, *J. Mol. Biol. 294*, 1375-1385.

[46] Koo, B. W., Hebda, J. A., and Miranker, A. D. (2008) Amide inequivalence in the fibrillar assembly of islet amyloid polypeptide, *Protein Eng. Des. Sel. 21*, 147-154.

[47] Fox, A., Snollaerts, T., Casanova, C. E., Calciano, A., Nogaj, L. A., and Moffet, D. A. (2010) Selection for Nonamyloidogenic Mutants of Islet Amyloid Polypeptide (IAPP) Identifies an Extended Region for Amyloidogenicity, *Biochemistry 49*, 7783-7789.

[48] Nanga, R. P. R., Brender, J. R., Xu, J. D., Hartman, K., Subramanian, V., and Ramamoorthy, A. (2009) Three-Dimensional Structure and Orientation of Rat Islet Amyloid Polypeptide Protein in a Membrane Environment by Solution NMR Spectroscopy, *J. Am. Chem. Soc. 131*, 8252-8261.

[49] Radovan, D., Smirnovas, V., and Winter, R. (2008) Effect of Pressure on Islet Amyloid Polypeptide Aggregation: Revealing the Polymorphic Nature of the Fibrillation Process, *Biochemistry 47,* 6352-6360.

[50] Hall, D., Hirota, N., and Dobson, C. M. (2005) A toy model for predicting the

rate of amyloid formation from unfolded protein, *J. Mol. Biol. 351*, 195-205.

[51] Abedini, A., and Raleigh, D. P. (2009) A role for helical intermediates in amyloid formation by natively unfolded polypeptides?, *Phys. Biol. 6*, 15005.

[52] Kirkitadze, M. D., Condron, M. M., and Teplow, D. B. (2001) Identification and characterization of key kinetic intermediates in amyloid beta-protein fibrillogenesis, *J. Mol. Biol. 312*, 1103-1119.

[53] Singh, Y., Sharpe, P. C., Hoang, H. N., Lucke, A. J., McDowall, A. W., Bottomley, S. P., and Fairlie, D. P. (2010) Amyloid Formation from an alpha-Helix Peptide Bundle Is Seeded by 3(10)-Helix Aggregates, *Chemistry* In press.

[54] Nerelius, C., Sandegren, A., Sargsyan, H., Raunak, R., Leijonmarck, H., Chatterjee, U., Fisahn, A., Imarisio, S., Lomas, D. A., Crowther, D. C., Stromberg, R., and Johansson, J. (2009) alpha-Helix targeting reduces amyloid-beta peptide toxicity, *Proc. Natl. Acad. Sci. U. S. A. 106*, 9191-9196.

[55] Saraogi, I., Hebda, J. A., Becerril, J., Estroff, L. A., Miranker, A. D., and Hamilton, A. D. (2009) Synthetic alpha-Helix Mimetics as Agonists and Antagonists of Islet Amyloid Polypeptide Aggregation, *Angew. Chem. Int. Ed. Engl. 49,* 736-739.

CHAPTER 5. NMR STRUCTURE IN A MEMBRANE ENVIRONMENT REVEALS PUTATIVE AMYLOIDOGENIC REGIONS OF THE SEVI PRECURSOR PEPTIDE $PAP_{248-286}$

This chapter is a version of a manuscript published in J. Am. Chem. Soc. (2009) 131, 17972-17979.[4]

5.1 ABSTRACT

Semen is the main vector for HIV transmission worldwide. Recently, a peptide fragment ($PAP_{248-286}$) has been isolated from seminal fluid that dramatically enhances HIV infectivity by up to 4-5 orders of magnitude. $PAP_{248-286}$ appears to enhance HIV infection by forming amyloid fibers known as SEVI, which are believed to enhance the attachment of the virus by bridging interactions between virion and host-cell membranes. We have solved the atomic-level resolution structure of the SEVI precursor $PAP_{248-286}$ using NMR spectroscopy in SDS micelles, which serve as a model membrane system. $PAP_{248-286}$, which does not disrupt membranes like most amyloid proteins, binds superficially to the surface of the micelle, in contrast to other membrane-disruptive amyloid peptides that generally penetrate into the core of the membrane. The structure of $PAP_{248-286}$ is unlike most amyloid peptides in that $PAP_{248-286}$ is mostly disordered when bound to the surface of the micelle, as opposed to the α-helical structures typically found of most amyloid proteins. The highly disordered nature of the SEVI peptide may explain the unique ability of

[4] Nataliya Popovych helped in setting up the NMR experiments. Subramanian Vivekanandan helped with data processing. Jeffrey Brender helped in writing the manuscript. This study was supported by the funds from NIH (DK 078885 to A.R.).

SEVI amyloid fibers to enhance HIV infection as partially disordered amyloid fibers will have a greater capture radius for the virus than compact amyloid fibers. Two regions of nascent structure (an α-helix from V262-H270 and a dynamic $\alpha/3_{10}$ helix from S279-L283) match the prediction of highly amyloidogenic sequences and may serve as nuclei for aggregation and amyloid fibril formation. The structure presented here can be used for the rational design of mutagenesis studies on SEVI amyloid formation and viral infection enhancement.

5.2 INTRODUCTION

Despite the rapid progress of the AIDS pandemic, the HIV virus is a surprisingly weak pathogen in vitro with only <0.1% of virus particles succeeding in infecting a host cell [*1, 2*]. Emerging evidence suggests that difficulties in virus attachment to the host cell in vitro, rather than intrinsic deficiencies in viral particles, are the source of this low infection rate. Because the half-life of free virions of HIV is very short in comparison to the probability of a virion randomly encountering the appropriate receptor, most virions will decay before initiating a successful infection cycle unless they can rapidly attach to the cell membrane surface where the search for the cell receptor proceeds by inherently more efficient two-dimensional diffusion [*3, 4*]. Viral attachment to the cell surface entry of the virus into the host cell therefore appears to be the primary barrier to HIV infection in vitro [*5*].

The difference between in vitro and in vivo infection rates suggests this process is much more efficient in vivo than in vitro and that cofactors absent in

vitro but present in vivo may be responsible for this difference. A clear candidate has emerged from a recent screening of a large library of peptides and low molecular weight proteins (<50 kDa) found in human semen. This screening identified SEVI (semen-derived enhancer of viral infection), a naturally occurring 39 amino acid fragment from prostatic acid phosphatase (PAP) that enhanced the rate of HIV infection dramatically across a broad range of HIV phenotypes [*6-8*].

Limiting dilution assays showed a truly remarkable enhancement by 4-5 orders of magnitude when HIV viral loads more closely resembling the actual conditions during sexual transmission were used, with only 1-3 virions necessary to establish a persistent infection in CEMx M7 dendritic cells in the presence of SEVI [*6*]. Furthermore, SEVI's ability to increase viral infectivity is not limited to the HIV virus, as it also exerts a similar effect on the XMRV retrovirus [*9*].

Because the structures of SEVI are not known in any form, it is difficult to make predictions about the interactions of SEVI with the cell membrane that facilitate HIV viral attachment. Some degree of aggregation of the peptide is necessary for activity as freshly prepared, monomeric solutions of SEVI are ineffective at promoting viral infectivity and the enhancement of HIV infectivity increases with time as SEVI is incubated in solution [*6*]. It has been established that SEVI is an amyloidogenic peptide and that amyloid fibers of the peptide are more effective than the monomeric peptide in promoting HIV cell binding and membrane fusion [*6*]. This is in agreement with previous studies that have shown a more modest enhancement of infectivity of enveloped viruses by other

amyloidogenic proteins, such as A*β* and α-synuclein [*10*]. While some degree of oligomerization seems to be a requirement for SEVI-enhanced infectivity, amyloid formation does not seem to be an absolute requirement for the enhancement of HIV infection by $PAP_{248-286}$ as it occurs well before the formation of amyloid fibers [*6*].

These interactions are likely to be highly dependent on specific structural details as other amyloid proteins that share the same gross cross-*β* sheet structure as SEVI show a much lower enhancement of infectivity. To understand the mechanism by which SEVI promotes the bridging of viral and host cell membranes, we have solved the high-resolution structure of the SEVI precursor $PAP_{248-286}$ in a membrane mimicking environment (SDS micelles) using NMR spectroscopy. The structure of $PAP_{248-286}$ possesses an unusual amount of disorder as compared to other amyloid proteins, which may explain the much greater ability of SEVI to enhance HIV infection as compared to amyloid fibers formed from other proteins [*6*]. From the structure and bioinformatic analysis of the $PAP_{248-286}$ sequence, we have also identified a putative amyloidogenic region of the $PAP_{248-286}$ sequence.

5.3 MATERIALS AND METHODS

5.3.1 *NMR Sample Preparation*. SEVI refers to the amyloid form of peptides derived from fragments of prostatic acid phosphatase (PAP). Of these peptides, the fragment $PAP_{248-286}$ was chosen for this study, as amyloid fibers formed from $PAP_{248-286}$ are the most effective at enhancing HIV infection. The $PAP_{248-286}$ peptide was synthesized and purified to >95% purity by Biomatik (Toronto, ON).

Because the large size of the amyloid form of the peptide precludes its study by solution NMR, peptide aggregation must be prevented for the duration of the experiment to obtain a high-resolution structure of the peptide. The removal of preformed aggregates of the peptide that can act as nuclei for further peptide aggregation is essential to arrest this process; accordingly, the peptide was dissolved first in a strongly disaggregating 1:1 solution of trifluoroacetic acid (TFA) and hexafluoroisopropanol (HFIP) at a concentration of 5 mg/mL to break up preformed amyloid fibers [11]. The TFA/HFIP solution was evaporated by a stream of nitrogen gas, and the resulting film was redissolved in pure HFIP at a concentration of 2 mg/mL. HFIP was removed by lyophilization under high vacuum for 24 h. Samples were prepared for NMR measurements by dissolving 3.4 mg of lyophilized peptide in 20 mM phosphate buffer at pH 7.3 containing 10% D_2O, 120 mM NaCl, and 200 mM perdeuterated SDS (Cambridge Isotopes Laboratory) to a final concentration of 2.5 mM. The choice of SDS micelles, neutral pH, and the addition of 120 mM NaCl was based on previous experiments showing the electrostatic nature of $PAP_{248-286}$ membrane binding and the ability of $PAP_{248-286}$ to cause substantial vesicle aggregation, particularly at acidic pH [*11*]. Samples prepared with zwitterionic DPC (dodecylphosphocholine) micelles aggregated rapidly and gave rise to a very broad and weak signal, while samples prepared without 120 mM NaCl displayed poorer resolution and showed visible aggregation within 24 h.

5.3.2 ***NMR Data Collection and Processing*****.** All NMR spectra of $PAP_{248-286}$ embedded in SDS micelles were recorded at 37 °C using a 600 MHz Bruker

Avance NMR spectrometer equipped with a TXI cryoprobe. Backbone and side-chain assignment of peptide was achieved using 2D ^{1}H-^{1}H TOCSY (total correlation spectroscopy) recorded at a 80 ms mixing time and 2D ^{1}H-^{1}H NOESY (nuclear Overhauser enhancement spectroscopy) recorded at 100 and 300 ms mixing times. Both spectra were recorded using 16 scans and 512 points in the indirect dimension, with a recycle delay of 1.5 s. Complex data points were acquired for quadrature detection in both frequency dimensions for the 2D experiments. All spectra were zero-filled in both dimensions to yield matrices of 2048 x 2048 points. Proton chemical shifts were referenced to the water proton signal at 4.7 ppm. All 2D spectra were processed using NMRPIPE and TopSpin software and analyzed using SPARKY [*12, 13*]. Resonance assignments were carried out using a standard approach reported elsewhere [*14*].

5.3.3 *Structure Calculations*. Structure calculations were performed using the X-PLOR-NIH program. A total of 286 NOEs, derived from the NOESY acquired at 300 ms mixing time, were categorized into three distance categories based on the cross-peak volumes obtained from SPARKY analysis: strong (1.8-2.9 Å), medium (1.8-4.5 Å), and weak (1.8-6.0 Å). These restraints were further used in the structure calculations: 145 restraints were intraresidue, and 141 were inter-residue NOEs (Table 5-1). The torsion angle restraints were obtained from the TALOS program using the Hα chemical shift values [*15*]. An extended structure of $PAP_{248-286}$ was used as a starting point for the hybrid molecular dynamics simulated annealing (SA) protocol at a temperature of 4000 K for the generation of an initial 100 structures [*16, 17*]. Explicit hydrogen-bond restraints were not

used in the calculations. Subsequently, these structures were refined using a further SA step and energy minimization. The final refinement was carried out using the refine_gentle.inp protocol, which gradually introduces the van der Waals radii. The few ambiguous angles found in the loop region were assigned an additional 60° of conformational freedom as compared to their predicted values. Out of the 100 structures generated, an ensemble of eight conformers with low RMSD was selected for further analysis. The covalent geometry of the conformers generated was analyzed using PROCHECK_NMR [*18*].

Table 5-1. Statistical information for the $PAP_{248-286}$ structural ensemble.

Distance constraints		
	Total	286
	Intra-residual	145
	Inter-residual	141
	Sequential (i - j = 1)	106
	Medium (i – j = 2, 3, 4)	35
Structural statistics		
	NOE violations (Å)	0.0318 ± 0.0045
	Dihedral angle restraint violations (º)	0.7816 ± 0.1550
	RMSD for bond deviations (Å)	0.0024 ± 0.0003
	RMSD for angle deviations (º)	0.4037 ± 0.0160
	RMSD of all backbone atoms (Å)	
	Val 262 – His 270	0.15 ± 0.05
	Pro 278 – Leu 283	0.74 ± 0.43
	RMSD of all heavy atoms (Å)	
	Val 262 – His 270	0.57 ± 0.12
	Pro 278 – Leu 283	1.60 ± 0.60
Ramachandran plot		
	Residues in most favored region (%)	65.8
	Residues in additionally allowed region (%)	29.8
	Residues in additionally allowed region (%)	3.7
	Residues in disallowed region (%)	0.7

5.4 RESULTS

5.4.1 ***Assignments, Constraints and NMR Structure.*** The structure of $PAP_{248-286}$ in SDS micelles was determined using solution NMR through 2D ^{1}H-^{1}H TOCSY and NOESY data collected as mentioned in the Materials and Methods. Sample preparation was the key step in obtaining high-resolution spectra of

$PAP_{248-286}$. In an effort to optimize spectral resolution and sensitivity, several 1D ^{1}H chemical shift spectra were acquired over a temperature range of 25-45 °C, and the best compromise between sensitivity and resolution was found to be near 37 °C.

The 2D ^{1}H-^{1}H NOESY spectra display numerous, relatively well-resolved cross-peaks, with a significant degree of spectral dispersion in the amide region indicating the presence of at least a partial degree of secondary structure throughout the peptide (Figure 5-1). This is an indication of secondary structure

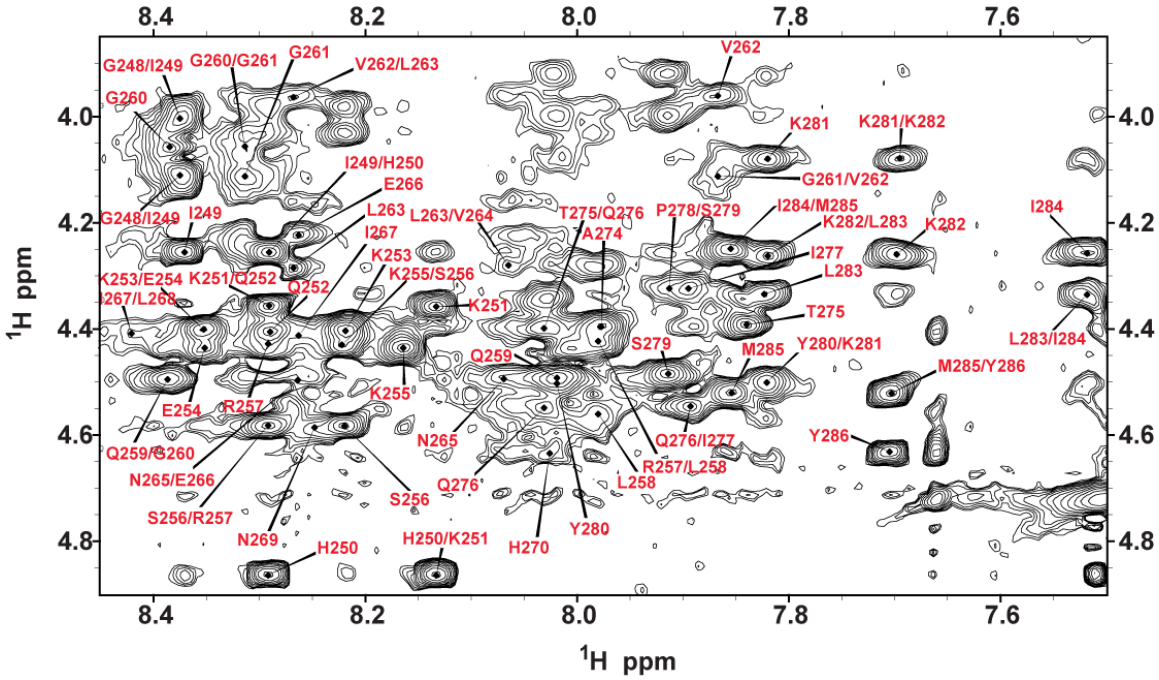

Figure 5-1. The fingerprint region of a 2D ^{1}H-^{1}H NOESY spectrum of SDS micelles containing $PAP_{248-286}$ showing NOE connectivities among Hα nuclei.

formation in the peptide, as a completely disordered structure would have both poor chemical shift dispersion due to the similarity of chemical shift values in the random coil state and poor NOE cross-peak intensity due to the high mobility of the structure. In the V262-H270 and Y280-I284 regions, inter-residue $d_{\alpha HNH}(i,i+3)$,

$d_{\alpha HNH}(i,i+4)$, and $d_{\alpha H\beta H}(i,i+3)$ NOE connectivities along with negative chemical shift indices provide unequivocal evidence for helical structure (Figures 5-2 and 5-3). Similarly, the CD spectra of $PAP_{248-286}$ in SDS micelles and trifluoroethanol solutions exhibit the double minima at 208 and 222 nm characteristic of partial α-helical content. The remainder of the peptide has chemical shift index values consistent with disordered conformations, although the NOE crosspeak intensity pattern, which is more sensitive to transient structure formation, shows strong sequential $d_{NHNH}(i,i+1)$ peaks indicative of transient α-helical or *β*-sheet formation.

Figure 5-2. NOE intensity plot for the amino acid residues of $PAP_{248-286}$ showing the NOE connectivity among residues. Thicker lines correspond to stronger NOE intensities.

To create the structure of $PAP_{248-286}$, all NOEs were converted into distances and modeled using the classical simulated annealing protocol built in XPLOR-NIH. Out of the 100 refined $PAP_{248-286}$ structures, 26 did not have NOE violations of >0.5 Å, dihedral angle restraint violations of >5°, have bonds that

deviate from ideality by a RMS difference of >0.01 Å, or have bond angles that deviate from ideality by a RMS difference of >2°. Out of the structures that passed the acceptance criteria, an ensemble of eight conformers was further selected for the final analysis as a representation of the transient structure formed by the disordered $PAP_{248-286}$ on the micelle. Statistical information on the peptide structure along with a summary of the backbone and side-chain NOEs used for secondary structure assignment is provided in Table 5-1 and Figure 5-4.

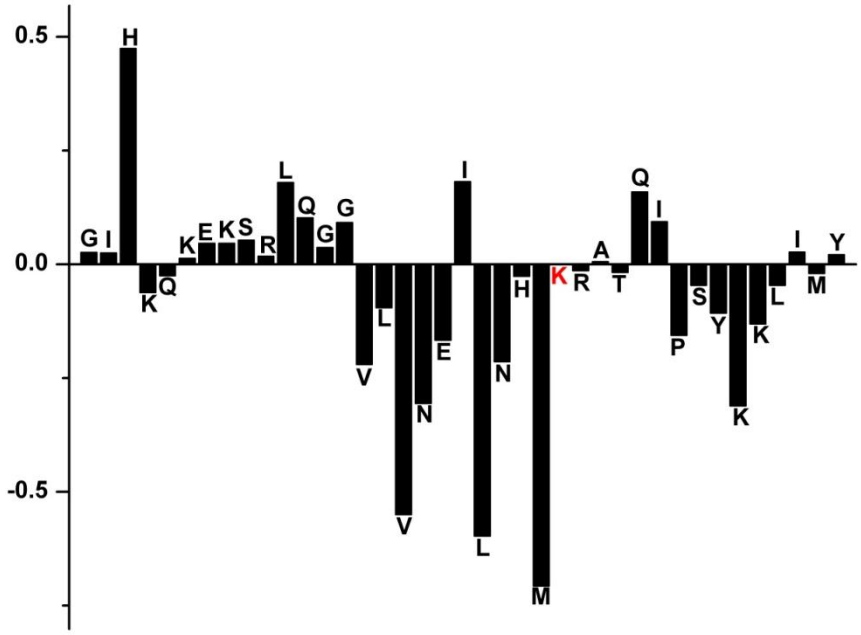

Figure 5-3. α-Proton chemical shift index (CSI) for $PAP_{248-286}$ showing the disordered N-terminal end (CSI near zero) and the central and C-terminal helical regions (CSI < -0.1). The Hα chemical shift of K272 was not detected (red). The CSI was calculated by subtracting the Hα chemical shifts values measured for the peptide from the random coil shifts values for the respective amino acid reported in the literature.

The secondary structure representation of $PAP_{248-286}$ from these eight conformers is shown in Figure 5-5A. The structure of the $PAP_{248-286}$ peptide can be separated into three distinct regions: a highly flexible N-terminal region (G248-G261), a rigid α-helical central region (V262-H270), and a flexible C-terminal

region (M271-Y286) containing a short 3_{10} or α-helix (S279-L283). The RMSD for the C- and N-terminal ends is very large, reflecting a high degree of disorder in these regions. The central region from V262-H270 is more ordered, and a superposition of the eight low-energy conformers gives an RMSD of 0.15 ± 0.05 Å for the backbone atoms from V262-H270, and an RMSD of 0.57 ± 0.12 Å for all heavy atoms. Analysis of the Ramachandran plot, for the final eight conformers of the $PAP_{248-286}$, shows that 65.8% of the residues fall in the most favored region, while the rest of the residues fall in the additionally allowed (29.8%), generously allowed (3.7%), and disallowed (0.7%) regions of the plot as shown in Figure 5-6.

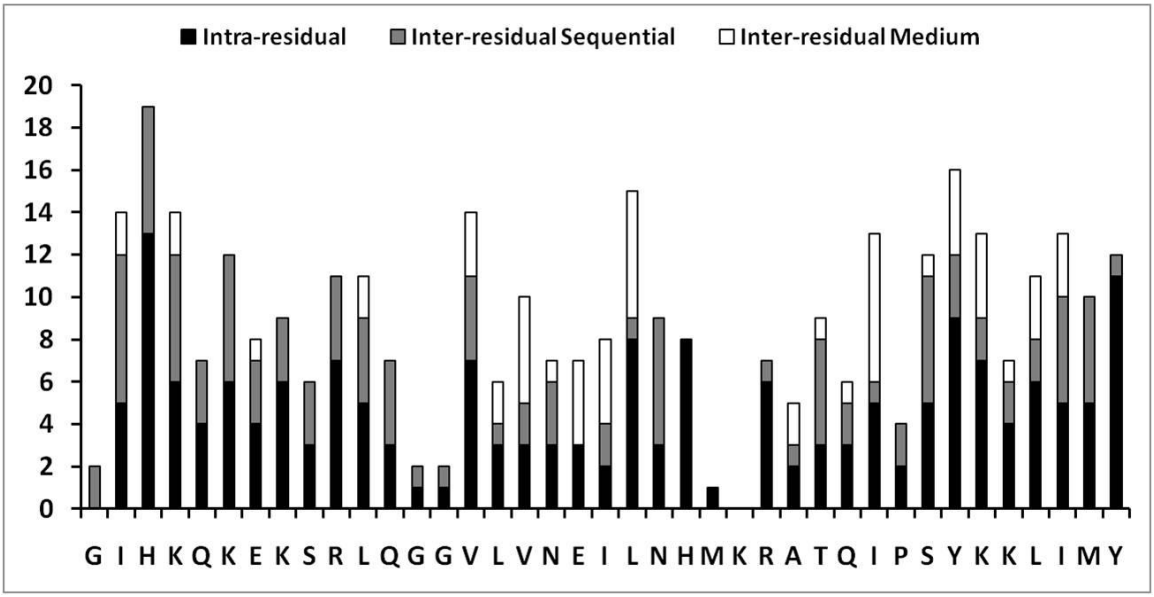

Figure 5-4. Histogram of the number of NOEs detected versus the residue number showing the number of intraresidue, sequential (i - j = 1), and medium range (i - j = 2, 3, 4) NOEs detected. Long-range (i - j > 4) NOEs were not observed.

5.4.2 *Positioning of the $PAP_{248-286}$ in the Micelle*. The paramagnetic quencher Mn^{2+} was used to determine the membrane orientation of the $PAP_{248-286}$. The

signal intensities of the nuclei that are in close proximity to the Mn^{2+} ion are decreased due to the increase in the relaxation rate of the nuclei. Because manganese ions cannot penetrate into the hydrophobic interior of the micelle, changes in signal intensity reflect the exposure of the amino acid residues of the peptide to the solvent. To identify the exposure of specific residues to solvent more precisely, 2D ^{1}H-^{1}H TOCSY spectra were used to monitor the changes in the chemical shift of the α-proton peaks after the addition of 0.8 mM $MnCl_2$. It is

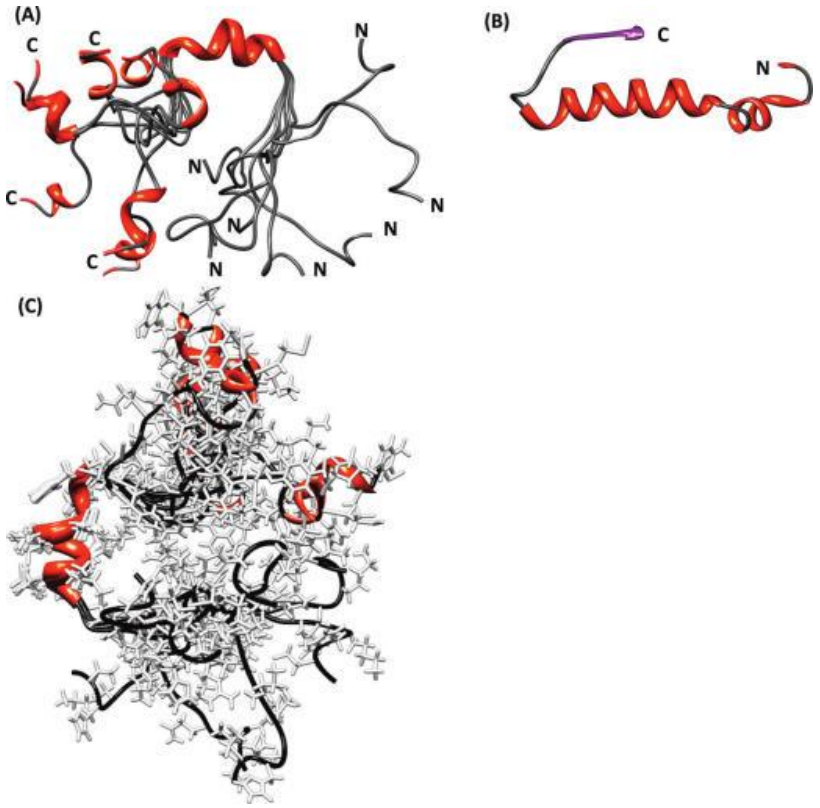

Figure 5-5. (A) Secondary structure representation of an overlaid ensemble of NMR-derived conformers for $PAP_{248-286}$ showing the helical region from V262-H270, the highly flexible N- and C-termini, and the short helix from S279-L283. (B) Secondary structure representation of $PAP_{248-286}$ extracted from the crystal structure of human PAP. In the crystal structure, residues L283-Y286 are in a β-sheet conformation, while residues K251-I277 are in a helical conformation with a distortion at G261. (C) All-atom representation of the $PAP_{248-286}$ conformational ensemble.

interesting to note that all of the peaks were completely quenched by a moderate

(0.8 mM) concentration of Mn^{2+}, except the α-protons of Ile 249 and Lys 251 and the *β*-protons of His 250 as shown in Figure 5-7. The near complete quenching of the residues of $PAP_{248-286}$ is in contrast to other amyloidogenic peptides, which are bound to the surface of detergent micelles but show only a partial reduction in the peak intensity after the addition of as much as 1.2 mM $MnCl_2$, and suggests the depth of penetration of $PAP_{248-286}$ is significantly less [*19, 20*]. Partial rather than complete quenching of the residues near the N-terminus of the peptide suggests this cluster of residues is either buried further into the micelle than the remainder of the peptide or the mobility of these residues is altered so that the rotational reorientation time of these residues is shorter than the electron spin relaxation time [*21-23*].

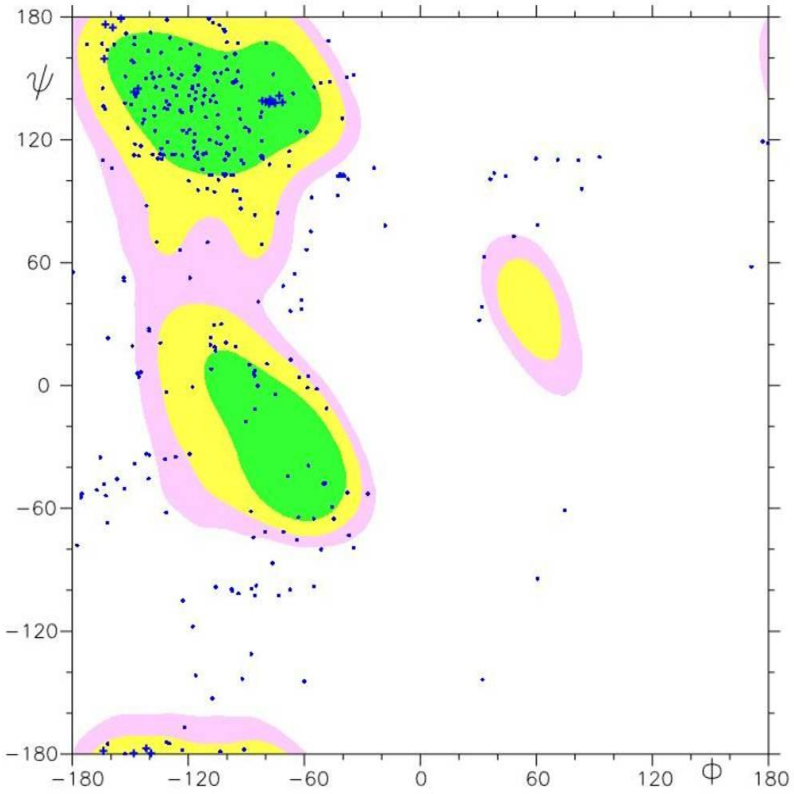

Figure 5-6. Ramachandran plot showing the phi and psi angles for the ensemble of conformers of the $PAP_{248-286}$ peptide.

5.5 DISCUSSION

Like many amyloidogenic short peptides and some amyloidogenic proteins, monomeric $PAP_{248-286}$ is predominantly unstructured in solution. However, $PAP_{248-286}$ is most active in the form of large aggregates with the characteristic β-sheet conformation of amyloid proteins (SEVI fibers). The structure of the final SEVI product is an obvious target for therapeutic intervention to block the action of SEVI, but the structures of intermediates along

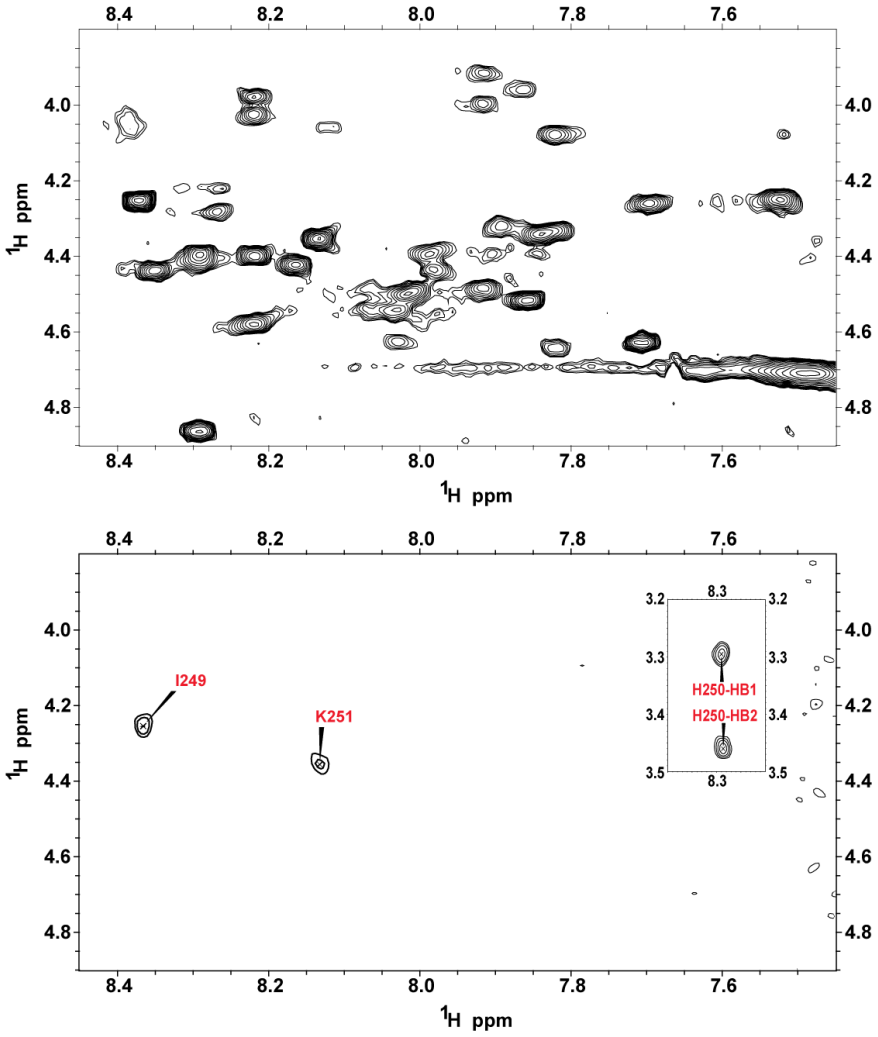

Figure 5-7. Fingerprint region of a 2D ^{1}H-^{1}H TOCSY spectrum of SDS micelles containing $PAP_{248-286}$ after the addition of 0.8 mM $MnCl_2$. The complete quenching of almost all peaks indicates that the peptide is well exposed to the solvent and does not penetrate deeply into the micelle.

the aggregation pathway of $PAP_{248-286}$ may ultimately be just as fruitful as therapeutic targets. The significance of the intermediate state is due to the energetics of the aggregation process; amyloid fibers are thermodynamically very stable but are kinetically difficult to form due to the low probability that multiple aggregation prone segments will align in the correct orientation required for the precise self-assembly of the very ordered amyloid fiber. For this reason, aggregation of completely disordered proteins usually gives rise to amorphous aggregates rather than structured oligomers, [*24-26*] a fact that has been exploited by small molecule inhibitors that stabilize the disordered state of the monomer and divert aggregation from potentially toxic protofibrillar species to nontoxic amorphous aggregates [*8, 27*]. Preorganization of the monomeric state can overcome some of the difficulties associated with self-assembly by restricting the degrees of freedom of motion in the native state and aligning aggregation-prone sites in the molecule in the proper orientation for intermolecular association [*28, 29*].

Taken these considerations into account, it can be seen that knowledge of the conformational preferences of the monomeric state of an amyloidogenic peptide can give substantial insight into the pathways of aggregation and eventual structure of the amyloid fiber [*19, 20, 30-32*]. However, the transient structure present in intrinsically disordered proteins is difficult to detect experimentally. Amyloidogenic proteins, particularly unstructured ones, are notoriously difficult to crystallize. The structural investigation of largely unstructured proteins by solution NMR is difficult due to poor chemical shift

dispersion and the structural heterogeneity of the ensemble, which gives rise to substantial line-broadening due to conformational exchange among members of the ensemble on the submillisecond timescale [*33*]. The most structured regions of the peptide, which are the regions of most interest for the reasons mentioned above, are usually the victim of the most severe line-broadening. Another serious complication is the aggregation of the peptide, which severely aggravates the line-broadening due to conformational exchange and severely limits the observation time available before the aggregated protein is too large for solution NMR experiments. These limitations can be partially overcome by using trifluoroethanol or hexafluoroisopropanol solvent systems, which stabilize helical states of the peptide and reduce or eliminate aggregation at high concentrations [*34-37*]. The structure-promoting solvents are used to stabilize transient structures in the natural conformational ensemble, which is overall disordered [*38*]. However, the use of these solvent systems can be questioned as they can give rise to artificial levels of structure that are not present in the biological system [*39-42*].

Many of these limitations can be overcome by the use of detergent micelles to stabilize the monomeric protein, which offer a more biologically relevant environment than organic solvents as amyloid proteins are often found in intimate association with cellular membranes and many of their biological effects derive from this association [*43-49*]. SEVI in particular is thought to act by binding to the cell membrane surface and neutralizing the natural repulsion that exists between the membranes of the HIV virion and the target cell [*6, 7*]. Unlike

mixtures of organic solvents and water, detergent micelles are heterogeneous like real cell membranes, having a hydrophobic core similar to the phospholipid bilayer and a polar interface between the micelle and solution. Detergents also have the additional advantage of trapping the aggregation-prone protein in a monomeric state due to the small size of the detergent micelle and the large electrostatic repulsion that exists between each micelle. This property is essential for limiting the rapid loss of signal due to aggregation of the peptide.

$PAP_{248-286}$ is largely disordered on the membrane surface, unlike many amyloid peptides. $PAP_{248-286}$ binds to the surface of the SDS micelle in a largely disordered manner. The complete quenching of the signal of almost every residue at a relatively low concentration of Mn^{2+} suggests the binding of $PAP_{248-286}$ is almost entirely electrostatic, as previously inferred based on differential scanning calorimetry and the loss of $PAP_{248-286}$ infection promoting activity in mutants lacking cationic residues [*7, 11*]. The superficial binding of $PAP_{248-286}$ to the surface may explain the apparent lack of toxicity of $PAP_{248-286}$ as the ability of amyloid peptides to disrupt membranes is frequently correlated with the penetration of the peptide into the hydrophobic part of the bilayer membrane [*6, 19, 20, 50, 51*].

Most unstructured amyloidogenic peptides readily adopt an α-helical conformation when bound to membranes due to the amphipathic and hydrophobic nature of most amyloidogenic sequences. A common motif among amyloid peptides bound to detergent micelles is the helix-turn-helix motif, in which an amphipathic helix is separated from a more polar helix by a short

flexible linker region. Most high-resolution structures of amyloidogenic peptides bound to detergent micelles show some variation of this motif, although a considerable degree of conformational flexibility is present in most of the peptides as the location of the linker region and the length of the helical regions of the peptide can vary substantially depending on the experimental conditions [*52-55*]. The structure of $PAP_{248-286}$ is consistent with this general trend; however, the helical content is lower than other amyloid peptides, and the structure is dominated by long flexible regions joining short helices rather than by the well-defined helices separated by short linker regions that are typical of other amyloid peptides.

While the α-helical regions of the membrane-bound monomer of amyloid peptides are not found in the final amyloid product, regions that are disordered in the membrane-bound state frequently remain so throughout the aggregation pathway. For example, the N-terminus of $A\beta_{1-42}$ and the C-terminus of α-synuclein are disordered in both SDS micelles and in the structure of the amyloid fiber [*56-61*]. However, the disordered regions of these peptides are composed of negatively charged residues and not poised to interact favorably with the negatively charged cell membrane. On the other hand, the disordered N-terminus of $PAP_{248-286}$ has a high percentage of positively charged lysine and arginine residues, which have a high affinity for surface of cell membranes. If the conformational flexibility and superficial electrostatic membrane binding found in monomeric $PAP_{248-286}$ is also present in the structure of the membrane-bound SEVI amyloid fiber, these structural characteristics may help explain the unique

proficiency of SEVI among amyloid proteins to enhance HIV infection. Flexible, highly charged cationic polymers like polylysine share SEVI's ability to enhance retroviral infection rates and share many common characteristics with the structure and membrane binding mode proposed here [*11, 62, 63*]. Like $PAP_{248-286}$, these polymers bind exclusively electrostatically to the membrane surface without penetration into the headgroup region, undergo helix-to-*β*-sheet transitions, and retain a considerable amount of flexibility when bound to the surface [*64-66*]. Disordered regions frequently have higher interaction rates than structured regions in proteins because the interaction volume (radius of capture) is larger for the disordered state than a compact, folded one [*67, 68*]. This is especially true if, like the association of proteins with lipids, binding is based on multiple weak, nonspecific interactions rather than a single specific interaction site [*69*]. Although a considerable degree of conformational reorganization is required to form the SEVI amyloid fiber, an unusual degree of disorder in the SEVI amyloid fiber may facilitate the membrane bridging interactions implicated in the enhancement of HIV infection by both SEVI and polylysine [*68*]. In addition, disordered regions in the amyloid fiber may facilitate the endocytosis of SEVI fibers. Many endocyotic proteins have extensive disordered regions, which appear to allow the capture of endocyotic nucleation factors across a large cytosolic volume [*69*]. A high degree of disorder in the SEVI amyloid fiber would likely enhance the rate of endocyotic internalization relative to other amyloid fibers, which internalize the HIV virion if it is bound to the SEVI fiber at the time [*70*]. The structure of SEVI amyloid fibers remains unsolved, and only limited

mutagenesis work has been done [*6, 7*]. Further structural work on the SEVI amyloid fiber is likely to yield informative insights into the mechanism of HIV enhancement by SEVI and serve as a test of this hypothesis.

Nascent helical structure in A274-I284 and V262-H270 may nucleate amyloid formation. Two regions of nascent helical structure may be nucleation sites for amyloid formation. The first region consists of a stable, regular α-helix extending from V262 to H270, and the second region consists of two dynamic or transient α- or 3_{10} helices extending from A274-Q276 and Y280-I284 separated by a kink or distortion at residues I277-S279. The propensity for helical conformations in these regions may be essential for fiber formation, as a helix to-*β*-strand transition is a common intermediate step in the amyloidogenesis of many amyloid proteins [*30, 71*]. The importance of helical intermediates in amyloid formation can be seen by the fact that the induction of helical structure through either the addition of a helix-promoting solvent or by membrane binding can dramatically enhance the rate of amyloidogenesis [*71*]. Mutational analyses of amyloid proteins with helical intermediates have shown that the helical intermediate should be metastable to efficiently promote *β*-strand formation. The stability of the helices in these regions may be critical for determining the ultimate rate of amyloidogenesis; if the helices are excessively stabilized by mutations in the sequence or by helix stabilizing drugs, the peptide can be kinetically trapped as a helical intermediate; conversely, a very unstable helix is insufficiently populated to impact the kinetics [*72, 73*].

The limited amount of mutagenesis data currently available on SEVI

suggests the nascent, dynamic helix at the C-terminus is essential for amyloidogenesis. Analyses of truncated versions of the $PAP_{248-286}$ peptide have shown that deletions at the C-terminal end of the peptide in the region of the dynamic helix significantly reduce both amyloid formation and HIV promotion [*6*]. On the other hand, deletions at the N-terminal end, which is disordered in the NMR structure, have little effect. The metastable 3_{10} helices that are present in some of the structures at the C-terminus are particularly suited for promoting intermolecular interactions and *β*-strand formation [*30*]. Because of the more extended conformation of the 3_{10} helix as compared to an α-helix, the grooves of the 3_{10} helix are larger and more easily accommodate the side-chains of another peptide. Furthermore, the *β*-turns that comprise the 3_{10} helix are less stable than the α-helix and can be easily destabilized to form *β*-strands, [*30*] as shown by the crystal structure of PAP in which L283-Y286 is part of a *β*-strand on the surface of the protein [*74*].

The proposed amyloid nucleation sites are consistent with predictions of amyloidogenic regions. The increasing number of known amyloidogenic proteins has made possible the use of bioinformatic tools to predict amyloidogenic regions within proteins. The AGGRESCAN algorithm uses the inherent aggregation propensities of individual amino acids determined from mutational data on the A*β* peptide to find “hot spots”, short (~5 residue) stretches of amino acid that serve as nucleating centers for amyloid formation [*75, 76*]. A color-mapped representation of the aggregation propensity from AGGRESCAN on the $PAP_{248-286}$ structure is provided in Figure 5-8. As shown in Figure 5-8, the

predictions of AGGRESCAN substantially match the helical regions of the NMR structure. AGGRESCAN predicts two aggregation "hot spots" in $PAP_{248-286}$: G260-E266, which is approximately within the V262-H270 helical region, and K281-Y286 in the area of both the dynamic helix at the C-terminal end and the L283-Y286 sequence identified by activity studies on truncated peptides. The PASTA algorithm uses pairwise energy functions to determine the probability that a given stretch of residues can be in a parallel or antiparallel *β*-strand [*77, 78*]. Similar to the prediction of AGGRESCAN, PASTA predicts that residues 262-270 are prone to form parallel *β*-sheets (energy score of -6 for residues 262-270 in a parallel alignment; stretches of residues in the *β*-sheet conformation in known fiber structures generally have a score of >4).

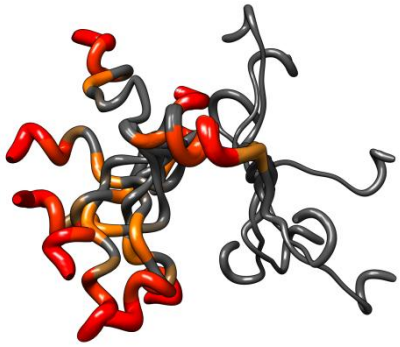

Figure 5-8. Prediction of the amyloidogenic propensity of the $PAP_{248-286}$ sequence by AGGRESCAN. Red, orange, and gray colors indicate regions of high, moderate, and low amyloidogenic propensity, respectively.

Because amyloid formation is almost always deleterious to a protein's normal function and general cellular health, there is substantial evolutionary pressure against amyloid formation. One method of preventing amyloid formation is to flank particularly amyloidogenic sequences with "gatekeeper residues", evolutionarily conserved sequences that are either enriched in residues that are

either strong *β*-sheet breakers (glycine or proline residues) or highly charged sequences that enhance the electrostatic repulsion between proteins and therefore minimize aggregation [79]. The ordered 262-270 region of $PAP_{248-286}$ fits this pattern, being terminated on the N-terminal side by a double glycine repeat (GG) and flanked by a highly charged sequence (QKEK) nearby. Similarly, the C-terminal side of this sequence is flanked by a proline residue (P278) and a nearby lysine repeat (KK), which would also serve to limit the aggregation of the Y280-Y286 amyloidogenic region. This pattern of gatekeeper residues is conserved in all PAP sequences determined so far, suggesting that one of the functions of these residues is to limit the propensity of PAP to aggregate. The observation that $PAP_{248-286}$ with all of the cationic amino acids mutated to alanine has a higher tendency to aggregate gives some support to this hypothesis [7].

5.6 CONCLUSION

We have solved the first high-resolution structure of the SEVI precursor peptide $PAP_{248-286}$ as a first step toward understanding the structural factors that drive $PAP_{248-286}$ to form the amyloid fibers that are identified as the form responsible for increasing HIV infectivity. $PAP_{248-286}$ has an unusual amount of structural disorder when bound to the membrane as compared to other amyloid proteins, which may facilitate the binding of virus particles by maximizing the radius of capture for incoming virus particles. The disordered N-terminal end also has a high percentage of positively charged residues, which can interact with multiple lipids on the virus surface. Furthermore, the combination of structural

disorder and high positive charge at the N-terminus of $PAP_{248-286}$ may be linked to the high affinity of the SEVI amyloid fiber for the HIV virus and the remarkable enhancement of HIV infectivity by the SEVI amyloid fiber if this disorder persists in the amyloid state as predicted. Although the peptide is mostly disordered, two ordered regions of the peptide are consistent with bioinformatic predictions of high amyloidogenic propensity. The regions of nascent structure in the peptide bear further investigation, especially by mutational analysis to identify residues that are particularly responsible for controlling SEVI formation.

REFERENCES

[1] Dimitrov, D. S., Willey, R. L., Sato, H., Chang, L. J., Blumenthal, R., Martin, M. A. (1993) Quantitation of human immunodeficiency virus type 1 infection kinetics. *J. Virol. 67*, 2182-2190.

[2] Rusert, P., Fischer, M., Joos, B., Leemann, C., Kuster, H., Flepp, M., Bonhoeffer, S., Gunthard, H. F., Trkola, A. (2004) Quantification of infectious HIV-1 plasma viral load using a boosted in vitro infection protocol. *Virology 326*, 113-129.

[3] Perelson, A. S., Neumann, A. U., Markowitz, M., Leonard, J. M., Ho, D. D. (1996) HIV-1 dynamics in vivo: virion clearance rate, infected cell life-span, and viral generation time. *Science 271*, 1582-1586.

[4] Berg, H. C., Purcell, E. M. (1977) Physics of chemoreception. *Biophys. J. 20*, 193-219.

[5] Eckert, D. M., Kim, P. S. (2001) Mechanisms of viral membrane fusion and its inhibition. *Annu. Rev. Biochem. 70*, 777-810.

[6] Munch, J., Rucker, E., Standker, L., Adermann, K., Goffinet, C., Schindler, M., Wildum, S., Chinnadurai, R., Rajan, D., Specht, A., Giménez-Gallego, G., Sánchez, P. C., Fowler, D. M., Koulov, A., Kelly, J. W., Mothes, W., Grivel, J. C., Margolis, L., Keppler, O. T., Forssmann, W. G., Kirchhoff, F. (2007) Semen-derived amyloid fibrils drastically enhance HIV infection. *Cell 131*, 1059-1071.

[7] Roan, N. R., Munch, J., Arhel, N., Mothes, W., Neidleman, J., Kobayashi, A., Smith-McCune, K., Kirchhoff, F., Greene, W. C. (2009) The cationic properties of SEVI underlie its ability to enhance human immunodeficiency virus infection. *J. Virol. 83*, 73-80.

[8] Hauber, I., Hohenberg, H., Holstermann, B., Hunstein, W., Hauber, J. (2009) The main green tea polyphenol epigallocatechin-3-gallate counteracts semen-mediated enhancement of HIV infection. *Proc. Natl. Acad. Sci. U.S.A. 106*, 9033-9038.

[9] Hong, S. H., Klein, E. A., Das Gupta, J., Hanke, K., Weight, C. J., Nguyen, C., Gaughan, C., Kim, K. A., Bannert, N., Kirchhoff, F., Munch, J., Silverman, R. H. (2009) Fibrils of prostatic acid phosphatase fragments boost infections with XMRV (xenotropic murine leukemia virus-related virus), a human retrovirus associated with prostate cancer. *J. Virol. 83*, 6995-7003.

[10] Wojtowicz, W. M., Farzan, M., Joyal, J. L., Carter, K., Babcock, G. J., Israel, D. I., Sodroski, J., Mirzabekov, T. (2002) Stimulation of enveloped virus infection by beta-amyloid fibrils. *J. Biol. Chem. 277*, 35019-35024.

[11] Brender, J. R., Hartman, K., Gottler, L. M., Cavitt, M. E., Youngstrom, D. W., Ramamoorthy, A. (2009) Helical conformation of the SEVI precursor peptide

PAP248-286, a dramatic enhancer of HIV infectivity, promotes lipid aggregation and fusion. *Biophys. J. 97*, 2474-2483.

[12] Delaglio, F., Grzesiek, S., Vuister, G. W., Zhu, G., Pfeifer, J., Bax, A. (1995) NMRPipe: a multidimensional spectral processing system based on UNIX pipes. *J. Biomol. NMR 6*, 277-293.

[13] Goddard, T. D., Kneller, D. G. (1999) *SPARKY 3*, University of California: San Francisco, CA.

[14] Wuthrich, K. (1986) *NMR of Proteins and Nucleic Acids*, John Wiley and Sons: New York.

[15] Cornilescu, G., Delaglio, F., Bax, A. (1999) Protein backbone angle restraints from searching a database for chemical shift and sequence homology. *J. Biomol. NMR 13*, 289-302.

[16] Nilges, M., Gronenborn, A. M., Brunger, A. T., Clore, G. M. (1988) Determination of three-dimensional structures of proteins by simulated annealing with interproton distance restraints. Application to crambin, potato carboxypeptidase inhibitor and barley serine proteinase inhibitor 2. *Protein Eng. 2*, 27-38.

[17] Stein, E. G., Rice, L. M., Brunger, A. T. (1997) Torsion-angle molecular dynamics as a new efficient tool for NMR structure calculation. *J. Magn. Reson. 124*, 154-164.

[18] Laskowski, R. A., Rullmann, J. A. C., MacArthur, M. W., Kaptein, R., Thornton, J. M. (1996) AQUA and PROCHECK-NMR: programs for checking the quality of protein structures solved by NMR. *J. Biomol. NMR 8*, 477-486.

[19] Nanga, R. P., Brender, J. R., Xu, J., Veglia, G., Ramamoorthy, A. (2008) Structures of rat and human islet amyloid polypeptide IAPP(1-19) in micelles by NMR spectroscopy. *Biochemistry 47*, 12689-12697.

[20] Nanga, R. P., Brender, J. R., Xu, J., Hartman, K., Subramanian, V., Ramamoorthy, A. (2009) Three-dimensional structure and orientation of rat islet amyloid polypeptide protein in a membrane environment by solution NMR spectroscopy. *J. Am. Chem. Soc. 131*, 8252-8261.

[21] Tuzi, S., Hasegawa, J., Kawaminami, R., Naito, A., Saito, H. (2001) Regio-selective detection of dynamic structure of transmembrane alpha-helices as revealed from (13)C NMR spectra of [3-13C]Ala-labeled bacteriorhodopsin in the presence of Mn2+ ion. *Biophys. J. 81*, 425-434.

[22] Bloembergen, N. (1957) Proton relaxation times in paramagnetic solutions. *J. Chem. Phys. 27*, 572-573.

[23] Solomon, I. (1955) Relaxation processes in a system of two spins. *Phys. Rev. 99*, 559-565.

[24] Chimon, S., Shaibat, M. A., Jones, C. R., Calero, D. C., Aizezi, B., Ishii, Y. (2007) Evidence of fibril-like β-sheet structures in a neurotoxic amyloid intermediate of Alzheimer's β-amyloid. *Nat. Struct. Mol. Biol. 14*, 1157-1164.

[25] Lambert, M. P., Barlow, A. K., Chromy, B. A., Edwards, C., Freed, R., Liosatos, M., Morgan, T. E., Rozovsky, I., Trommer, B., Viola, K. L., Wals, P., Zhang, C., Finch, C. E., Krafft, G. A., Klein, W. L. (1998) Diffusible, nonfibrillar ligands derived from Abeta1-42 are potent central nervous system neurotoxins. *Proc. Natl. Acad. Sci. U.S.A. 95*, 6448-6453.

[26] Ferreira, S. T., Vieira, M. N. N., De Felice, F. G. (2007) Soluble protein oligomers as emerging toxins in Alzheimer's and other amyloid diseases. *IUBMB Life 59*, 332-345.

[27] Ehrnhoefer, D. E., Bieschke, J., Boeddrich, A., Herbst, M., Masino, L., Lurz, R., Engemann, S., Pastore, A., Wanker, E. E. (2008) EGCG redirects amyloidogenic polypeptides into unstructured, off-pathway oligomers. *Nat. Struct. Mol. Biol. 15*, 558-566.

[28] Knight, J. D., Hebda, J. A., Miranker, A. D. (2006) Conserved and cooperative assembly of membrane-bound alpha-helical states of islet amyloid polypeptide. *Biochemistry 45*, 9496-9508.

[29] Hall, D., Hirota, N., Dobson, C. M. (2005) A toy model for predicting the rate of amyloid formation from unfolded protein. *J. Mol. Biol. 351*, 195-205.

[30] Harrison, R. S., Sharpe, P. C., Singh, Y., Fairlie, D. P. (2007) Amyloid peptides and proteins in review. *Rev. Physiol. Biochem. Pharmacol. 159*, 1-77.

[31] Bertoncini, C. W., Rasia, R. M., Lamberto, G. R., Binolfi, A., Zweckstetter, M., Griesinger, C., Fernandez, C. O. (2007) Structural characterization of the intrinsically unfolded protein beta-synuclein, a natural negative regulator of alpha-synuclein aggregation. *J. Mol. Biol. 372*, 708-722.

[32] Schweitzer-Stenner, R., Measey, T., Hagarman, A., Eker, F., Griebenow, K. (2006) Salmon calcitonin and amyloid beta: two peptides with amyloidogenic capacity adopt different conformational manifolds in their unfolded states. *Biochemistry 45*, 2810-2819.

[33] Hsu, S. T. D., Bertoncini, C. W., Dobson, C. M. (2009) Use of protonless

NMR spectroscopy to alleviate the loss of information resulting from exchange-broadening. *J. Am. Chem. Soc. 131*, 7222-7223.

[34] Tomaselli, S., Esposito, V., Vangone, P., van Nuland, N. A. J., Bonvin, A., Guerrini, R., Tancredi, T., Temussi, P. A., Picone, D. (2006) The alpha-to-beta conformational transition of Alzheimer's Abeta-(1-42) peptide in aqueous media is reversible: a step by step conformational analysis suggests the location of beta conformation seeding. *ChemBioChem 7*, 257-267.

[35] Valerio, M., Porcelli, F., Zbilut, J. P., Giuliani, A., Manetti, C., Conti, F. (2008) pH effects on the conformational preferences of amyloid beta-peptide (1-40) in HFIP aqueous solution by NMR spectroscopy. *ChemMedChem 3*, 833-843.

[36] Crescenzi, O., Tomaselli, S., Guerrini, R., Salvadori, S., D'Ursi, A. M., Temussi, P. A., Picone, D. (2002) Solution structure of the Alzheimer amyloid beta-peptide (1-42) in an apolar microenvironment. Similarity with a virus fusion domain. *Eur. J. Biochem. 269*, 5642-5648.

[37] Cort, J. R., Liu, Z., Lee, G. M., Huggins, K. N., Janes, S., Prickett, K., Andersen, N. H. (2009) Solution state structures of human pancreatic amylin and pramlintide. *Protein Eng. Des. Sel. 22*, 497-513.

[38] Jao, S. C., Ma, K., Talafous, J., Orlando, R., Zagorski, M. G. (1997) Trifluoroacetic acid pretreatment reproducibly disaggregates the amyloid β-peptide. *Amyloid: Int. J. Exp. Clin. Invest. 4*, 240-252.

[39] Buck, M. (1998) Trifluoroethanol and colleagues: cosolvents come of age. Recent studies with peptides and proteins. *Q. Rev. Biophys. 31*, 297-355.

[40] Hong, D. P., Hoshino, M., Kuboi, R., Goto, Y. (1999) Clustering of fluorine-substituted alcohols as a factor responsible for their marked effects on proteins and peptides. *J. Am. Chem. Soc. 121*, 8427-8433.

[41] Gast, K., Siemer, A., Zirwer, D., Damaschun, G. (2001) Fluoroalcohol-induced structural changes of proteins: some aspects of cosolvent-protein interactions. *Eur. Biophys. J. 30*, 273-283.

[42] Kumar, S., Modig, K., Halle, B. (2003) Trifluoroethanol-induced beta --> alpha transition in beta-lactoglobulin: hydration and cosolvent binding studied by 2H, 17O, and 19F magnetic relaxation dispersion. *Biochemistry 42*, 13708-13716.

[43] Hebda, J. A., Miranker, A. D. (2009) The interplay of catalysis and toxicity by amyloid intermediates on lipid bilayers: insights from type II diabetes. *Annu. Rev. Biophys. 38*, 125-152.

[44] Brender, J. R., Durr, U. H. N., Heyl, D., Budarapu, M. B., Ramamoorthy, A. (2007) Membrane fragmentation by an amyloidogenic fragment of human Islet Amyloid Polypeptide detected by solid-state NMR spectroscopy of membrane nanotubes. *Biochim. Biophys. Acta 1768*, 2026-2029.

[45] Engel, M. F. (2009) Membrane permeabilization by Islet Amyloid Polypeptide. *Chem. Phys. Lipids 160*, 1-10.

[46] Bystrom, R., Aisenbrey, C., Borowik, T., Bokvist, M., Lindstrom, F., Sani, M. A., Olofsson, A., Grobner, G. (2008) Disordered proteins: biological membranes as two-dimensional aggregation matrices. *Cell Biochem. Biophys. 52*, 175-189.

[47] Aisenbrey, C., Borowik, T., Bystrom, R., Bokvist, M., Lindstrom, F., Misiak, H., Sani, M. A., Grobner, G. (2008) How is protein aggregation in amyloidogenic diseases modulated by biological membranes? *Eur. Biophys. J. 37*, 247-255.

[48] Beyer, K. (2007) Mechanistic aspects of Parkinson's disease: alpha-synuclein and the biomembrane. *Cell Biochem. Biophys. 47*, 285-299.

[49] Lashuel, H. A., Lansbury, P. T. (2006) Are amyloid diseases caused by protein aggregates that mimic bacterial pore-forming toxins? *Q. Rev. Biophys. 39*, 167-201.

[50] Smith, P. E., Brender, J. R., Ramamoorthy, A. (2009) Induction of negative curvature as a mechanism of cell toxicity by amyloidogenic peptides: the case of islet amyloid polypeptide. *J. Am. Chem. Soc. 131*, 4470-4478.

[51] Brender, J. R., Hartman, K., Reid, K. R., Kennedy, R. T., Ramamoorthy, A. (2008) A single mutation in the nonamyloidogenic region of islet amyloid polypeptide greatly reduces toxicity. *Biochemistry 47*, 12680-12688.

[52] Coles, M., Bicknell, W., Watson, A. A., Fairlie, D. P., Craik, D. J. (1998) Solution structure of amyloid beta-peptide(1-40) in a water-micelle environment. Is the membrane-spanning domain where we think it is? *Biochemistry 37*, 11064-11077.

[53] Patil, S. M., Xu, S., Sheftic, S. R., Alexandrescu, A. T. (2009) Dynamic alpha-helix structure of micelle-bound human amylin. *J. Biol. Chem. 284*, 11982-11991.

[54] Ulmer, T. S., Bax, A., Cole, N. B., Nussbaum, R. L. (2005) Structure and

dynamics of micelle-bound human alpha-synuclein. *J. Biol. Chem. 280*, 9595-9603.

[55] Motta, A., Andreotti, G., Amodeo, P., Strazzullo, G., Morelli, M. A. C. (1998) Solution structure of human calcitonin in membrane-mimetic environment: the role of the amphipathic helix. *Proteins 32*, 314-323.

[56] Heise, H., Hoyer, W., Becker, S., Andronesi, O. C., Riedel, D., Baldus, M. (2005) Molecular-level secondary structure, polymorphism, and dynamics of full-length alpha-synuclein fibrils studied by solid-state NMR. *Proc. Natl. Acad. Sci. U.S.A. 102*, 15871-15876.

[57] Vilar, M., Chou, H. T., Luhrs, T., Maji, S. K., Riek-Loher, D., Verel, R., Manning, G., Stahlberg, H., Riek, R. (2008) The fold of alpha-synuclein fibrils. *Proc. Natl. Acad. Sci. U.S.A. 105*, 8637-8642.

[58] Del Mar, C., Greenbaum, E. A., Mayne, L., Englander, S. W., Woods, V. L. (2005) Structure and properties of alpha-synuclein and other amyloids determined at the amino acid level. *Proc. Natl. Acad. Sci. U.S.A. 102*, 15477-15482.

[59] Shao, H. Y., Jao, S. C., Ma, K., Zagorski, M. G. (1999) Solution structures of micelle-bound amyloid beta-(1-40) and beta-(1-42) peptides of Alzheimer's disease. *J. Mol. Biol. 285*, 755-773.

[60] Luhrs, T., Ritter, C., Adrian, M., Riek-Loher, D., Bohrmann, B., Doeli, H., Schubert, D., Riek, R. (2005) 3D structure of Alzheimer's amyloid-beta(1-42) fibrils. *Proc. Natl. Acad. Sci. U.S.A. 102*, 17342-17347.

[61] Petkova, A. T., Ishii, Y., Balbach, J. J., Antzutkin, O. N., Leapman, R. D., Delaglio, F., Tycko, R. (2002) A structural model for Alzheimer's beta -amyloid fibrils based on experimental constraints from solid state NMR. *Proc. Natl. Acad. Sci. U.S.A. 99*, 16742-16747.

[62] Davis, H. E., Rosinski, M., Morgan, J. R., Yarmush, M. L. (2004) Charged polymers modulate retrovirus transduction via membrane charge neutralization and virus aggregation. *Biophys. J. 86*, 1234-1242.

[63] Landazuri, N., Le Doux, J. M. (2004) Complexation of retroviruses with charged polymers enhances gene transfer by increasing the rate that viruses are delivered to cells. *J. Gene. Med. 6*, 1304-1319.

[64] Tribet, C., Vial, F. (2008) Flexible macromolecules attached to lipid bilayers: impact on fluidity, curvature, permeability and stability of the membranes. *Soft Matter 4*, 68-81.

[65] Zloh, M., Ramaswamy, C., Sakthivel, T., Wilderspin, A., Florence, A. T. (2005) Investigation of the association and flexibility of cationic lipidic peptide dendrons by NMR spectroscopy. *Magn. Reson. Chem. 43*, 47-52.

[66] Lee, J. H., Gustin, J. P., Chen, T. H., Payne, G. F., Raghavan, S. R. (2005) Vesicle--biopolymer gels: networks of surfactant vesicles connected by associating biopolymers. *Langmuir 21*, 26-33.

[67] Shoemaker, B. A., Portman, J. J., Wolynes, P. G. (2000) Speeding molecular recognition by using the folding funnel: the fly-casting mechanism. *Proc. Natl. Acad. Sci. U.S.A. 97*, 8868-8873.

[68] Tompa, P. (2009) Structural disorder in amyloid fibrils: its implication in dynamic interactions of proteins. *FEBS J. 276*, 5406-5415.

[69] Dafforn, T. R., Smith, C. J. (2004) Natively unfolded domains in endocytosis: hooks, lines and linkers. *EMBO Rep. 5*, 1046-1052.

[70] Miyauchi, K., Kim, Y., Latinovic, O., Morozov, V., Melikyan, G. B. (2009) HIV enters cells via endocytosis and dynamin-dependent fusion with endosomes. *Cell 137*, 433-444.

[71] Abedini, A., Raleigh, D. P. (2009) A role for helical intermediates in amyloid formation by natively unfolded polypeptides? *Phys. Biol. 6*, 15005.

[72] Brender, J. R., Lee, E. L., Cavitt, M. A., Gafni, A., Steel, D. G., Ramamoorthy, A. (2008) Amyloid fiber formation and membrane disruption are separate processes localized in two distinct regions of IAPP, the type-2-diabetes-related peptide. *J. Am. Chem. Soc. 130*, 6424-6429.

[73] Nerelius, C., Sandegren, A., Sargsyan, H., Raunak, R., Leijonmarck, H., Chatterjee, U., Fisahn, A., Imarisio, S., Lomas, D. A., Crowther, D. C., Stromberg, R., Johansson, J. (2009) Alpha-helix targeting reduces amyloid-beta peptide toxicity. *Proc. Natl. Acad. Sci. U.S.A. 106*, 9191-9196.

[74] Jakob, C. G., Lewinski, K., Kuciel, R., Ostrowski, W., Lebioda, L. (2000) Crystal structure of human prostatic acid phosphatase . *Prostate 42*, 211-218.

[75] de Groot, N. S., Pallares, I., Aviles, F. X., Vendrell, J., Ventura, S. (2005) Prediction of "hot spots" of aggregation in disease-linked polypeptides. *BMC Struct. Biol. 5*, 18-32.

[76] Conchillo-Sole, O., de Groot, N. S., Aviles, F. X., Vendrell, J., Daura, X., Ventura, S. (2007) AGGRESCAN: a server for the prediction and evaluation of "hot spots" of aggregation in polypeptides. *BMC Bioinformatics 8*, 65-81.

[77] Trovato, A., Seno, F., Tosatto, S. C. E. (2007) The PASTA server for protein aggregation prediction. *Protein Eng. Des. Sel.* 2007, *20*, 521-523.

[78] Trovato, A., Chiti, F., Maritan, A., Seno, F. (2006) Insight into the structure of amyloid fibrils from the analysis of globular proteins. *PLoS Comput. Biol. 2*, 1608-1618.

[79] Reumers, J., Maurer-Stroh, S., Schymkowitz, J., Rousseau, F. (2009) Protein sequences encode safeguards against aggregation. *Hum. Mutat. 30*, 431-437.

CHAPTER 6. CONCLUSIONS AND FUTURE DIRECTIONS

In type II diabetics, IAPP is the major component of the amyloid deposits found in the β-cells of pancreas. While initial studies on this peptide largely focused on identifying and characterizing the amyloidogenic segment of the peptide, emerging evidence supports the hypothesis that the intermediate helical species bound to the membrane are the highly toxic species. In particular, it has been shown that membrane aggregation (residues 1-19) and amyloid formation (residues 20-29) are two separate processes and the sequences responsible for these events are located in different regions within the same peptide. But the membrane bound α-helical intermediate structures of both the truncated or full length peptide were not available for IAPP.

In order to provide insights into the misfolding pathway, as described in Chapter 2, we have solved the high-resolution structures and found the membrane orientations of human and rat $IAPP_{1-19}$ using NMR experiments on dodecylphosphocholine micelles. The 1-19 fragment was chosen because previous studies suggested that this region is responsible for most of the membrane damage induced by hIAPP. While both peptides have similar α-helical folds, a drastic difference in their membrane topologies was observed. The rat $IAPP_{1-19}$ is bound to the surface of the micelle whereas the human $IAPP_{1-19}$ penetrates much deeper into the micelle. The structure determined here may

hold insights into both the normal physiological action of IAPP and the damage to *β*-cell membranes caused by the pathological aggregation of IAPP.

As discussed in Chapter 3, we extended our study to full-length rat IAPP, which forms an intermediate α-helical structure when bound to the membrane but does not form amyloid fibrils. In order to address this behavior of the peptide, we have solved the three-dimensional structure of full length rat IAPP in dodecylphosphocholine micelles. By comparing the rat IAPP structure with other toxic and nontoxic variants of IAPP, we have identified two structural features that correlate with the toxicity of the peptide. Rat IAPP is bound to the surface in a manner similar to that of the nontoxic rat $IAPP_{1-19}$ and low-pH human $IAPP_{1-19}$ peptides and does not penetrate deeply into the micelle like the toxic neutral pH human $IAPP_{1-19}$ peptide. The position of the N-terminal disulfide bridge has been identified as another factor that may modulate aggregation and toxicity. The nontoxic rat IAPP structure has a relatively rigid N-terminus that is bent toward the hydrophobic face of the amphipathic helix, whereas more toxic forms of IAPP have a more flexible N-terminus that is positioned away from the amphipathic helix. A comparison of the rat IAPP structure to other homologous peptides that share the same receptors, human IAPP, and fragments from the human IAPP sequence shows rat IAPP does not possess the *β*-turn seen in these peptides that is required to activate the receptor, but this region is flexible and may form a *β*-turn upon binding to the receptor.

While the structure of human IAPP with a non-amidated C-terminus was solved in SDS micelles at an acidic pH of 4.9, it would be interesting to see if

amidation at the C-terminus and change in the His18 protonation state would have any influence on the structure of the human IAPP peptide at physiological pH. Therefore, as presented in Chapter 4, we have solved the structure of human IAPP with an amidated C-terminus in SDS micelles at pH 7.3. When compared with the non-amidated C-terminus human IAPP structure solved at pH 4.9, both structures have an overall kinked helix motif, with residues 7-17 and 21-28 in a helical conformation. However, the C-terminus of amidated human IAPP is structured, with a 3_{10} dynamic helix from Gly33-Asn35, while the C-terminus is disordered in the structure of recombinant human IAPP solved at acidic pH. In addition, the angle between the N- and C-terminal helices is constrained to 85º instead of the free rotation present in the structure of recombinant human IAPP. These differences observed in our structure might play an important role in the aggregation process of human IAPP.

Recently another amyloid peptide known as SEVI was discovered by Munch et al, in 2007 which drastically enhances the infection of HIV. But the structures of the SEVI are not known in any form making it difficult to predict the interactions of this peptide with the cell membrane that facilitate HIV viral attachment. Therefore, as elaborated in Chapter 5, we have solved the first high-resolution structure of the SEVI precursor peptide $PAP_{248-286}$ as a first step toward understanding the structural factors that drive $PAP_{248-286}$ to form the amyloid fibers, which are identified as the form responsible for increasing HIV infectivity. $PAP_{248-286}$ has an unusual amount of structural disorder when bound to the membrane as compared to other amyloid proteins, which may facilitate the

binding of virus particles by maximizing the radius of capture for incoming virus particles. The disordered N-terminal end also has a high percentage of positively charged residues, which can interact with multiple lipids on the virus surface. Furthermore, the combination of structural disorder and high positive charge at the N-terminus of $PAP_{248-286}$ may be linked to the high affinity of the SEVI amyloid fiber for the HIV virus and the remarkable enhancement of HIV infectivity by the SEVI amyloid fiber, if this disorder persists in the amyloid state as predicted. Although the peptide is mostly disordered, two ordered regions of the peptide are consistent with bioinformatic predictions of high amyloidogenic propensity.

All of the NMR structural studies, performed here involve utilization of the micelles. While micelles have a hydrophilic head group and a hydrophobic tail similar to that of the lipids and have the ability to trap these peptides in a non-aggregated state, they differ from the real cell membrane by having a curved surface rather than a planar surface. Therefore, these structural studies can be further extended to bicelles or planar lipid bilayers that possess a planar curvature. However, the lipid-induced rapid aggregation of IAPP is a major challenge for high-resolution structural studies using NMR spectroscopy. Even optimization of conditions to prepare isotropic bicelles containing IAPP for solution NMR studies is challenging.

It would be also interesting to see if the transition from α-helical intermediate to β-sheet could be studied at the atomic-level by monitoring the change in chemical shift of the residues upon titrating the micelle bound α-helical

intermediate with bicelles consisting of a mixture of different lipids. In this context, it is worth exploring the structure of the peptide using aligned bicelles for solid-state NMR measurements using sophisticated techniques like BB-PISEMA, HIMSELF/HERSELF, PELF, PELF-mixing, and DREPT [*1-6*]. These techniques have successfully been applied to solve the high-resolution images of membrane-associted cytochrome b5 embedded in large bicelles.

Since the oligomers are known to be cytotoxic to the cell membrane, any further research progress in trapping these oligomers suitable for NMR structural studies would be the key in understanding the mechanism of cytotoxicity as well as to design the novel drugs for treatment of these amyloid diseases. Trapping the oligomers in lipid bilayers and applying solid-state NMR techniques for high-resolution studies could be the best approach to overcome these challenges.

REFERENCES

[1] Yamamoto, K., Lee, D. K., Ramamoorthy, A. (2005) Broadband-PISEMA solid-state NMR spectroscopy. *Chem. Phys. Lett. 407*, 289-293.

[2] Dvinskikh, S. V., Yamamoto, K., Ramamoorthy, A. (2006) Heteronuclear isotopic mixing separated local field NMR spectroscopy. *J. Chem. Phys.125*, 034507.

[3] Yamamoto, K., Dvinskikh, S. V., Ramamoorthy, A. (2006) Measurement of heteronuclear dipolar couplings using a rotating frame solid-state NMR experiment. *Chem. Phys. Lett. 419*, 533-536.

[4] Soong, R., Smith, P. E., Xu, J., Yamamoto, K., Im, S-C., Waskell, L.,

Ramamoorthy, A. (2010) Proton-evolved local-field solid-state NMR studies of cytochrome b5 embedded in bicelles, revealing both structural and dynamical information. *J. Am. Chem. Soc. 132*, 5779-5788.

[5] Xu, J., Smith, P. E., Soong, R., Ramamoorthy, A. (2011) A proton spin diffusion based solid-state NMR approach for structural studies on aligned samples. *J. Phys. Chem. B. 115*, 4863-4871.

[6] Xu, J., Soong, R., Im, S-C., Waskell, L., Ramamoorthy, A. (2010) INEPT-based separated-local-field NMR Spectroscopy: A unique approach to elucidate side-chain dynamics of membrane-associated proteins. *J. Am. Chem. Soc. 132*, 9944-9947.